Modelling study on the influence of wave conditions on tidal inlet dynamics

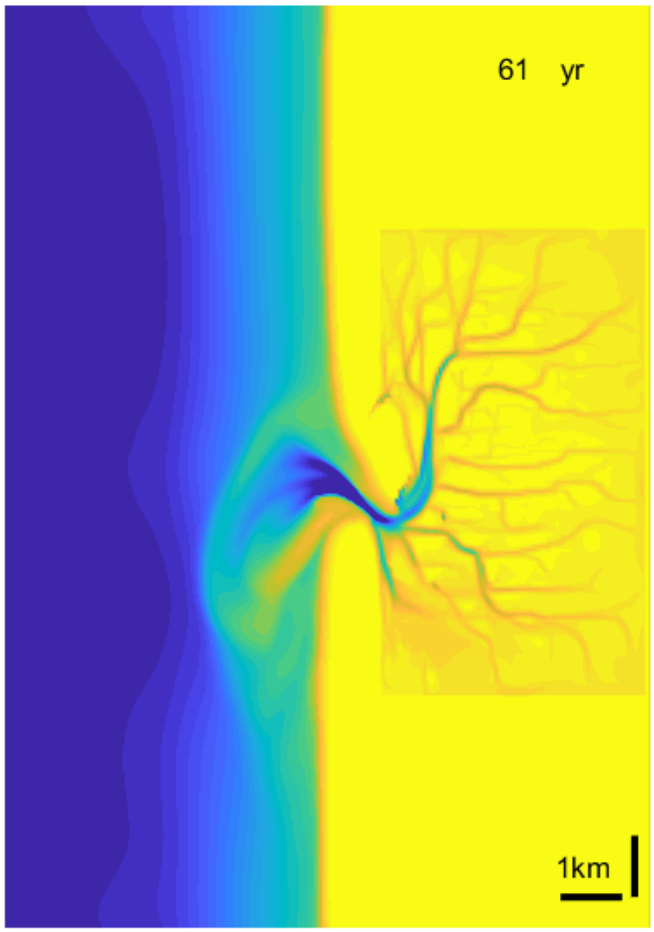

Master Earth Surface and Water, Coastal Dynamics and Fluvial Systems track

Faculty of Geosciences, Department of Physical Geography

Author:

Max Hoogland

Supervisors:

Prof. dr. M.G. Kleinhans

Dr. M. van der Vegt

Utrecht University

Abstract

Tidal inlets at barrier coasts are the meeting point between wave energy and tidal currents, these dynamic systems often include cyclic patterns of channel rotation and breaching. The effect of different wave conditions on the dynamics of these systems is still unknown. Different wave height or direction result in a different sediment balance and greatly influence morphology in these systems. In this study a depth averaged (2DH) numerical model using Delft3D/SWAN is used based on a setup including a wave climate used for studying basin infilling (Boechat Albernaz et al., 2023). The classes used in the wave climate were also used for new model runs with single wave conditions of varying height and direction. For the wave climate scenario, cyclic behavior of the ebb-tidal delta was observed but this seems to have an erosional origin instead of originating in sediment bypassing processes. Other scenarios did not show cyclic behavior to the same extent. Why remains unclear. The size development of the tidal inlet depends on balance between alongshore drift, which brings sediment to the inlet, and the tidal currents through the inlet. The sediment exchange in the model was limited by the limited supply of sediment through alongshore transport at lower wave energy or the reducing inlet size at higher wave energy. Various runs show that the inlet narrows at higher wave energy or widens at low wave energy. In most runs, large amounts of sediment were deposited in both the basin and ebb- tidal delta until they reached a steady state. Both the basin and the ebb- tidal delta were found to be a large sink of sediment. Due to a phase difference between the tidal currents in alongshore and cross-shore direction, the outflow of the ebb current tends to bend in the opposite direction to the tidal propagation and alongshore transport. In most model runs, this mechanism caused the main ebb channel to bend southward together with the ebb- tidal delta. Low waves from the southwest, opposed to the ebb channel, caused the ebb- tidal delta to grow larger. Low waves from the northwest push the ebb channel more towards the shore, this reduced the ebb- tidal delta volume because of the smaller seaward extent of the ebb- tidal delta. For higher waves, the waves from the southwest pushed the entire ebb- tidal delta in downdrift direction. Single wave conditions have a profoundly different effect on the morphology of the ETD and tidal inlet systems, they force the system in one direction opposed to a wave climate where waves with different heights and directions provide a more balanced image. As was previously shown, the empirical relations that predict inlet dimensions show a very different trend than the model used in this study. The mode of erosional cyclic behavior found in our results remains inconsistent with previous model studies.

Table of Contents

1 Introduction

Barrier islands are long and flat sandy islands that lie parallel to the coast. They are built up by waves, currents and wind and they occur in shallow seas around the world. The most well-known examples of barrier coasts are the Wadden Sea in northwestern Europe and the western and southern coasts of the United States. Barrier coasts are important coastal landscapes because they contribute to biodiversity and they form a first line of defense from floods at low lying coastal areas. In protecting and conserving barrier coasts, ebb- tidal deltas play an important role. Ebb- tidal deltas are shoals that form at the end of the ebb channel in a tidal inlet which, due to their shallow depth, enforce early wave breaking and energy dissipation. This reduces the wave energy and thus erosional force that reaches the mainland (FitzGerald, 1988). A second function of ebb- tidal deltas is that they can be a temporary source of sediment, for both the connected tidal basin as the adjacent barrier islands. Due to recent and future developments, ebb- tidal deltas are under threat because of sand volume loss. This has been linked to land reclamation, dam construction and sea level rise combined with natural processes (Elias et al., 2012; Ridderinkhof, Hoekstra, et al., 2016; Wang et al., 2018). Barrier coasts and tidal basins are especially vulnerable to drowning under sea level rise and nourishment on ebb tidal deltas has been proposed to mitigate the loss of these land areas and ecosystems. As it is likely that for preservation and protection of barrier systems human interventions are necessary in the future, there is a need for better understanding and prediction of the dynamics of ebb- tidal deltas. Numerical modelling is an important tool to better understand these complex systems and supplemented with field measurements, this can be used to reliably predict future behavior. This study will explore how different wave conditions influence the tidal inlet and ebb- tidal delta in an idealized modelled setting.

1.1 Ebb tidal deltas

An ebb- tidal delta (from here on referred to as ETD) is a shoal formed on the seaward side of a tidal inlet by different forces that move great volumes of sand. They form at the intersection where a tidal inlet channel meets with a longshore current. Here, due to the combination of the jet like ebb current and wave action, the sediment is stored in a large shoal, gets bypassed or is transported into the basin (De Swart & Zimmerman, 2009). The ebb jet transports sediment from the back basin or sediment that is intercepted from the longshore transport seaward. Where the jet current disperses it loses its transport capacity, from there wave action transports sediments back towards shore. The flood currents, in contrast, occur as an almost radial inflow and therefore have a far smaller impact on the morphology seaward of an inlet (Tambroni & Seminara, 2006). The size of the ETD is related to relative magnitude of wave and tidal energy which was classified by (Hayes, 1979). This leads to a more direct relationship that was found between ETD and tidal inlet size, and tidal prism, which is the volume of water flowing through an inlet during half a tidal cycle (Davis & Hayes, 1984). Empirical relationships were defined between the volume of the ETD (V) and tidal prism (P) (Equation 1;(Walton & Adams, 1976) and between the cross-sectional area (A) and tidal prism (P) (Equation 2; (O'Brien, 1969).

$$V = 1.89 \times 10^{-5} \times P^{1.23}$$

Equation 1

$$A = 3.04 \times 10^{-5} \times P^{1.05}$$

Equation 2

These relations are secondarily affected by delivery of sand through wave energy, as with higher wave energy more sand is transported back onshore. More recently, the physical processes behind these relationships are being quantitatively researched through numerical modelling, which allows for more specific model inputs. The volume and morphology of the ETD, which is determined by tidal prism, nearshore slope and the interaction between waves and tidal currents, is also found to be changing over time due to the effects of inlet sediment bypassing or changeable wave conditions (Davis R & Dalrymple R, 2012).

The general features of ETDs and where they are situated in their environment in relation to other morphological entities are shown in Figure 1. These environments are highly dynamic, and ETDs often show cyclic behavior which can express itself in varying forms depending on the relative magnitude of wave and tidal energy as well as local geological factors. This cyclic behavior of ETDs consists of sediment bypassing processes where sediment from the longshore drift is temporarily stored in the ETD around the inlet channel, which in turn is a sediment source that feeds the downdrift coast.

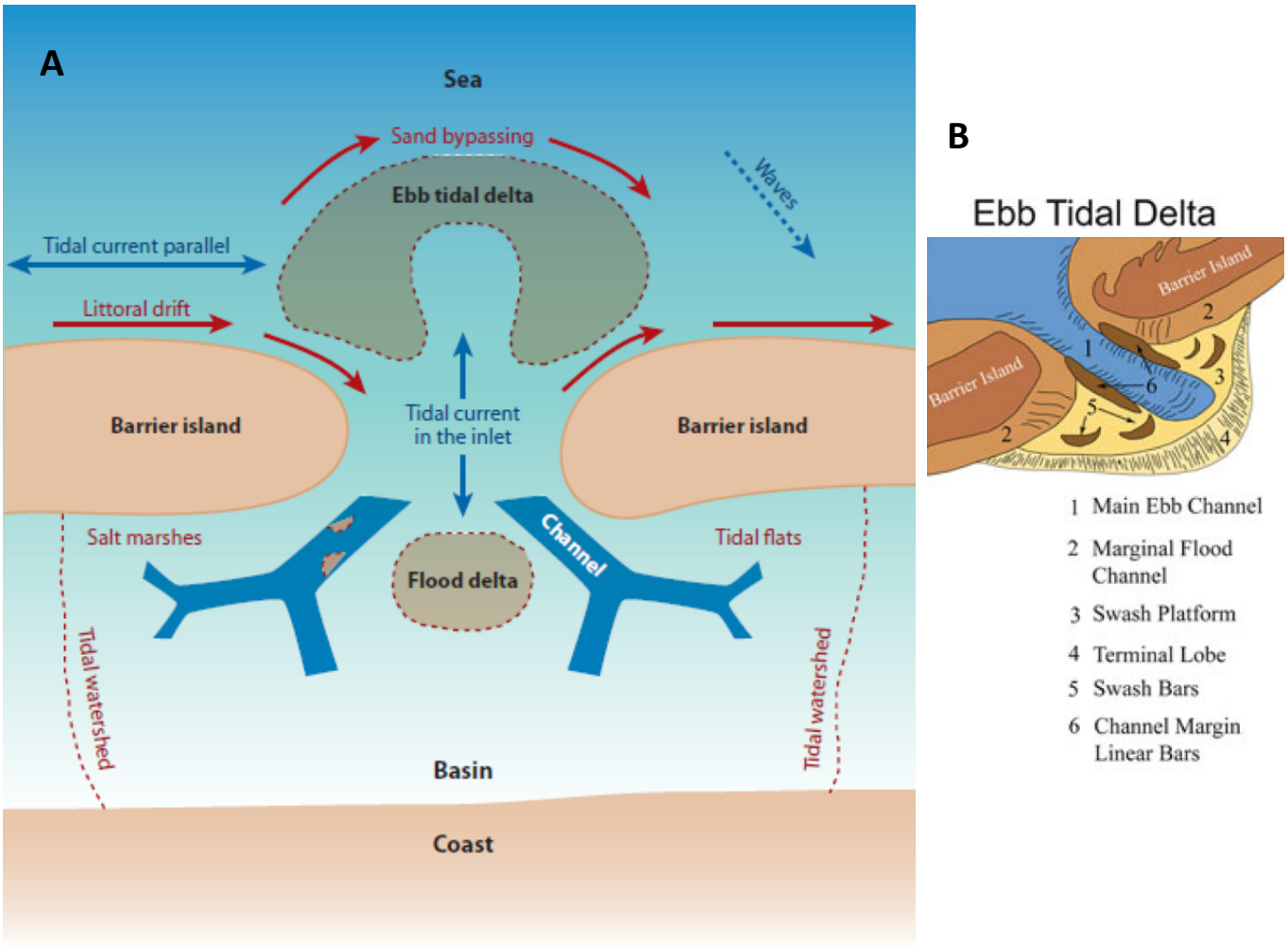

Figure 1, A; sketch of an idealized tidal inlet system, showing geomorphologic elements and the dominant physical processes and phenomena (De Swart & Zimmerman, 2009). B; conceptual ebb tidal delta model with more detailed geomorphological elements (Hayes, 1979).

1.2 Sediment bypassing processes

Sediment bypassing occurs as waves and currents form swash bars and margin bars that grow and migrate downdrift and toward the coast (Figure 1a). The bars formed on the ETD often merge and periodically attach to the beach or a spit (

Figure 2). Different modes of sediment bypassing using conceptual models (Fitzgerald et al., 2000). These models have different morphological evolutions, cyclical behavior and inlet stability influenced by the relative magnitude of wave and tidal energy. Stable inlet processes (

Figure 2 B) are defined by a stable inlet that doesn't migrate, here bars form alongside the channel and on the swash platform, which merge and weld to the coast, this leads to cyclic fluctuation of the sediment volume on the ETD. Inlet migration and spit breaching (

Figure 2 A) is defined by a migrating inlet channel that is pushed in downdrift direction by a growing spit, here the ETD migrates with the location of the inlet until a spit breaching occurs and the cycle starts over. Ebb tidal delta breaching (

Figure 2 C) is defined by the downdrift migration of the channel and its associated margin bars, these bars push the ebb channel towards the coast until eventually the ebb channel breaches through these bars. The cyclic behavior of this delta breaching involves alternating between a single channel and double channel configurations. Figure 3 shows a model of a tidal inlet that is wave dominated. These inlets are usually small, have sand shoals that are pushed close to the mouth and the ETD is shaped like a fan with shallow channels running over it. The shallow nature of the ETD and the gentle fan shape allow the longshore drift to transport sediment along the ETD without much bypassing and exchange with the basin. Other described types of sediment bypassing at tidal inlets are variations on

Figure 2 A and C which differ in the location where the main inlet channel breaches through the spit or shoals. The presence of man-made or hard geological structures, such as a jetty or a headland, will also have different bypassing mechanisms at play.

1.2.1 Cyclic behavior

The volume of the ETD changes over time due to the channel shoal cycles and sediment bypassing processes. The average period of this cyclic behavior of the ETD correlates to the tidal prism and for the Wadden Sea, this ranges from 4 to 130 years, with larger tidal prisms favoring longer timescales (Ridderinkhof et al., 2016). The closure of portions of the Wadden Sea has decreased the basin size for some of the inlets there. This reduced the tidal prism for each of these tidal inlet systems which in turn affected the morphological behavior both in the basin and the ETD (Wang et al., 2012). After such a change in tidal prism, the system transitions to a new state of morphological equilibrium. For the Wadden Sea, this meant that the infilling rate of the basin increased, and the size of the ETD decreased as most of the extra sediment was supplied by the ETD (Elias et al., 2012). Storm events also have a great impact on the morphodynamics of ETDs as they are associated with high wave energy and large amounts of sediment get transported. During these events, shoals can both form and breach in a short period of time. These small-scale changes in shoals don't affect the ETD and inlet dynamics as a whole but can trigger a new sediment bypassing cycle (Elias et al., 2012). These subtle dynamics make it difficult to capture the morphological behavior of ETDs using empirical relations or conceptual models and shows the need for more complete numerical modelling.

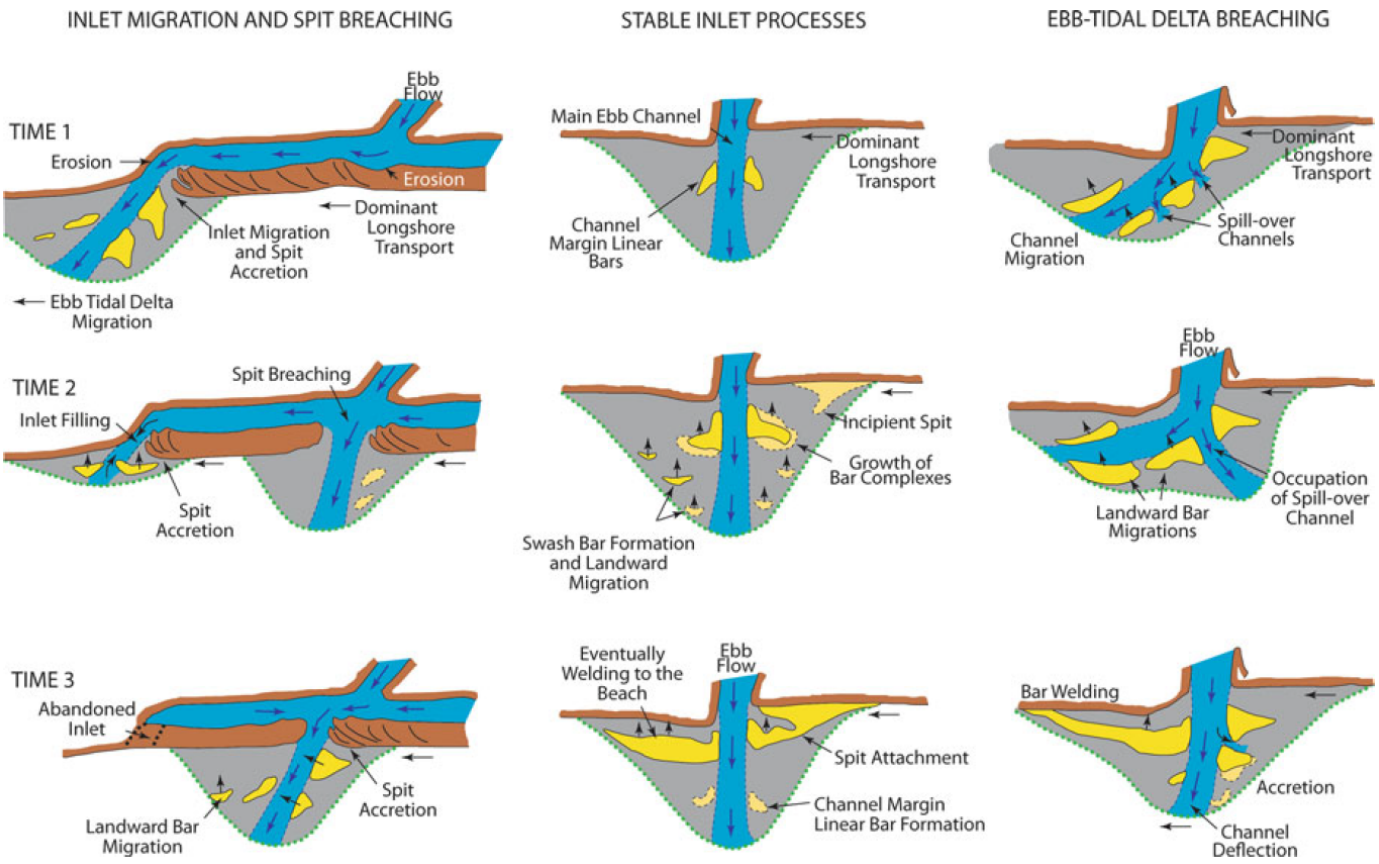

Figure 2, conceptual models of sediment bypassing processes at tidal inlets. (Fitzgerald et al., 2000)

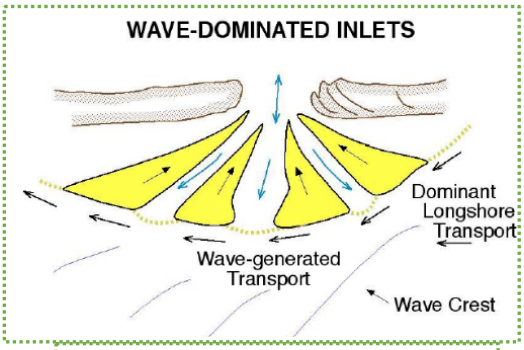

Figure 3, conceptual model of wave dominated inlet. (Fitzgerald et al., 2000)

1.3 Ebb- tidal deltas in numerical modelling

Numerical modeling studies on tidal inlets have produced increasingly promising results in reproducing the conceptual model from (Fitzgerald et al., 2000). Cayocca (2001), showed that littoral drift is the largest factor in shoal formation and migration, and that new channels only breach under the presence of tides. While wave induced transport can push any ETD in downdrift direction, a model focused on the influence of tides showed that tidal asymmetry can result in updrift oriented inlet channels. The presence of a phase difference between alongshore and cross-shore tidal currents, causes currents to

leave the inlet in an opposite to the tidal propagation thus resulting in a channel with an updrift orientation when considered without waves (van der Vegt et al., 2009). Dastgheib et al. (2008) and Nahon et al. (2012) both produced models where channel rotation and subsequent breaching was shown. These models showed more shoreward breaching of the ETD for more wave dominated coasts to outer delta breaching and stable inlet processes (Fitzgerald et al., 2000) for mixed energy and tide dominated coastal conditions. Unfortunately, no study was done to the underlying mechanisms and their dependence on waves and tides. Ridderinkhof, et al. (2016) researched migration and growth of shoals on ETDs and included multiple wave heights and a wave climate in their model. They did not reach a full shoal formation cycle but gave important insight in the physical processes behind shoal formation. The model used multiple wave conditions in a seasonal (serial) configuration to simulate storm events. This showed that shoal formation has thresholds related to minimum water depth, sand volume and local wave height. Shoals on ETDs grow as a result of local imbalances between wave conditions and bathymetry. These imbalances were caused by either incidental or local high wave energy through storm events or redistribution of sediment subsequent increase in refracted wave energy. Mechanisms behind shoal migration are both wave driven, and tide driven residual currents over the shoal. The balance between these residual currents determines the speed and direction of the shoal migration, while in most cases this migration is shoreward. Lenstra et al. (2019) used an idealized Delft3D/Swan model, that showed cyclic behavior as described earlier. This study demonstrates what the relative roles of wave and tidal forcing are during the different phases of cyclic behavior on ETDs. The cyclic dynamics of ETDs were further researched by Lenstra K. J. H. (2020) and this produced a model that showed cycles of multiple modes of sediment bypassing depending on tidal prism vs longshore drift ratios (Bruun & Gerritsen, 1960).

It was found that transport due to wave skewness is important for the coherence of shoals during migration (Ridderinkhof, de Swart, et al., 2016). Lenstra K. J. H. (2020) notes that the parameterization of wave related bed transport produced issues regarding the steepening of the shoreface. Wave skewness and asymmetry parameterization was improved upon by Ruessink et al. (2012), which was based on extensive field measurements, explicitly calculates both parameters. Previous methods, including the default method within Delft3D (Isobe & Horikawa, 1982), did not explicitly calculate skewness and asymmetry and were mostly derived from lab experiments. The new parameterization was implemented in Delft3D to predict wave driven sediment transport (Albernaz et al., 2019). The new method was included in Boechat Albernaz et al. (2023) and proved to prevent excessive shoreline erosion or accretion in the model and represents the sand transport along the coast better.

1.3.1 New model with wave climate

Most of previously described model studies on ETDs only use constant wave conditions with a single wave direction. This could possibly change the outcome, as in a natural system, wave conditions form a spectrum. The new model by Boechat Albernaz et al. (2023) includes a wave climate with different wave conditions run in parallel using the Mormerge method (Roelvink, 2006). This showed promising results with some form of cyclic behavior of the ETD with alternating single and double channel configurations. This study however, focused on basin infilling and the dynamics of the ETD weren't discussed in more detail.

In Figure 4, the behavior of a model run by Boechat Albernaz et al. (2023) is shown. Here, bed elevation is shown for each 10 years of the modeled tidal inlet system with the wave climate (further information on the model conditions, see section 2.1). We see that the model run starts with deepening the inlet

channel and developing a channel network within the basin. After 10 years a large ebb channel has formed in southward direction. From 20 to 40 years the channel mouth becomes wider, the inlet moves southward with longshore current, and the northern barrier retreats landward, confining the inner part of the channel. During this period the ETD grows and shows behavior akin to ebb tidle delta breaching processes (

Figure 2 C). After 40 years the angle of the inner channel rotates from a shore normal orientation to a SE-NW orientation, and the behavior of the ETD changes to switching between a single and double channel configuration similar to outer delta shifting (Fitzgerald et al., 2000).

The previously explained differences and challenges in modelling ETD dynamics will be further explored in this study. Boechat Albernaz et al. (2023) will be the starting point and together with the literature, including empirical relationships, and conceptual models, we enhance our understanding of tidal inlet dynamics.

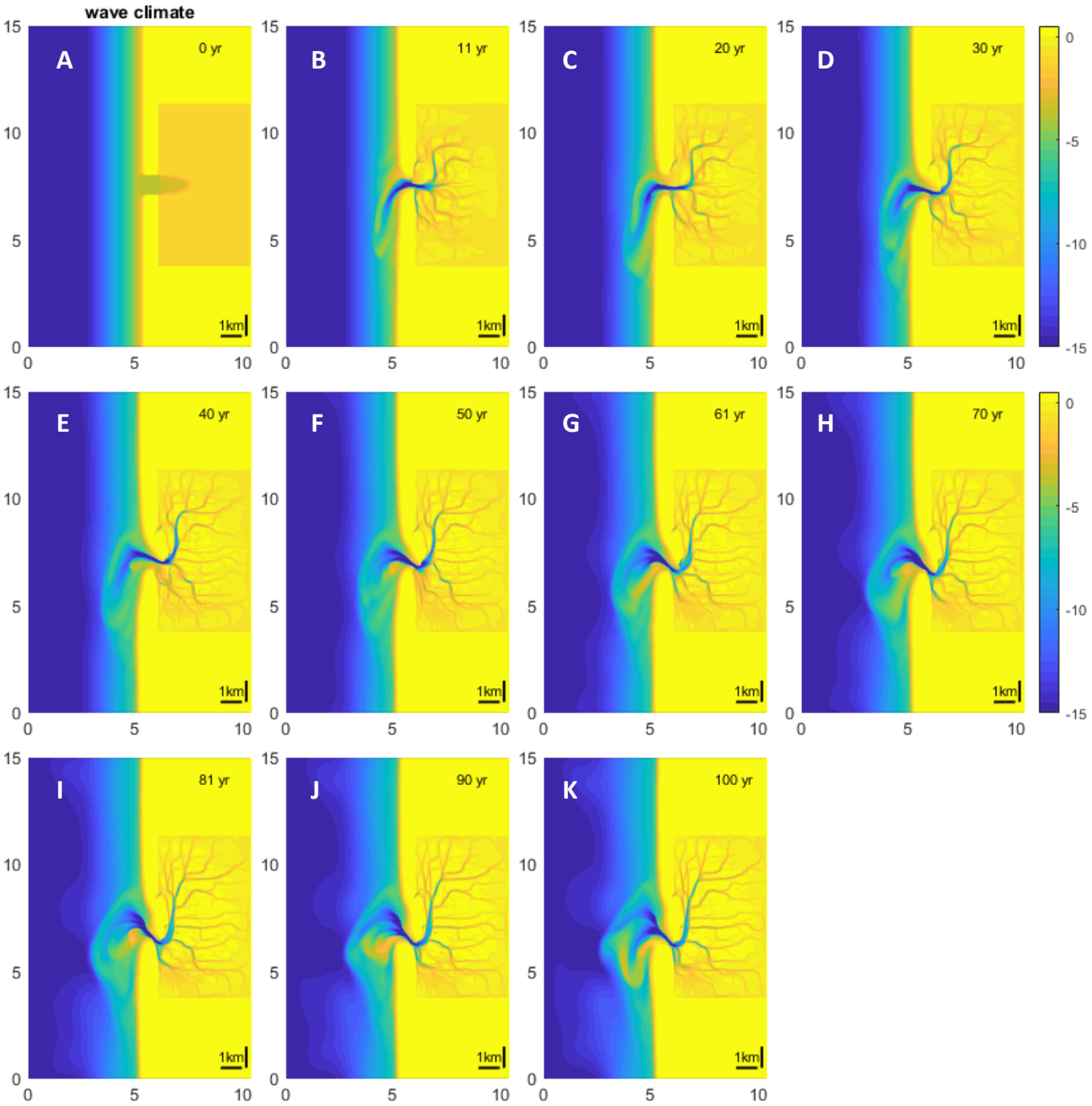

Figure 4, wave climate run time series

1.4 Research questions

The aim of this research is to provide and improve our insight into the cyclic behavior of ETDs and what the effect of different single wave conditions on the ETD morphology is. Within this we look at (1) how a wave climate and a single wave differently affect the behavior of tidal inlet morphology. (2) What the effect of wave height and direction is on the dynamics of tidal inlet systems, and (3) what role does wave direction play on the mode of sediment bypassing at a tidal inlet?

Previous research demonstrated how the combination of tides and waves can cause cyclic behavior of ETDs and how a wave climate influences shoal migration differently than a single wave of different heights. It is well understood how wave direction relates to alongshore transport, but it is still unknown what the effect of wave direction interacts with the morphology of tidal inlets, the ETD and sediment bypassing processes. In this research, by working with a wave climate with different wave directions in parallel, and dissecting this into multiple wave conditions, we hope to unravel how different wave conditions force the dynamics of tidal inlets.

The morphological properties we analyze to provide insight in these research questions are: (1) cyclic behavior of the ETD, (2) sediment transport balances in the tidal inlet, (3) tidal prism and cross-sectional area of the inlet.

2 Method

2.1 Model

For this research we built further on the research by Boechat Albernaz et al. (2023), from which we received data and model settings to do supplementing model runs. The morphodynamic model that is used here was first developed by (Boechat Albernaz et al., 2023). It is performed in a depth-averaged (2DH) configuration of Delft3D (Deltares, 2020, FLOW2D3D Version 6.03.00.62434). This version includes the parameterization of near bed wave orbital motion by (Albernaz et al., 2019) which improved shallow wave-induced sediment transport. The waves were simulated with the SWAN spectral wave model (Booij et al., 1999) which is embedded within Delft3D-WAVE. For the sediment transport the VR04 predictor was applied (Van Rijn et al., 2004), improved according to Albernaz et al. (2019) for the computation of near-bed wave orbital velocities. The VR04 predictor was used because it is well calibrated for both wave- and current-driven sediment transport. The mud fractions are treated as cohesive sediments and their deposition and erosional fluxes are computed according to the Partheniades-Krone method (Lesser et al., 2004).

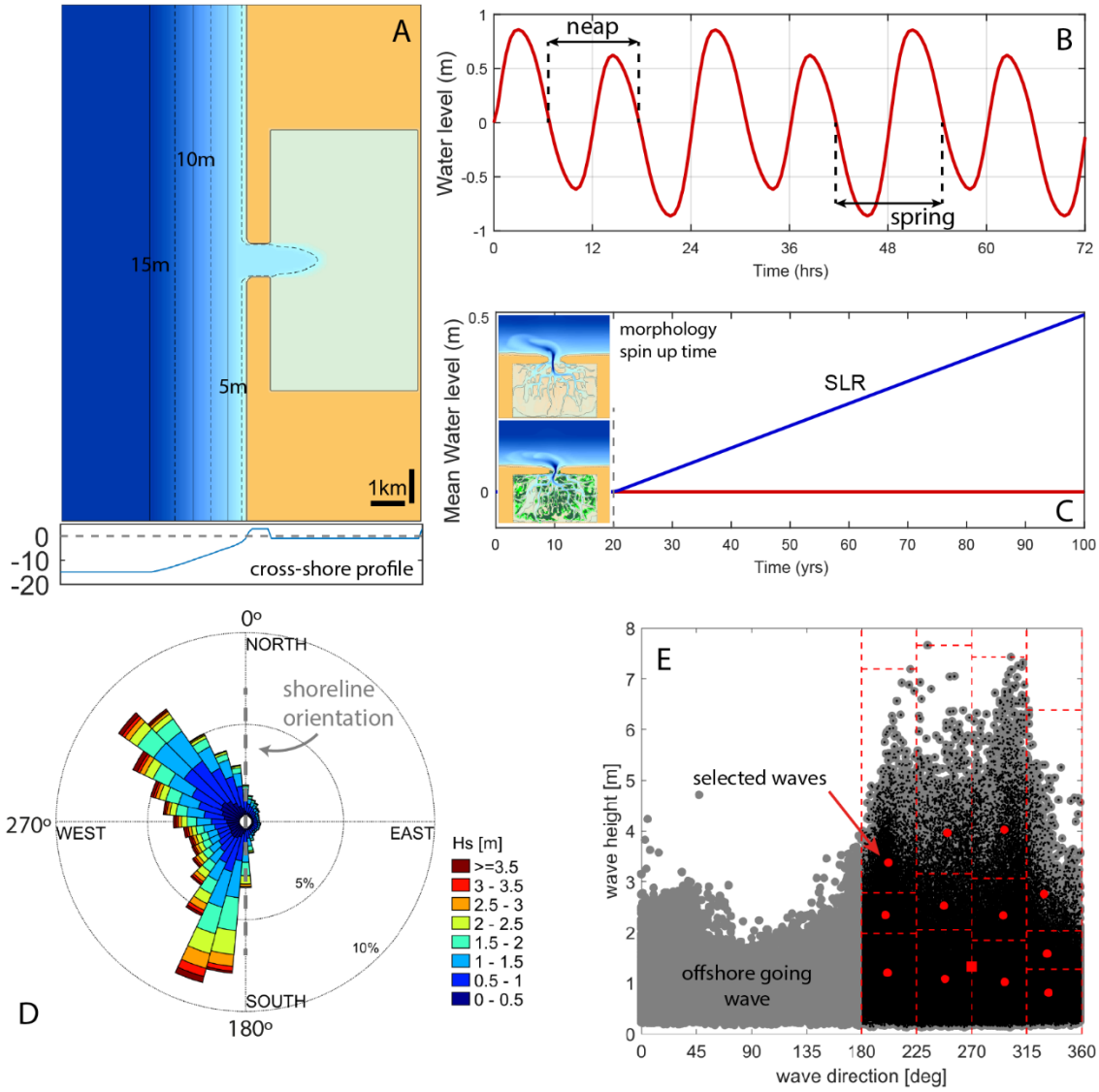

Figure 5, Delft3D model layout and boundary conditions. (a) plan view of model domain and cross- shore profile. The alongshore domain was reduced for visualization purposes; (b) morphological tides; (c) implementation of sea level rise not used in this study; (d) Wave polar histogram for significant wave height (Hs); (e) and the reduction and schematization to wave bins for modelling. The wave data was recorded at the IJmuiden 'Munitiestortplaats' between 1990 and 2016. Directions were rotated by 30o for application in the model domain with the same relative angle. Dots indicate selected wave conditions, and the square indicates the time-averaged condition (Boechat Albernaz et al., 2023).

Wave	Wave height	Wave period	Wave direction
#	(Hs) m	(Tp) sec	deg
1	1.20	4.1	201
4	1.08	4.2	248
5	2.53	5.5	247
6	3.96	6.5	250
7	0.80	3.5	270
8	1.02	4.7	297
9	2.33	5.7	296
10	4.02	6.9	296
11	0.81	4.2	333

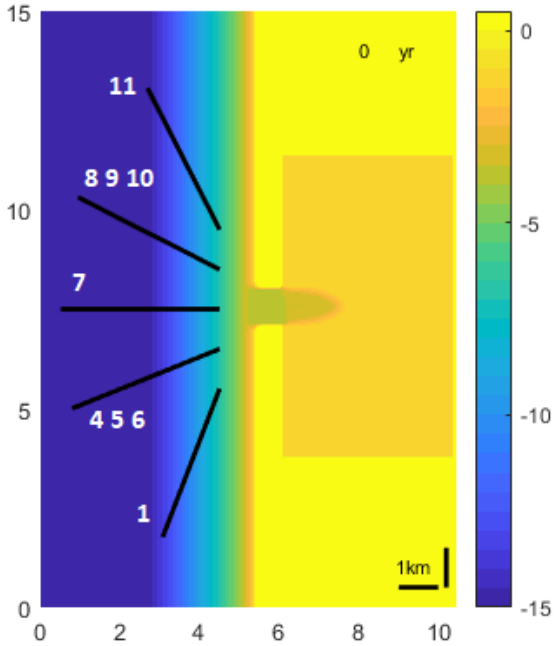

Figure 6, Left: table of used waves with height, direction and period, right: visualization of wave directions.

2.1.1 Model domain and settings

The domain for the model simulations was adopted from (Boechat Albernaz et al., 2023), the idealized conditions used in the model are broadly inspired by a mixture of what is found in the Wadden Sea (Figure 1). The model domain consists of a 20 by 5.5 km idealized coast with a cross shore profile based on a time-spatial averaged nearshore bed profile obtained from the JARKUS database (Rijkswaterstaat, 2017). This coast was connected to a shallow basin of 1 m depth and 4.4 and 7.7 km dimensions via a single 1 km wide inlet enclosed by coastal barriers.

The sediment in the model consists of four fractions: 200 and 125 µm sand, silt, and clay. The sediment will distribute itself in the model to represent different environments, from a wave-exposed coast to protected mud flats. The sediment supply was defined at the coastal boundaries as equilibrium concentration for the sand fractions, while silt and clay combined was set to 15 mg/L.

The tidal conditions were inspired on North Sea records and was directly copied from (Boechat Albernaz et al., 2023). The model consists of alongshore propagating morphological tides running from south to north in the model domain (Figure 5 A). The tidal components were rounded to integer hours, with 0.75 M2 amplitude, 0.075 m M4, 0.035 m M6 and a diurnal component of 0.2 m. The tidal cycle is depicted in Figure 5 B and shows a semi-diurnal cycle with daily disparity between high and low amplitude cycles.

In the research by (Boechat Albernaz et al., 2023) the wave climate was reduced to 12 wave bins with equal energy (with $E \approx H_s^2$). An average wave as a 13^{th} wave added to replace the offshore and parallel waves (Figure 5 E), the details of these wave bins are shown in **Error! Reference source not found.**. The wave climate was divided in four directions which were subsequently divided into 3 bins with equal energy with low, medium, and high waves.

2.1.2 New runs

To further investigate the intricacies of modellimg the tidal inlet system, new model runs were conducted for separate waves. For the new runs, the wave settings were picked from the separate waves present in the wave climate of Boechat Albernaz et al. (2023) to show what the influence of different individual waves is on the tidal inlet morphology. To represent an array of different wave directions and wave heights, 9 different waves were used (Figure 6). These separated wave conditions correspond to Boechat Albernaz et al. (2023) and are categorized into three wave height categories and five categories based on wave direction. The wave direction categories are visualized in Figure 6, they can be divided into parallel and opposite to the tidal propagation and high and low angles of incidence. Added to this was a scenario with a shore normal wave (wave 7 Figure 6), that represents the parallel and offshore waves in the research by (Boechat Albernaz et al., 2023). For all directions a low wave scenario was run while for the scenarios with low angle of incidence, different wave heights were modeled. The wave height categories on wave height are defined as low (0.80 – 1.20 m), medium (2.30 – 2.60 m) and high (3.90 – 4.10 m) waves, which were compared to each other. In addition to these 9 model runs two more scenarios were looked at, a model run without waves and a run for wave 1 without tides. Initially it was planned to do more runs without tides but as results came in it became clear that without tidal energy the inlet channel would just slowly fill in.

2.1.3 Modelling time improvement

To speed up modelling time, a morphodynamic upscaling method is used which multiplies the morphological change per timestep. Delft3D includes morphological acceleration factor (morfac) (Ranasinghe et al., 2011). In Boechat Albernaz et al. (2023), the morfac varies for each wave according to wave duration, while in this study we used more rounded morfac values to better align the time series. For the high and medium waves, a lower morfac of 25 and 50 respectively, was chosen because the morphological changes per timestep may otherwise exceed the water depth resulting changes in bed elevations that are not physically possible. For the control scenario, with tides only, the morfac was set to 100 as it finished relatively quick. To make further run time improvement, the morfac and time step were doubled for all runs with low waves. To show the difference between a morfac of 100 and a run with the morfac and timestep doubled to 200 and 24s respectively, **Error! Reference source not found.** shows the bed level change of a cross section through the initial inlet location after around 26 years. The figure shows that the largest differences between the two runs occur within the basin, where the water is dispersed in multiple smaller channels. Here, a slight difference in the location of a smaller channel has a large effect on the cross section. Seaward of the inlet, our focus area of the ebb channel and ebb delta show relatively little difference between the two runs. For the larger morfac, the ebb delta and channel lie slightly more towards the shore than with a morfac of 100. Together with the similar bathymetric development in both model runs as observed in animations and time series, we chose to go ahead with this time saving strategy.

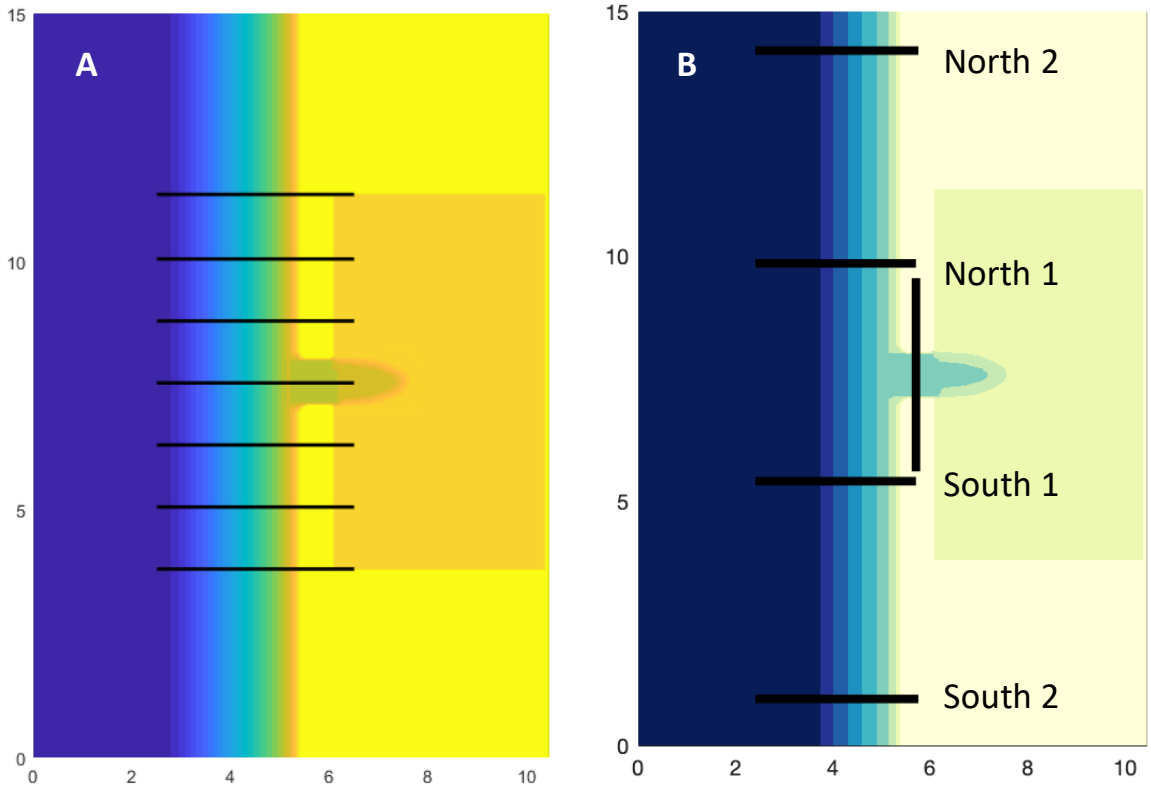

Figure 7, left: cross sections indicating the locations of timestacks. Right: measuring transects included in the model, through the inlet, and four transects perpendicular on the coast.

2.2 Analysis strategy

The data from the new model runs were analyzed together with a dataset from (Boechat Albernaz et al., 2023), this dataset includes the wave climate as previously discussed. The data analysis was done through looking at the morphological behavior of each dataset and their individual differences. The morphological behavior in our datasets is described using different parameters as well as observing the bathymetry through time.

First the observations of the bathymetry were discussed, using time series, animations, and time stacks. Through these observations, a lot can be said of the general morphological evolution of each wave condition, such as the direction and extent of the ETD and main ebb channel, the duration of the basin development, and inlet stability.

The time series include the bed elevation mapped out for several timesteps. In the results, a low wave condition and the wave climate are shown in more detail by showing the bed elevation for every 10 or 20 years of morphological time. For the rest of the datasets, the bed elevation is shown for two moments in time, with 20 and 100 years for the low wave conditions, while different timesteps were picked for the runs that were cut short by model instability.

For every wave scenario, timestacks were made on seven cross-sections perpendicular to the coast, covering the whole basin (Figure 7 A). The timestacks show the bed elevation of a single cross-section

changes through time. With this, you can plainly see recurring patterns that indicate periodically migrating bars on the shoreface.

2.2.1 Parameters

To get more insight in the morphologic behavior of the different model runs, we analyzed the longshore transport as well as different parameters related to the ETD. These parameters are ETD volume, tidal prism, cross-sectional area of the inlet and basin infilling. The longshore transport, along with tidal prism, were derived from measurement transects in the model (Figure 7 B). It was measured as sediment transport per second (m3/s) over a transect of 3350m. One of the transects goes through the inlet and four lie perpendicular on the coast, with two transects both north and south of the inlet. The transport was further processed to represent the average sediment transport over a tidal cycle.

The cross-sectional area and basin infilling were calculated according to the bed elevation, with the latter being defined as the relative increase of bed level. For the calculation of the ETD volume the method by Lenstra et al. (2021) was used. In this method a reference bathymetry, that represents a cross-section of the shoreface where it is undisturbed by the vicinity of a tidal inlet, was calculated first and then the difference between the reference and each cross-section in the range of the ETD was used to compute the total volume of the ETD.

The parameters described above help us to compare the different wave conditions in a more quantitative manner. The sediment transport data shows how much sediment is being moved and if this can be correlated to the rate of morphologic development of the ETD and basin. Furthermore, the tidal prism and cross-sectional area of the inlet were compared to the empirical relation of O'Brien (1969) as seen in Equation 2. This can be further compared to how the model runs in Boechat Albernaz et al. (2023) relate to this and other empirical relations.

3 Results

Each model run started with the same initial bathymetry, after which the system began developing. As this research is based on the wave climate scenario by Boechat Albernaz et al. (2023), we will describe the observations on the new model runs as shared or distinct behavior compared to the wave climate (Figure 4). We start with the low wave runs as they proved to have the most stable coastline, and within the low wave scenarios the run with an SSW wave (wave 1, Figure 8) was described first as it seemed the most similar to the wave climate.

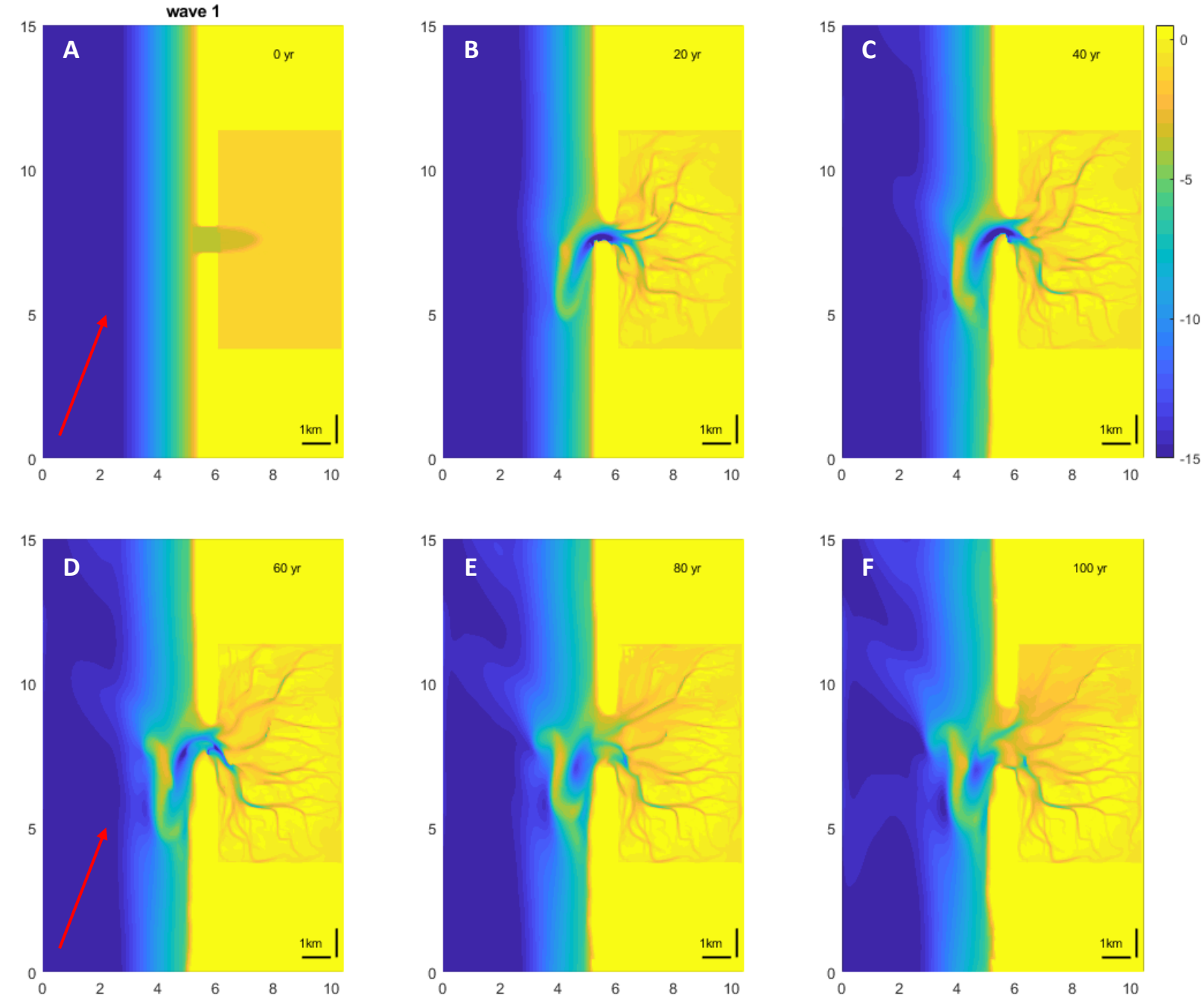

Figure 8, Time series of wave 1 scenario (1.2m, SSW), red arrow indicates incoming wave direction.

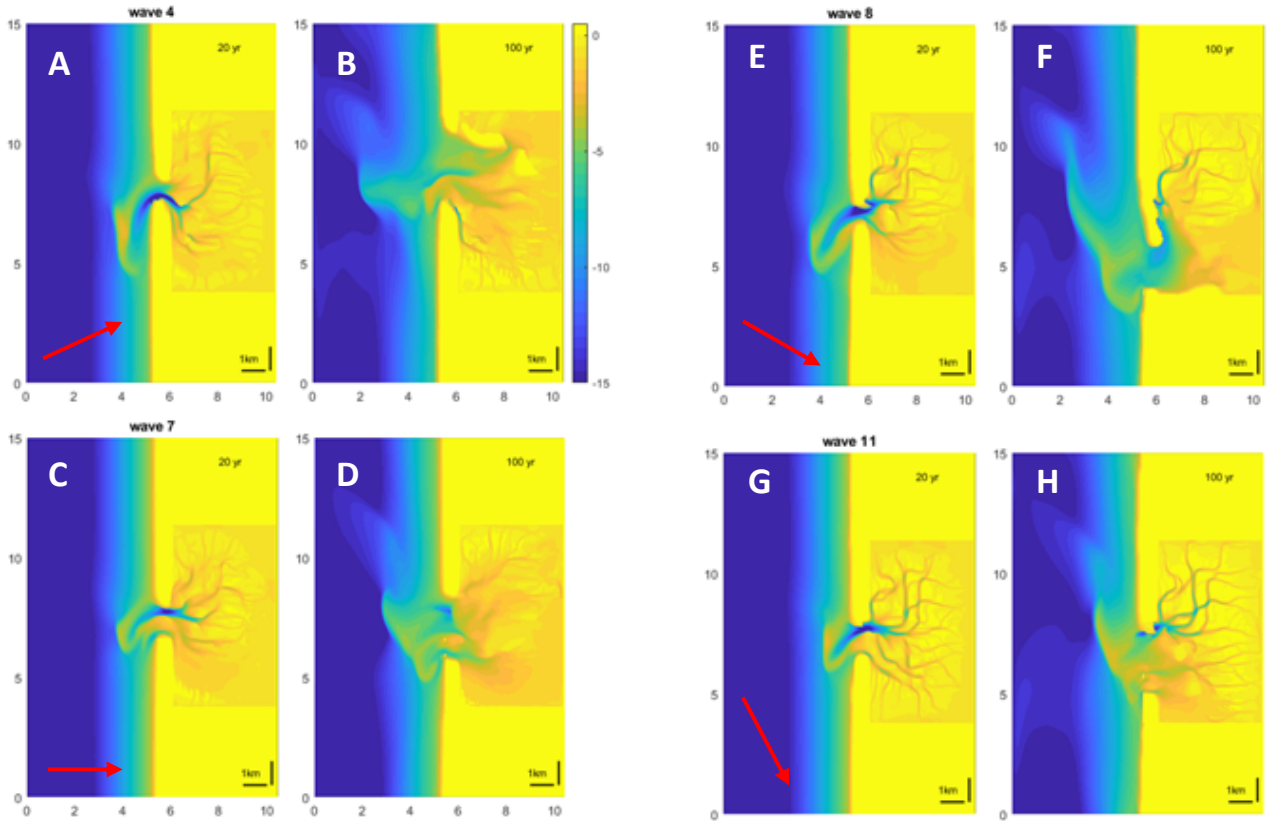

Figure 9, comparison of model bathymetry low waves (± 1m) at 20 and 100 years. Wave 4 WSW, 7 W, 8 WNW, 11 NNW. Red arrow indicates incoming wave directions.

3.1 New runs observations

The new wave runs with only one wave produced significantly different results. Low waves will be discussed first as they produced the most reliable results. For the higher waves, the models did not complete their full run time. These produced very steep cross shore profiles that are not reliable model outputs even with a reduced morfac. The control runs will then be discussed to see the forcings of tides or waves on their own.

3.1.1 Low waves

Wave 1 is a low wave run, with 1.2 m waves from SWS direction. From 20 to 40 years, this scenario starts up similarly as the wave climate, but the basin channels develop slower. After 40 years, the development of the inlet starts to deviate from the wave climate scenario. The inlet channel gets gradually wider as the barrier island on the north erodes, while the southern barrier does not grow in the same pace (Figure 8, C to F). This channel widening decreases the velocity of the flow through the inlet resulting in a shallower channel. This wide and shallow inlet leaves the basin vulnerable to wave erosion and this can be seen in Figure 8 E and F, as the relative deepening of the northwestern corner of the basin.

The ETD develops similarly as in the wave climate scenario where a swash platform builds slowly over time and channel margin bars form on both sides of the channel, most defined on the seaward side. When the channel gets wider the active channel on the ETD shortens resulting in the seaward margin bar functioning more as a terminal lobe. As time progresses, the channel slowly fills in and the features

on the ETD wash out until only a vague shallow area remains. The cross-sectional area of the channel first increases when the channel widens. But as the ETD gets pushed more shoreward, the inlet channel becomes shallower and with this the cross-sectional starts to decrease (Figure 8).

Comparing all low wave runs (± 1m) with each other (Figure 9), we see that they all go through the process of inlet widening and subsequently washing out of the ETD and the front of the basin. On the ETD, the channel margin bar develops more on the seaward (north) side of the channel, together with the terminal lobe, for waves that approach from the south (wave 1 and 4, Figure 8 and Figure 9 A and B), whereas waves 7, 8 and 11 (Figure 9 C to H) have a more visible channel margin bar on the landward (south) side of the channel. The inlet stability is lower for the waves with a slight oblique angle of incidence than for shore normal and very oblique waves. The inlet at waves 4 and 8 wanders more downdrift with the wave driven alongshore drift than in the other scenarios. Other observations are that the deep channel from the start of the run does not fill in completely for wave 8 and 11 after 100 years. At 20 years they both show that the northern barrier head migrates into the channel, but the deep parts fill in slowly and some remnants are still found at 100 years. Striking is that in the scenario with shorenormal waves, the southern barrier is eroding more than the northern barrier (Figure 9 C/D). The inlet in wave 7 at 20 years has two distinct channels, one being ebb dominated and one is flood dominated. This is also found and further explored in 3.1.3 in the scenario without waves.

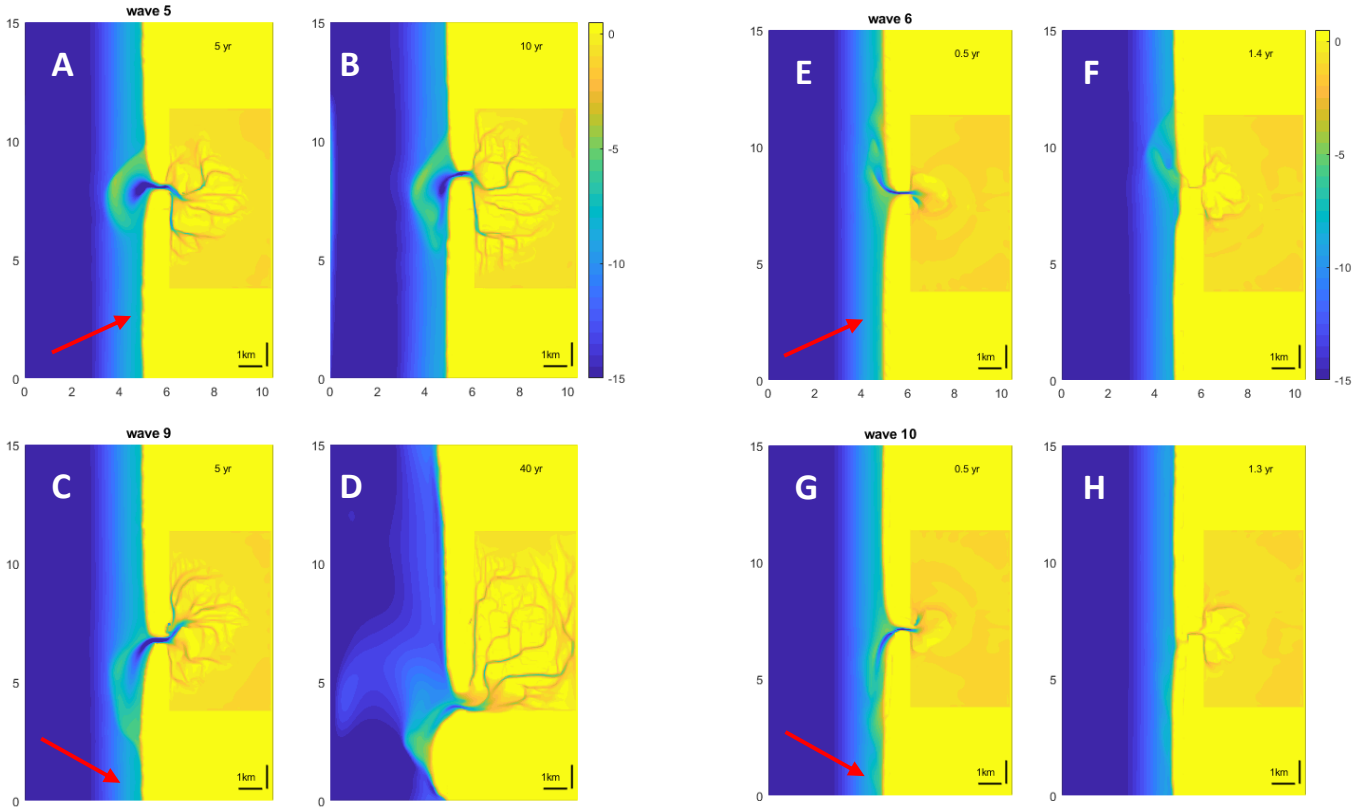

Figure 10, comparison of model bathymetry for above; medium waves (± 2.4m), wave 5 WSW and 9 WNW. Below; high waves (± 4m), wave 6 WSW and 10 WNW. Red arrow indicates incoming wave directions.

3.1.2 Medium and high waves

The medium wave runs (± 2.4m Figure 10 A to D) were done for slightly oblique angles of incidence, wave 5 (WSW) and wave 9 (WNW). These scenarios did not reach their intended run time of 100 years. This is because the coastline is not stable and the shoreface steepens to the point that the bed level changes are larger than the water depth, which is not possible. Figure 10 (A to D) shows that the inlet channel for waves 5 and 9 gets confined very quickly. This is caused by the large alongshore drift that deposits sediment on the upstream barrier island, while the tidal currents tend to keep the inlet open and active. Because of the narrow channel, the tidal prism decreases, and the basin develops slower than in the previously discussed scenarios due to less sediment transport. The channel stays narrow throughout the run and the inlet moves with the alongshore drift to the north (Figure 10 A/B) or south (Figure 10 C/D). For wave 9, the model was more stable, and here the channel got pushed all the way to the edge of the basin. What further strikes is that the channel and ETD in Figure 10, wave 5 doesn't reach as far in the direction opposite to the tide. This shows that the higher waves push the ETD more in downdrift direction than observed in scenarios with lower wave energy, the ETD is more shaped like a shield around the channel and the channel fans out over the terminal lobe like a wave-dominated inlet (Figure 3).

The ETD for wave 9 (Figure 10 C/D), this run only stopped after 40 years, shows more familiar development (like the wave climate and lower waves) in the earlier stages but pushed more shoreward by higher wave energy. Because the shoreface steepens and the inlet moves quickly with the longshore drift, the ETD loses the defined components through the run, but a shallower area remains on the path the ETD has been.

The scenarios with high waves (± 4m Figure 10 E to H), proved to be hard to capture in this model. The model stopped at around 1.5 years because of steepening of the shoreface. Another interesting observation is that for wave 6 (Figure 10 E/F), the high waves push the ebb channel with the wave direction to the north, indicating the forcing of the waves here is stronger than the tidal phase difference that forces the channel to bend south.

3.1.3 Control runs

The control run without tides (Figure 11 C/D) shows that waves alone close off the inlet, the offshore area changes very little and no ETD is formed. The cross-sectional area shows that the closing off starts only just at about 10 years. This is probably due to the closing off starts on the seaward side of the inlet and the cross-sectional area being measured more on the landward side of the inlet channel.

The simulation without waves (Figure 11 A/B) shows how the basin develops without waves. The inlet remains stable and not a lot of activity is observed outside the basin. There is no ETD forming seaward of the inlet and the whole inlet looks like a large flood delta. The inlet is split in two channels dividing the inlet into distinct ebb and flood channels. The southern, flood channel has an ebb shield where the current disperses and flows to the different tidal creeks. The northern, ebb channel has a similar shield where the

ebb current disperses at the mouth of the inlet. This clearly separated channel system resembles tidally dominated estuarine system.

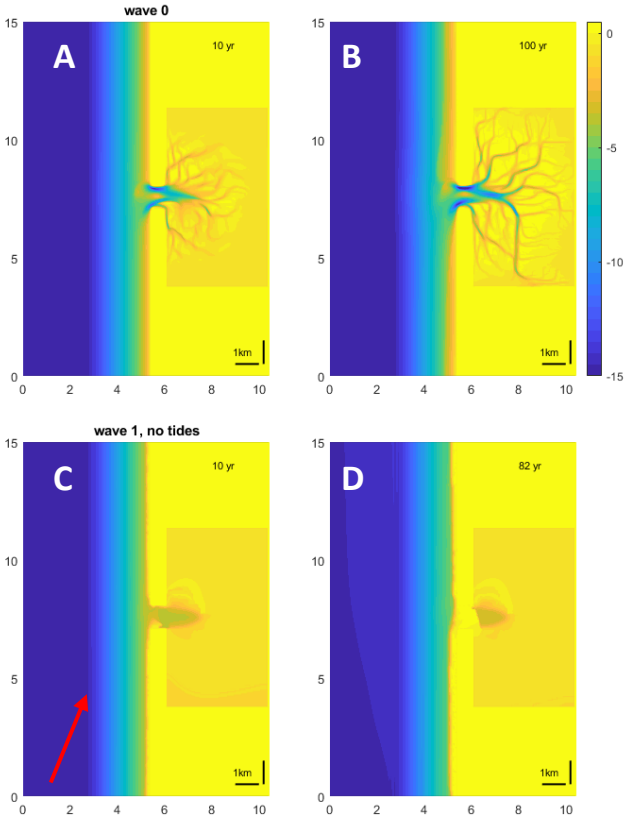

Figure 11, comparison of model bathymetry for control scenarios, wave 0 has no waves, only tides. And wave 1, no tides has only a wave of 1.2m from SWS. Red arrow indicates incoming wave direction.

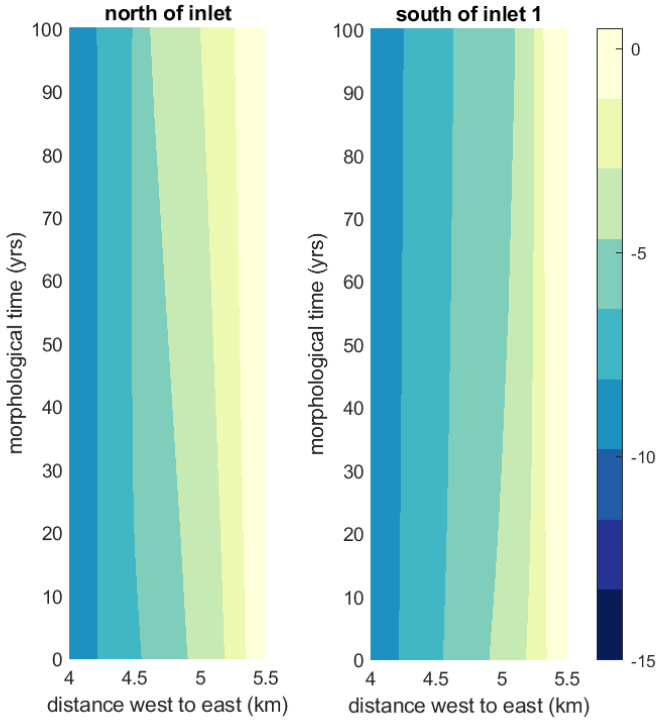

Figure 12, Bed elevation of cross-section through time, for scenario with no waves. Left: cross-section north of inlet, right: cross-section south of inlet.

3.2 Transport

Sediment transport in the model was measured through cross-shore transects (Figure 7 B). The transport was split between suspended load and bed load and the suspended load was found to be the largest fraction. For all the waves the suspended load and bed load transport are displayed separately and was further processed to represent average sediment transport per second. Figure 13 represent the suspended load and bed load transport, averaged for the two northern transects in panels A/B and for the southern transects in panels C/D. In Appendix B, more transport plots are available of the separate transports, and averaged transports of transects close to the inlet and far from the inlet. Figure 14 A/B shows the transport values in the same manner for higher waves, as these have a higher transport. Figure 14 C/D finally shows the net sediment flux between south and north of the inlet, this shows the amount of sediment that was trapped in the basin and the ETD.

We found that Suspended load transport was larger than the bed load component by a factor between 2 and 4. The sediment transport in most scenarios is northward through all transects, corresponding to the tidal propagation, with a few exceptions. We also see that the measured sediment transport north

of the inlet is lower than south of the inlet, and south of the inlet the sediment transport shows more fluctuations due to

Starting with the control runs, the scenario without waves shows the lowest transport of all scenarios as wave stirring does not occur here, however it is still clearly in northward direction. Furthermore, as the transport was averaged over a tidal cycle, the transport displayed for the no waves scenario in Figure 13 represents the residual sediment transport over a tidal cycle. We observed that the transport in this scenario is still affected by the morphology, as the value of northward transport is smallest for the transect just north of the inlet (Figure 13 A/B, Appendix B.I). Figure 12 shows that north of the inlet, more sediment deposition occurred on the shoreface, while south of the inlet the shoreface was more erosion dominated. This difference in transport between north and south of the inlet is shown in Figure 14 C/D and is also present in the other wave scenarios. It shows that the basin and ETD are a net sink of sediment as they build up in the model.

The scenario without tides has a wave of 1.2 m from SSW, so the longshore drift in this scenario is as expected to the north. This scenario shows a very average sediment transport compared to other scenarios, and both the suspended and bedload follow a similar path, only a different magnitude. It has a startup period and then, with some variations, stays on the same level for much of the run. What strikes is that south of the inlet Figure 13 C/D, the transport ramps up and then drops down a little two times during the run. We see that the infilling rate of the inlet fluctuates and the drop in sediment transport (Figure 14 C/D). This behavior of fluctuating infilling of the inlet was found in the animations but it does not reflect in other parameters.

The sediment transport for medium and high waves very clearly correspond to their wave direction and thus are less determined by the tidal propagation (Figure 14 A/B). The average sediment transport for these scenarios is in the direction of the wave propagation, for waves 5 and 6 (WSW) the transport is still northward but for waves 9 and 10 (WNW), the transport is to the south. For higher waves the transport is higher when the wave is higher, and it is less dependent on morphology. Wave 5 (2.53m WSW) and wave 10 (4.02m WNW) show higher transport than wave 9 (2.33m WNW) and wave 6 (3.96m WSW).

Low waves of ± 1m from shorenormal direction (W) also show a very regular sediment transport pattern. The average for both suspended and bedload transport behaves similar and is northward with a quick startup period and then slowly decreases over time with little fluctuations. South of the inlet (Figure 13 C/D) the fluctuations are a bit more visible as the southern barrier experiences more erosion than the northern barrier. This means that the “south 1” transect (Figure 7 B) is closer to the most morphologically active area of the model. The net influx of sediment to the ETD and basin is relatively low for this scenario as the amount of sediment transport north and south of the inlet are very similar (Figure 14 C/D).

Waves from a very oblique angle (NNW) show a very similar transport pattern to the shorenormal scenario, but with northward suspended load transport significantly higher south of the inlet than north of the inlet. This indicates that in the scenario with waves from NNW, more sediment stays between the measuring transects than with shorenormal waves, as shown in Figure 14 C/D.

The other low wave scenarios (± 1m) mostly show northward transport with exceptions found in wave 1 (SSW) and wave 8 (WNW). For wave 8 (WNW), the occurrence of southward transport (Figure 13 A/B)

can be attributed to the wave direction. Interestingly, this is only true for the transects north of the inlet. This scenario also records the highest transport values for suspended transport north of the inlet. South of the inlet (Figure 13 C/D), where incoming waves pass over the shallow ETD and they lose some of their energy, tides periodically become a relatively more important force of sediment transport. Here, the bed load transport is northward and suspended load shows fluctuations over time between northward and southward transport. This results in a relatively high flux of sediment to the basin and ETD, as sediment gets transported to the inlet from both sides (Figure 14 C/D).

Wave 1 (SSW) has the second highest suspended load transport south of the inlet (Figure 13 C), which can be contributed to the waves and tides pushing sediment in the same direction. This behavior is also seen for wave 4 (WSW), which records the highest northward suspended load transport both north and south of the inlet (Figure 13 A/C). These high transport values contribute to the relatively high flux of sediment to the basin and ETD (Figure 14 C/D). South of the inlet, these wave scenarios show a very irregular pattern in the transport data with large fluctuations. At 20 and later at 75 years, both suspended and bed load transport decrease for the SSW scenario, this is related to bed level changes of the ETD that affect this area of the coast (Figure 8 C/D). Bed load transport behaves very different for these scenarios, with waves from SSW showing southward transport north of the inlet that increases over time (Figure 13 B). Waves from WSW show a similar pattern for bed load transport, but it starts with relatively high northward transport values that decrease over time and eventually reaches net southward transport. This also contributes to net influx of sediment to the basin and ETD (Figure 14 C/D).

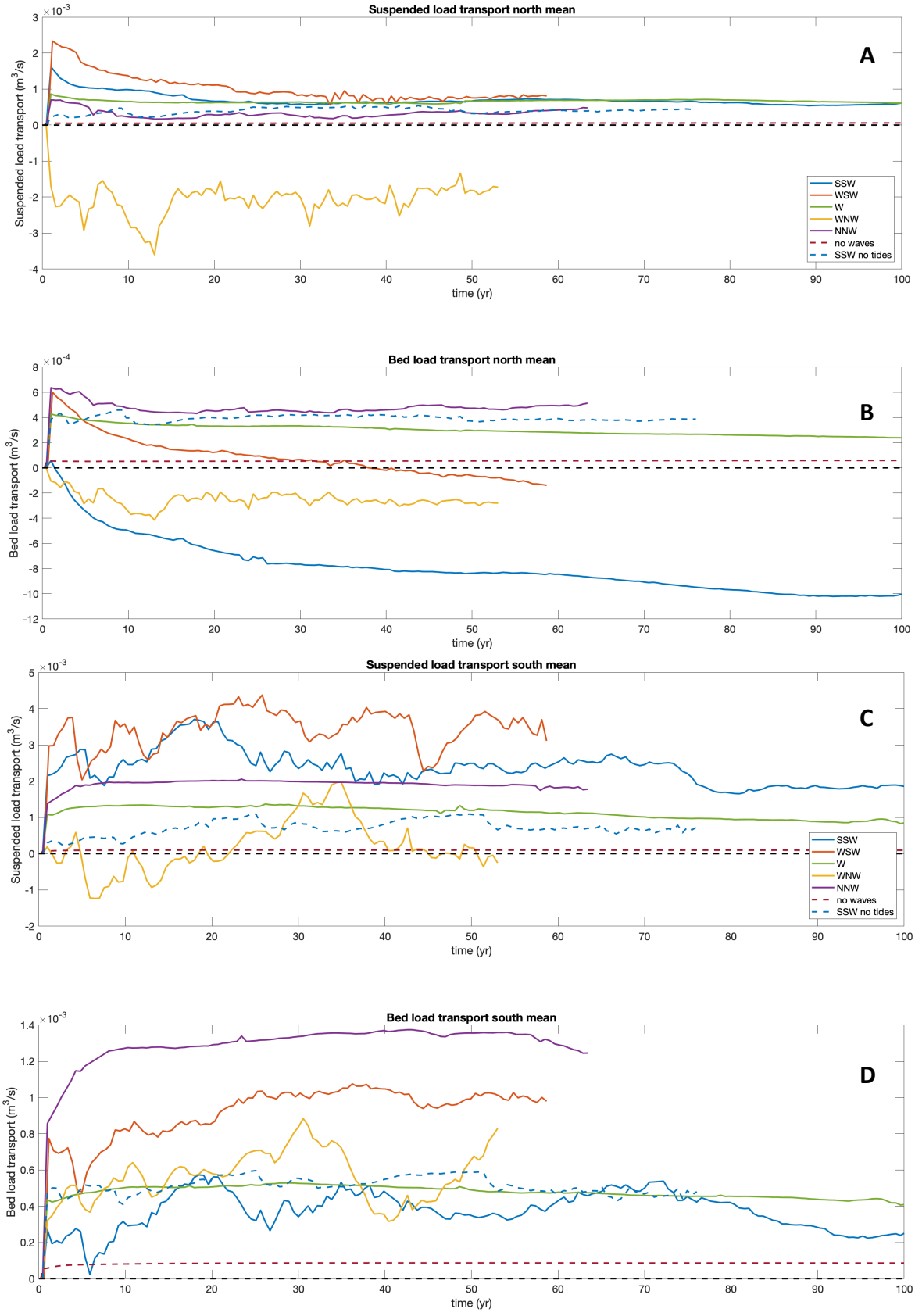

Figure 13, suspended load transport and bed load transport

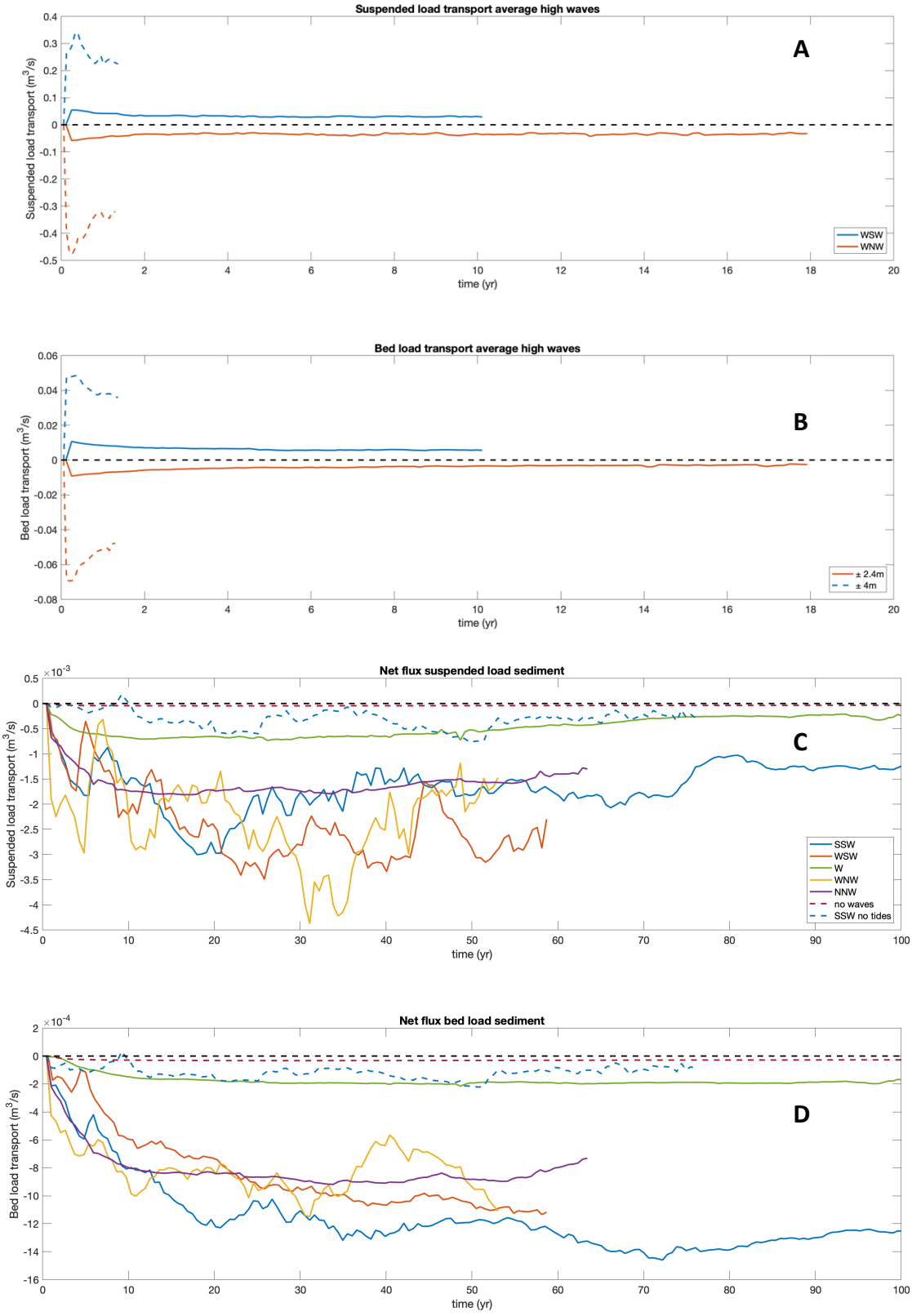

Figure 14, A and B, average suspended load and bed load transport for high waves scenarios, C and D; net flux from south to north, negative values represent trapped sediment in between the measuring transects.

3.3 Parameter analysis

To better understand what the effect of the different wave characteristics, such as angle of incidence or wave height, is on the tidal inlet morphology we analyzed different parameters. These parameters concern the tidal prism, cross-sectional area, and basin infilling rate, ETD volume. The tidal prism and cross-sectional area of the inlet are interconnected because the amount of water that flows through the inlet is restricted by the cross-sectional area, while the amount of water flowing through the inlet changes the inlet morphology and thereby the cross-sectional area. The development of the tidal prism indicates the strength of the tidal currents that, together with the alongshore sediment transport, play an important role in the formation of an ETD and the infilling of the basin. In this chapter we will analyze these parameters to find if the connections between them differ between different wave characteristics.

3.3.1 Tidal prism

The tidal prism (Figure 15 A) initially reduces for all scenarios after which the scenarios behave differently depending on wave height and direction. The tidal prism in the wave climate scenario keeps decreasing steadily throughout the model run, because although the channels in the front develop to distribute the water more efficiently through the basin this gets balanced by channel confinement and the increase of supratidal areas.

For high and medium ($\pm$ 4m and $\pm$ 2.4m respectively) wave scenarios the tidal prism decreases quickly because the inlet gets confined drastically and closes off completely for the high waves. For the low waves, the initial decrease of tidal prism (Figure 15 A) relates to the lack of channels distributing the water into the basin early in the model run. The influx of sediment also plays a role in the reduction of tidal prism, but this is the case more so later in the model run. We see that very oblique waves and the control scenario without waves have the largest reduction of tidal prism, while the opposite is true for waves that are closer to shore normal. After the initial decrease, the tidal prism for low waves shows a stable or increasing trend. This increase is caused by the widening of the inlet channel and the subsequent washing out of the supratidal areas in the front of the basin (Figure 8 D/E). The time at which the channel starts to widen and when washing out of the front of the basin (Figure 8 D/E) starts determines the start of the increasing trend of the tidal prism.

For wave 7 (W), we see a transition to increasing tidal prism at around 12 years, while wave 1 (SSW) has this transition around 70 years. This corresponds to the full bathymetry time series for wave 7 (Appendix A.I), where the inlet widening is visible at 20 years, while for wave 1 starts much later at 60 years. The tidal prism for the scenario without waves follows a similar profile as the wave climate as here, the tidal prism decreases initially because of the formation of a flood delta obstructing flow. Later, as channels in the basin develop further, the decrease continues but the rate at which the tidal prism decreases slows down. The basin infilling continues however, and with this the growing supratidal areas continue to decrease the tidal prism. For the wave climate scenario, the initial decrease of tidal prism is caused by the same mechanisms as described above, but the continued decrease can be attributed to the narrow channel later in the run.

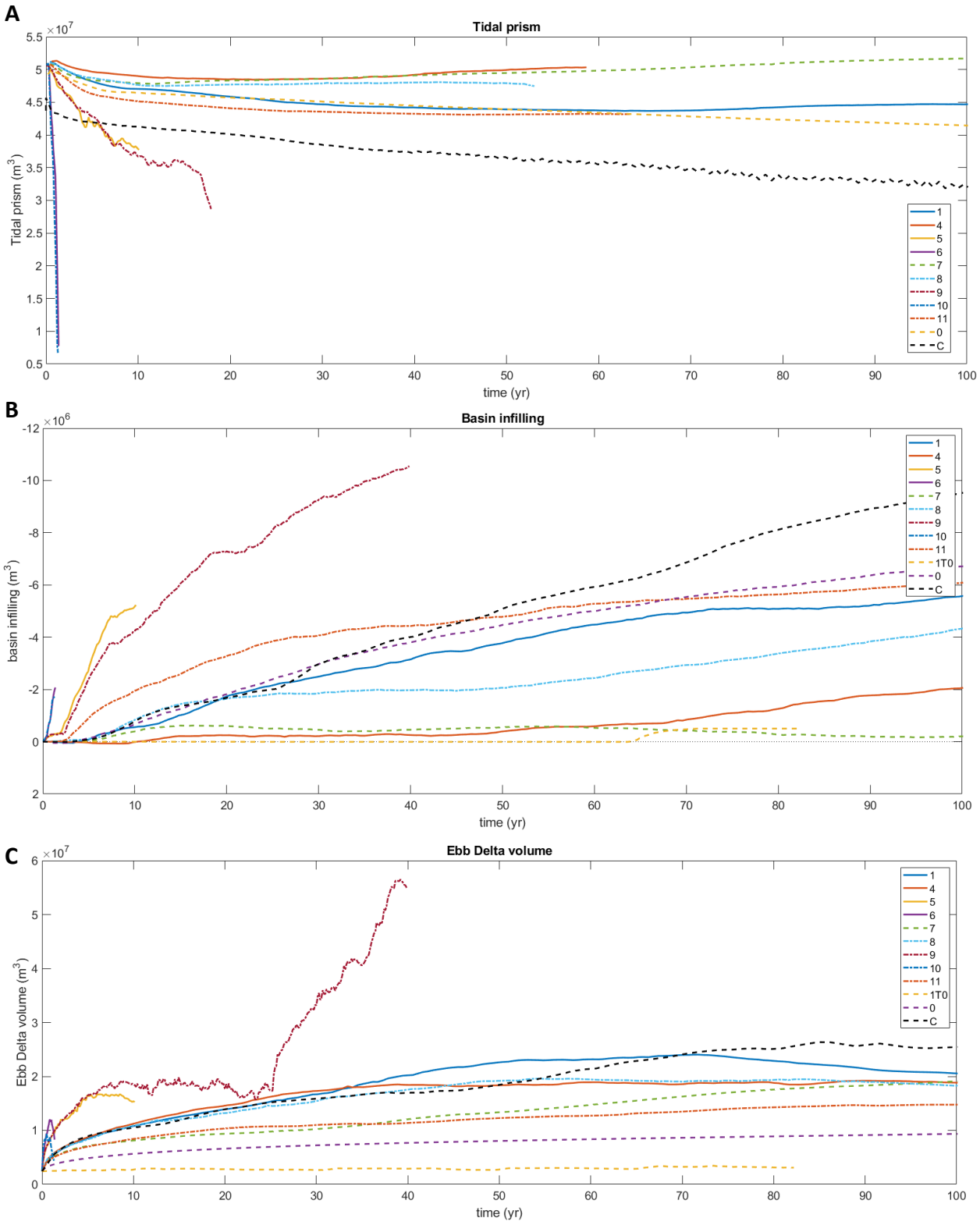

Figure 15, A: tidal prism over time for each wave scenario, B: basin infilling over time for each wave scenario, C: ebb- tidal delta volume over time for each wave scenario. The solid lines represent waves from SW, dashed dotted lines are waves from NW and dashed lines are other waves (control runs 0 and 1T0, shore normal 7, and wave climate C)

3.3.2 Basin infilling rate

The basin infilling rate (Figure 15 B) is the negative of the accommodation space and shows how much sediment is brought into the basin. The basin development for most scenarios starts with deepening of the inlet and development of channels. This is paired with a slight increase of the accommodation space followed by gradually infilling of the basin. The control scenario without tides shows that virtually no sediment is brought into the basin and the basin infilling only increases when the landward part of the inlet gets filled in.

Figure 15 shows that the basin gradually fills in over time all scenarios with the rate of the basin infilling differing for different wave heights. For high wave scenarios (Figure 15 B, wave 5, 6, 9, 10), the wave driven alongshore drift that feeds the transport into the basin is larger and therefore the rate with which the basin fills in is also larger. The other scenarios show a different behavior regarding the basin infilling, the basin volume stabilizes after a certain amount of time (Figure 15 B). The wave climate scenario again shows different behavior as the basin infilling continues presumably because of the presence of higher waves, a higher alongshore transport is present feeding sediment into the basin.

The stabilization of the basin infilling in low wave scenarios is indirectly caused by the erosion on the downdrift barrier, as the inlet does not close from the updrift side. This mechanism forms a very wide shallow inlet channel, leaving the basin behind the inlet vulnerable to wave erosion. The most striking example of this erosion process is wave 4 (WSW) at 100 years (Figure 9 A/B), where the basin is relatively deep for a large area behind the inlet. This erosion counters the infilling of the rest of the basin, resulting in stagnation of the overall infilling (Figure 15 B). Wave direction makes a lot of difference here for the low wave scenarios.

Wave 1 (SSW) behaves most similarly to the wave climate until the washing out of the basin occurs. Wave 11, from NNW, starts filling in rapidly (Figure 15) but this stops at around 30 years, when the inlet gets wider and erosion of the front of the basin begins. The scenario of wave 4, from WSW, seems to favor formation of the ETD (Figure 15) in the early stages, as a result of which the sediment flux towards the basin is smaller (Figure 15), the basin infilling then gets countered by widening of the inlet. Wave 7 (shorenormal), experiences similar progression of basin infilling as wave 4, but the ETD builds up slower, wave 8 is similar to wave 11, but more of the sediment goes to the ETD.

3.3.3 Ebb tidal delta volume

In the initial setup of the model run, the ETD is not yet present, so the sediment to build up the ETD comes from elsewhere. The buildup of the ETD is fed by sediment exported from the basin or from sediment captured from the alongshore drift which is then exported by tidal currents. Figure 15 C shows the volume of the ETD through time for each wave scenario. In general, the ETD volume for the wave climate and most low waves follow a similar progression, the buildup rate starts quick and slows down at around 10 years. The ETD for high wave scenarios builds up much quicker, as higher wave energy cause more sediment availability.

The control runs show the lowest values for ETD volume, in the scenario without tides there are no tidal currents that push sediment seaward, resulting in no ETD development. For the scenario without waves, the ETD does grow, but as there is very little alongshore transport to feed both the basin infilling and the ETD, the basin infilling gets favored over ETD buildup.

The low wave scenarios gradually build up the ETD to between 15 million and 20 million m^3 and for the wave climate this rises to 25 million m^3. The smaller ETD at 100 years for the low waves are a result of smaller alongshore transport rates and widening of the inlet, this reduces velocity and transport capacity of the tidal current. The subsequent washing out of the front of the basin, as described before, also affects the ETD volume. This stands out the most for wave 1, where the ETD volume decreases after 70 years.

The low wave runs show differences per direction, the ETD at wave 8 (WNW) follows the progression of the wave climate until 50 years when the ETD buildup stagnates, and the volume remains 20 million m^3 until the end of the run. The ETD at waves 1 and 4 (SSW and WSW) grows slightly quicker than the wave climate and other low waves early in the model run (between 10 and 40 years). This is a result of the northern margin bar gets more developed for waves from the south, the northern margin bar lies more seaward in deeper water and therefore it needs to accumulate more sediment to reach the same water depth as a more landward bar. For wave 11 the opposite mechanism is in play, as well as that the maximum seaward extent of the ETD at 20 years is some 500 m more landward than in the other low wave scenarios. Wave 7 (shore normal), as previously discussed, behaves in some respects similar to the scenario without waves in the beginning of the model. The ETD for wave 7 however, does develop and slowly reaches 20 million m^3 like other low wave scenarios.

The higher waves have a larger rate of building up the ETD at the start of the run. The ETD volume for medium waves (± 2.4m) stabilizes at slightly below 20 million m^3 at 5 years, showing a relation between the basin size and the ETD volume. For wave 9 (2.33m WNW), the ETD grows again after 25 years, but this is due to the growth of a sandbar further seaward which is not connected to the ETD and may be a result of the fast-moving inlet and shoreface steepening in the model. The high wave scenarios (± 4m) have a quick buildup of the ETD and then peak between 0.5 and 1 year after which the inlet closes and the large wave energy washes away the features of the ETD.

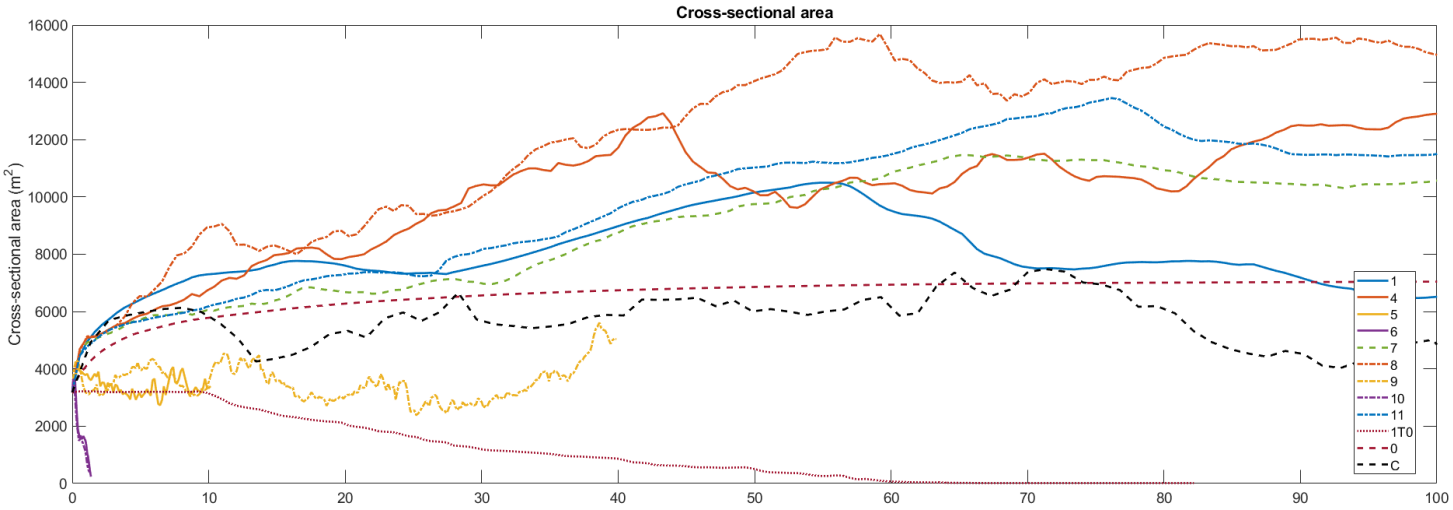

Figure 16, cross-sectional area over time for each wave scenario. The solid lines represent waves from SW, dashed dotted lines are waves from NW and dashed lines are other waves (control runs 0 and 1T0, shore normal 7, and wave climate C)

3.3.4 Cross-sectional area of the inlet

The cross-sectional area of the inlet channel (in this paragraph abbreviated to XA) is measured parallel to the coast and starts in the initial bathymetry at 3600m^2 (Figure 16). The XA grows as tides that flow in and out of the basin remove sediment from the channel. This can be seen in the scenario without waves, where the XA grows logarithmically as this system gradually moves to an equilibrium state.

This growth of XA happens initially for all scenarios, but as higher waves show significantly higher longshore transport (Figure 14), the infilling of the inlet channel quickly dominates over the tides that keep the inlet open. For high waves (± 4m), the inlet quickly fills in completely, and for medium waves (± 2.4m) the inlet channel stays open but gets narrow and deep (Figure 10 A to D), thereby having a fluctuating XA around the original 3600m^2. The control run without tides also shows the inlet being filled in gradually. This is because there are no tidal currents that remove sand from the inlet while the longshore transport keeps bringing in sediment.

All the other scenarios see their XA grow over time, compared to the run without waves, the addition of waves in these model runs cause the XA to grow faster in the beginning. As was described in 3.1.1, the low wave scenarios (± 1m) all start out with a deepening inlet channel and after a certain amount of time, the channel starts to widen (bed levels for every ten years can be found for each scenario in Appendix A). The deepening and subsequent widening of the inlet channel both increases the XA for all low wave scenarios (Figure 16).

What we see for the low wave scenarios is that as the basin inlet gets wider, a deep channel remains present. For wave 7 (W) and wave 11 (NNW), the deep part of the inlet is situated in the same place as the initial deep channel that formed in the beginning of the model run (Figure 9 C/D for wave 7 and G/H for wave 11). These remnants of the initial channel contribute greatly to the XA and can be attributed to the sediment transport being dominated by the tidal currents which focuses deposition to the ETD and basin. These remnants are also seen in waves 1, 4 and 8, but in lesser extent as the initial deep channel gets buried quickly by the moving of the barriers with the inlet during the first phase of the model. The wave climate scenario shows a different behavior (Figure 16 wave C). The XA first rapidly increases through deepening of the channel, similar to low wave scenarios (Figure 16 wave 1, 4, 7, 8 and 11).

After becoming deeper, the wave climate scenario shows that the channel gets confined (Figure 4 B to K) and the XA decreases after 10 years. Between 20 and 80 years, the XA for this scenario stabilizes and fluctuates around the same value as the control run without waves. No further correlation is found here, besides the tidal prism that shows a very similar downward trend for both these scenarios. Over time, the wave climate scenario shows that the inlet moves southwards and changes its orientation from east-west to southeast-northwest. During this process, the northern barrier grows behind the southern barrier and after ± 80 years, the northern barrier broadens and confines the channel over more of the cross-shore direction (Figure 4 I to K). This last part of the model run is characterized by a decrease in XA (Figure 16).

3.4 Cyclic behavior in wave climate scenario

As discussed in **Error! Reference source not found.**, the wave climate scenario from Boechat Albernaz et al. (2023) shows cyclic behavior where the ETD switches between a single and double channel configuration. Where first, between 20 and 30 years, this scenario showed behavior of shoal growth out on the ETD, that then gets breached by the channel and the shoal slowly migrates to the coast. Figure 17

A shows a time series of the wave climate scenario zoomed in on the ETD from 55 to 78 years. This shows another type of cyclic behavior where shoals started forming at the inlet that then travel outwards along the southern channel until eventually attaching to the coast. The ETD shifted to a configuration with two permanently present channels, with the northern channel being shielded by a shoal on the outer edge of the ETD. The southern channel shows the most morphologic activity, as this channel itself switched between a single and double channel configuration. This cyclic behavior has a period of between 5 and 10 years, depending on what counts as a whole cycle.

This behavior started from 40 years on, and the first cycle had a transitional pattern. The first cycle, from 40 to 55 years, had a shoal that started near the inlet mouth and then connects to a margin bar from the north side of the channel. The later cycles behaved more like depicted in Figure 17 A, they showed oscillating shoals that formed as a blob near the inlet along the southern channel and then rapidly moved along the southern channel margin over the ETD. This rapid movement along the channel margin is associated with a new channel forming. This new channel then slowly merges with the previously existing southern channel. On the outer ETD, the shoal slows down and moves gradually towards the shore, if two cycles follow each other up closely, the shoals of both cycles merge before attaching to the shore. Figure 17 A shows two cycles of the buildup of the shoal near the inlet and subsequent rapid moving of the shoal, one between 55 and 61 years, and one between 73 and 77 years.

During the images of 65 to 70 years, two more buildup phases occured, where just a part of the shoal moves along the southern channel margin and no channel formed. These half cycles are detected in the time stack (Figure 17 B), as well as in animations. In the time stack (Figure 17 B), the bed level of a cross-section south of the inlet is displayed through time. From 1 to 10 years, the ETD and the main ebb channel forming, and as the inlet starts moving southward and starts rotating, the ETD grows further seaward (15 to 25 years). From 25 years on, the outer bar on the ETD gets lower which corresponds to the ebb channel breaching as described earlier. Also at 25 years, the shoal on the landward (south) side of the channel starts to develop, which then from 40 years on becomes the main source of cyclic behavior.

The cyclic behavior we described was not observed in the analyzed parameters discussed in 3.3. For all low wave runs and the wave climate scenario, tidal prism, ETD volume, and basin infilling showed relatively steady increase or decrease, while the cross-sectional area showed too many fluctuations to correlate to the cyclic behavior. These fluctuations might correlate the formation of shoals in or around the inlet, but that would be somewhat arbitrary. For the single wave runs, the fluctuations in cross-sectional area are as much present as for the wave climate scenario, but they do not show large scale cyclic patterns in the bed level that are associated with sediment bypassing processes.

Specific behavior that can be observed is for low waves 4 and 8 from WSW and WNW respectively (Figure 18). Here we see periodically forming shoals, that in the animation are observed to form on the margin of the inlet at the barrier that erodes by the waves. This behavior looks like the blob like shoals forming on the barrier that erodes as shown in Figure 17 A. For wave 8, this behavior is only present early in the run while for wave 4 (WSW), this happens later in the run, when the inlet is very wide and the forming shoals originate from within the basin, as erosion washes out the front of the basin. This similarity shows that this behavior is more driven by erosion of the erosional barrier than sediment bypassing processes related to the ETD.

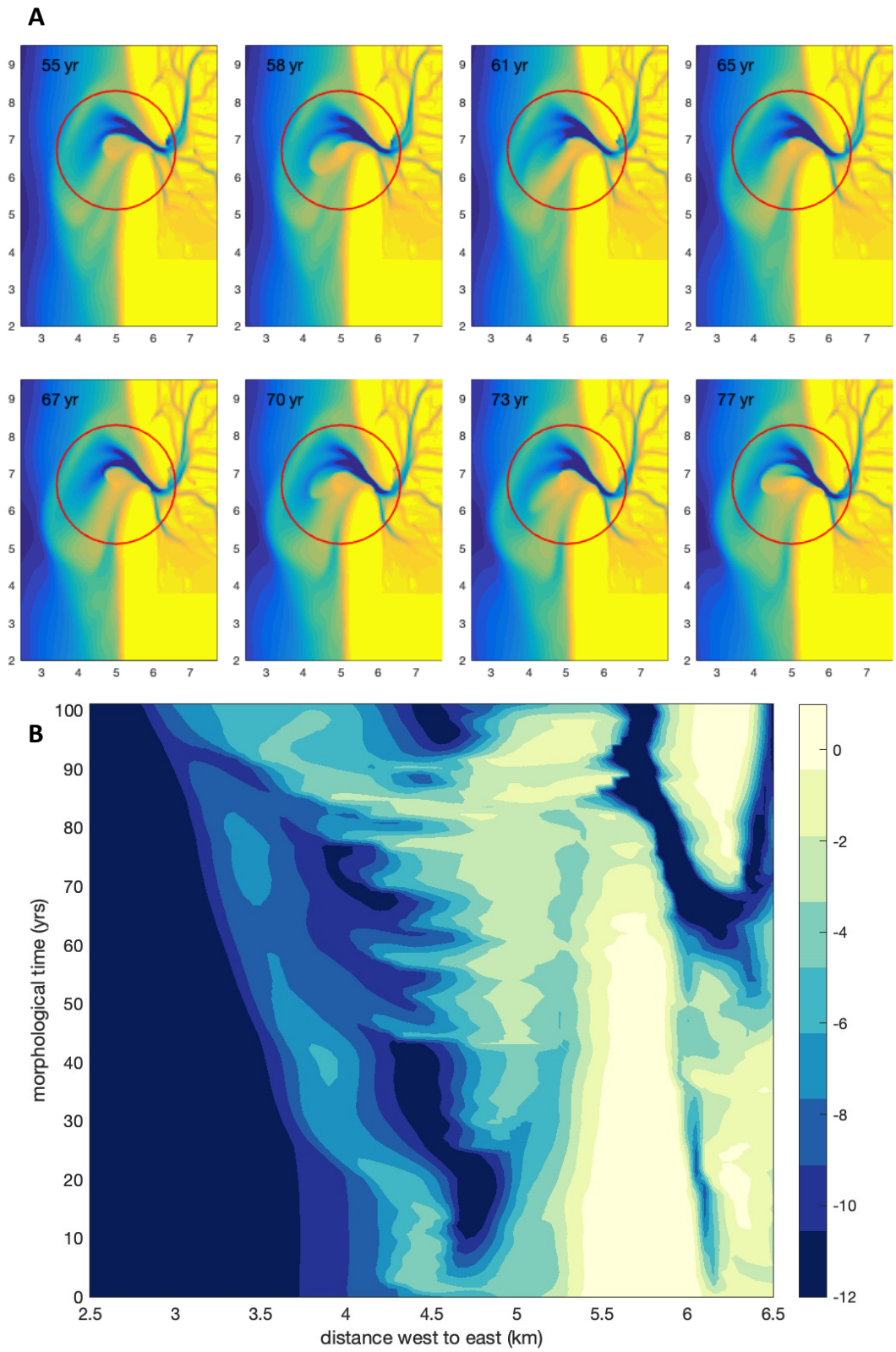

Figure 17, A; detailed view of the bed level of the wave climate scenario through time. Every three years, zoomed in on the inlet and ebb tidal delta. B; time stack of the water depth of a cross shore cross-section south of the inlet for the wave climate scenario.

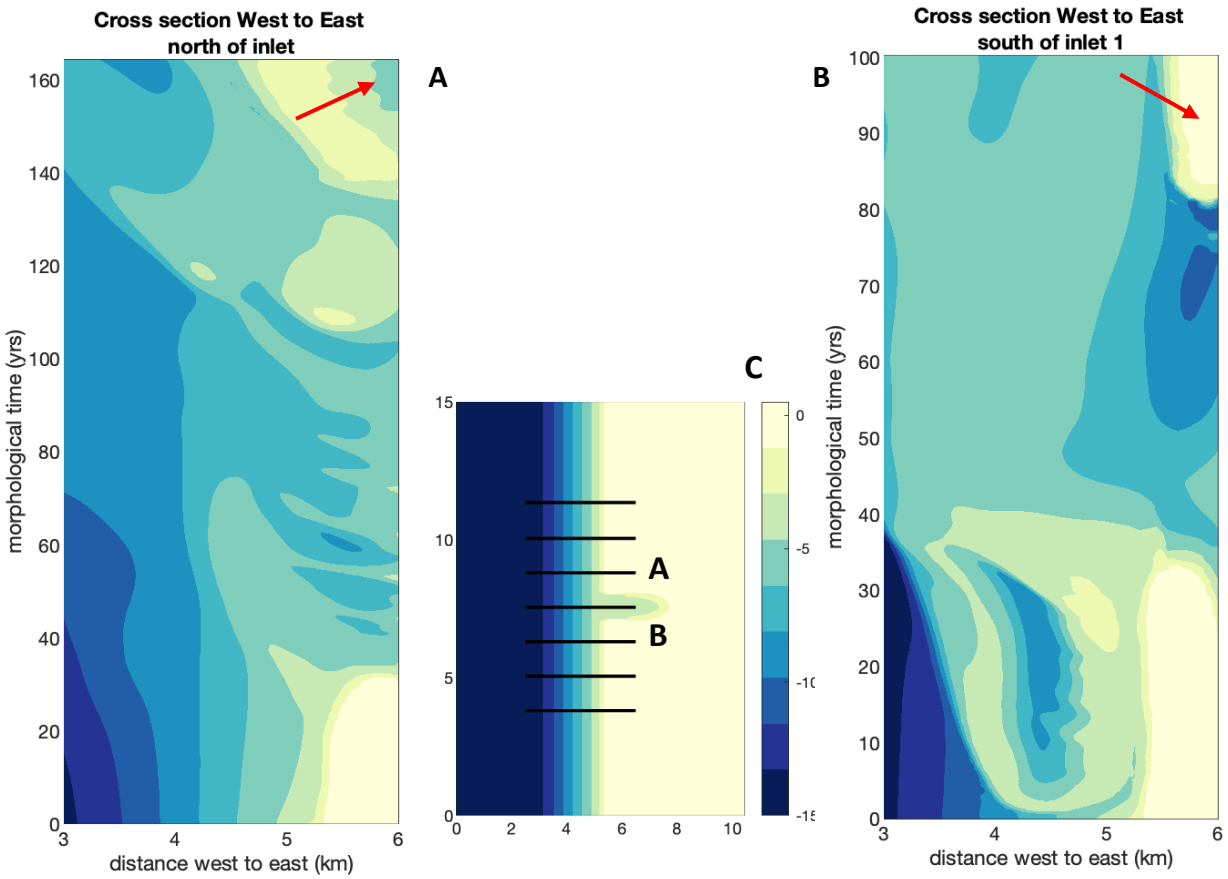

Figure 18, A: time stack of the water depth of a cross shore cross-section north of the inlet for a wave of ± 1m from WSW. B: time stack of the water depth of a cross shore cross-section north of the inlet for a wave of ± 1m from WNW. C: location of cross section. Red arrow indicates wave direction.

3.5 Findings

Height classes	Ebb channel orientation	Inlet width over time	Inlet stability/ location	Tidal prism	Basin infilling	ETD volume growth	X-sectional area	Alongshore transport	Sediment flux to basin and ETD
Wave climate	Southwest	Confines	Moves slowly south	Slow decrease	Gradual	Gradual and largest	Relatively constant	No data	No data
Low (± 1m)	Southwest	Widening	Moves slow with wave direction	Stable or increase	Stabilizes	Slow	Widening	Small northward	Small
Medium (± 2.4m)	South or shore normal	Confines quickly	Moves with wave direction	Decrease	Quick	Quick	Confines quickly	Large wave driven transport	Large
High (± 4m)	With wave direction	Fills in quickly	Moves very quick with wave direction	Quick decrease	Quick	Quick but erodes	Fills in quickly	Largest wave driven transport	Largest
No waves	No outer channel	Steady	No movement	Slow decrease	Slow	No visible morphology	Steady	Very small northward	Very small but most towards basin
No tides (± 1m)	No outer channel	Fills in	No movement	No tidal prism	No infilling	No ETD	Fills in	Small in wave direction	Very small
Direction classes	Comparing low waves relative to each other.								
NNW (330)	Most shore normal	Above average	Moves slowly south	Slow decrease	Quicker	Slowest	Average	More bedload	Low average
WNW (296)	Southwest	Above average	Moves quickly south	Stable	Slower	Gradual	Widens but remains deep	Wave driven southward transport present, north of inlet	Influx from both directions
W (270) (Shore normal)	Southwest	Above average	No movement	Stable to increase	Slow	Slow but gradual	Widens and develops two channels	Lower than average south of inlet	Very small
WSW (250)	South	Above average	Moves quickly north	Stable to increase	Slower	Gradual	Above average	Large in northward direction	Largest transport causes large influx
SSW (200)	South	Slower widening	Moves slowly north	Decrease but stabilizes	Stabilizes	Quick but erodes	Slow widening and shallow	Tide driven southward bed load transport present, north of inlet	Average, with largest bedload influx

Table 1, qualitative analysis of the progression of different parameters throughout the run per wave class. Color scale represents the relative amount, with blue to white to red representing low to average to high.

Table 1 gives an overview of the progression of the different parameters for each of the wave classes as defined in 2.1.2. This gives us a qualitative insight in how these parameters interact, in the upper section of the table, the wave height classes are compared to each other, as well as the control runs. In the lower section we looked at the differences between each wave direction, these scenarios were executed for low waves.

While a balance between waves and tides is needed to create an active tidal inlet system, the presence of tides is essential. The control scenario without tides experiences alongshore drift that is purely wave driven, and the sediment that is moved through in this model gets distributed evenly along the coast. No exchange with the basin results in no infilling of the basin, as well as no formation of an ETD. The inlet, as the sole unevenness in the initial bathymetry, slowly closes off, while most sediment continues to move updrift. In the scenario without waves, sediment transport is overall very low due to a lack of wave stirring. This results in low sediment availability, and we found that this was mostly directed by the tides into the basin. In the basin there was a lot of morphological activity, but our ETD volume shows there was only a small volume increase in seaward from the inlet (Figure 15 B/C).

Waves and tides are both an important factors in driving alongshore transport and removing one of these will drastically lower sediment supply needed for both the basin infilling and the buildup of an ETD. Meanwhile tidal are a driving force in the both alongshore and cross-shore transport of sediment, they play an important role in the exchange of sediment between the basin and the sea, and tides transport sediment in cross shore direction onto the ETD. Removing tides from the system this cross-shore redistribution of sediment will stop, and the inlet channel will fill in. The magnitude of the alongshore transport is dependent on wave angle and with increasing wave height increasingly more dependent on wave height. This drives the sediment availability for the tidal inlet system, where tidal currents act on the sediment balance by keeping the inlet open and transporting this sediment into the basin and in cross-shore direction out onto the ETD. Higher waves have more sediment availability, and when tides remain unchanged the morphological balance results in more narrow inlets until the alongshore transport closes off the inlet, this is shown Table 1 for medium and high waves. For high waves, $\pm$ 4m waves, the balance crossed a threshold at which the tides are too weak to keep the inlet open.

The alongshore sediment transport, as seen in Table 1, is largest for less oblique wave angles and both shore normal and very oblique wave angles show smaller alongshore transport. When wave driven alongshore transport becomes the dominant force through increasing wave energy and optimal wave angle, the wave angle also determines the direction of the alongshore transport.

Waves function as an erosional force as well, where the inlet gets filled in from updrift, the downdrift barrier erodes away. Wave angle and wave energy determine the stability of the inlet, the inlet channel therefore moves in the direction with the waves (Table 1). What strikes is that in the low wave scenarios, after a certain amount of time, the inlet channel starts to widen which does not happen in other scenarios. This causes tidal prism to rise in the later stages and it counters basin infilling and ETD growth as the front of the basin washes out. Evidence for what is causing this was not found.

The wave climate scenario is an intrinsic balance between all waves where different wave heights and directions result in a moderate progression of the parameters included in Table 1. The inlet slowly narrows but stays open and it moves slowly in the direction of the average wave energy. The ETD

development is most active in this scenario and basin infilling and tidal prism are and remain interconnected because of the constant cross-sectional area.

The wave direction was found to make a difference predominantly on the inlet stability, as alongshore transport is largest for slightly oblique angles of incidence. At more oblique angles the inlet moves slower in downdrift direction and with shore normal waves, the inlet widening happens on both barriers. For a low wave from SSW direction, it was found that the ETD volume develops more in the early phases of the model and this, together with lower alongshore transport causes the channel to start widening later in the run. On the opposite, waves from NNW direction cause the ETD to remain very short in cross-shore direction and this favors basin infilling and decrease of the tidal prism.

Another pattern shown in Table 1 is the difference between wave direction is from the same direction as the tidal propagation or opposite to this. The ebb channel orientation is towards southwest for most scenarios. For high waves from the south, the waves push against the front of the ETD and the channel to the north, rotating the channel. For medium waves from the south (Figure 10 A), the channel does not rotate fully northward, but remains more shore normal. Later in the run (Figure 10 B), the channel orientation rotated further southward. For low wave scenarios, we see that waves from the south cause the ebb channel to have a more southward orientation. Shore normal and waves from the north retain the southwestern orientation of the ebb channel. We found that if tides are relatively more important in determining the ebb channel orientation, the channel lies closer along the coast for waves that come in opposite to the ebb flow resulting in a more southward orientation.

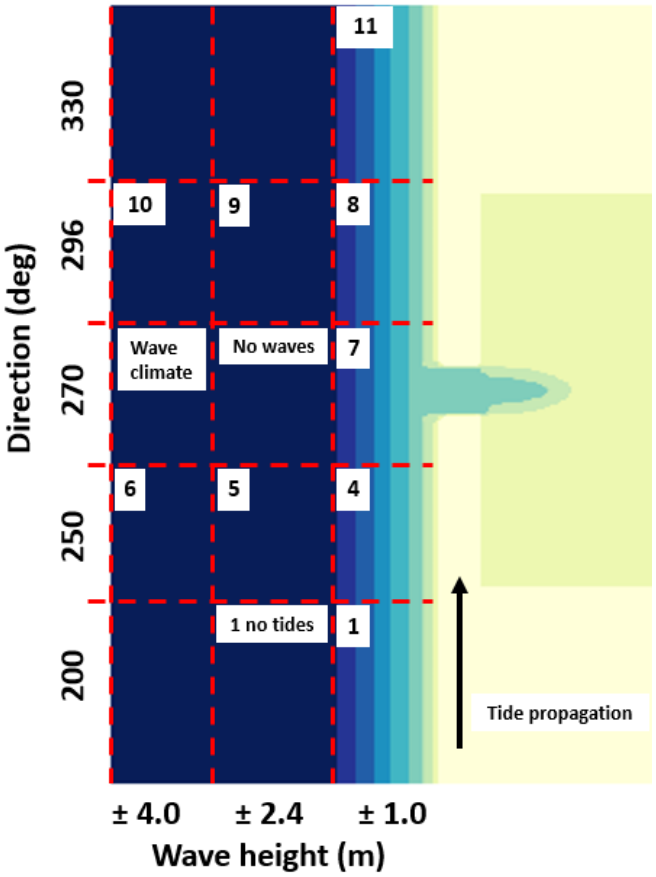

Figure 19, visual representation of wave classes.

4 Discussion

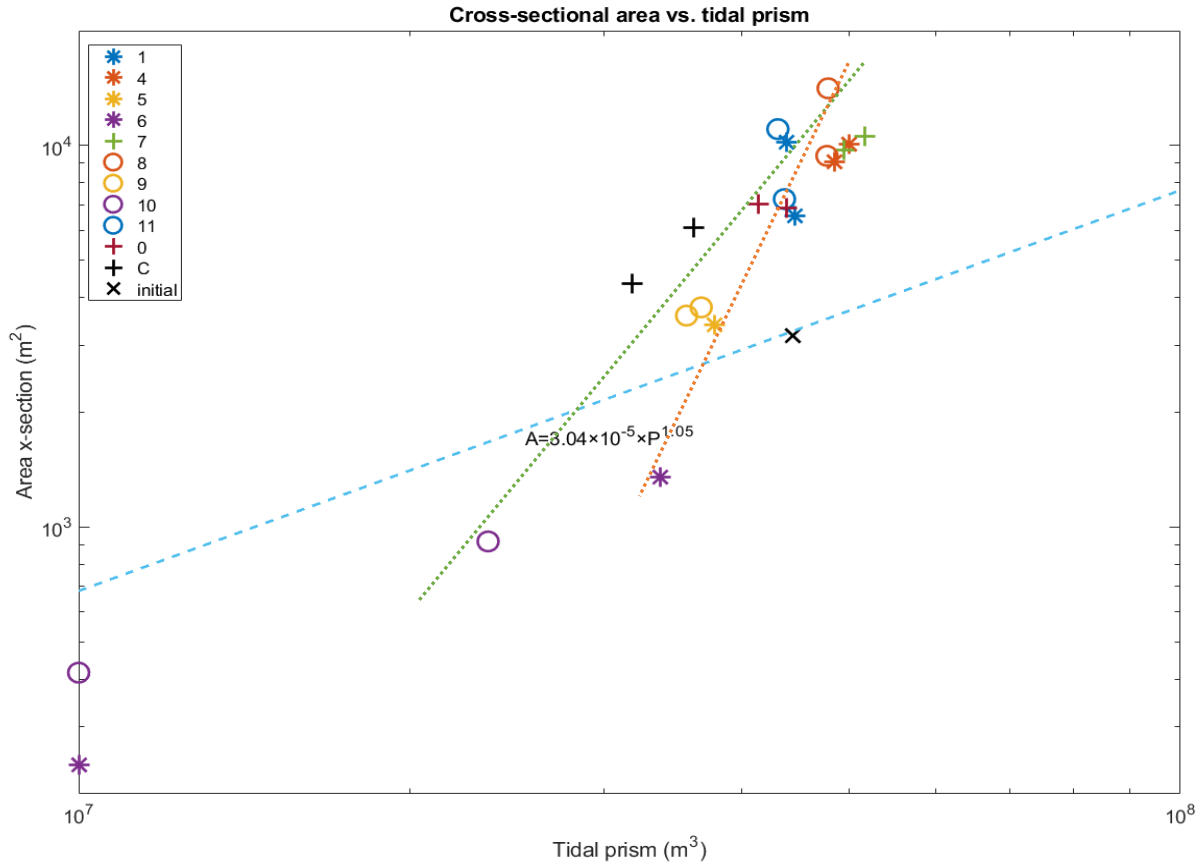

*Figure 20, Plot of cross-sectional area as a function of tidal prism for all model runs. * represent waves with a SW angle, O represent waves from NW, + respresent the control run (0), wave climate (C) and shore normal wave runs (7). Dashed line is the empirical relationship Equation 2* (O'Brien, 1969).

4.1 Model prediction and empirical theory

The tidal prism and cross-sectional area of the inlet are intrinsically linked through the amount of water that flows through the inlet. Previous research stated that in these complex inlet systems with multiscale feedbacks, the empirical relations such as Equation 2 are insufficient to predict long-term evolution of tidal inlet systems (Boechat Albernaz et al.). Most empirical relationships on inlet cross-section vs tidal prism are based on a relatively small dataset with specific characteristics (Leuven et al., 2018).

Figure 20 shows the cross-sectional area as a function of tidal prism together with the empirical relation Equation 2 (O'Brien, 1969). This shows that the empirical relation mostly underpredicts the cross-sectional area using only tidal prism as variable. This and other empirical relationships follow a similar structure and were found to follow a very different trend (Boechat Albernaz et al., 2023; Leuven et al., 2018). In most presented relationships, both parameters increase almost in a 1 to 1 ratio, while our data show an overall ratio of 1 to 5, with an increase of cross-sectional area of an order of magnitude for a tidal prism increase of a factor 2. Overall, we see that higher waves have a lower cross-sectional area and tidal prism, as high waves (in purple), sit below, and medium waves (in yellow), above but close to, the line of Equation 2. The model runs represented by (**+**) seem to have a trend closer to Equation 2, but

this is a mere coincidence as these runs are unrelated to each other representing the control run without waves, a model with shore normal waves and the wave climate. The data points of the wave climate are skewed by a different measurement of the tidal prism and tidal prism values are lower by some 5 million m^3. Waves from the southwest (*****) cause a steeper trend than waves from the northwest (**O**) which relates to the direction of tidal propagation.

Our results show that to predict the dimensions and systemic connections between different morphological parts of the barrier coast, a more complete model of the specific barrier coast is necessary.

4.2 Main findings of the model

The main finding in this research is that a tidal inlet system with a single wave does not behave in the same manner than when a whole wave climate acts on the same system. The differences were found to lie mainly in inlet stability, as with a single wave with higher energy, the inlet moves rapidly with the direction of the waves. With a wave climate with waves from multiple directions, there are waves from both sides pushing on the inlet, reducing the rate with which the inlet moves in one direction. There is still a dominant wave direction, southward in our model, but the movement of the inlet is greatly reduced compared to single wave scenarios. Unfortunately, the sediment transport data from the wave climate run was not available, and therefore we could not compare this to the single wave runs (Boechat Albernaz et al., 2023). We tried to work around this by estimating the relative amount of sediment transport through looking at the rate of morphological changes of the wave climate scenario, compared to our single wave runs with different conditions.

The sediment transport in most scenarios was northward for all measured transects, this is because the direction of alongshore transport for low waves was mostly determined by the tidal currents. We found exceptions on this northward transport for high and medium waves from NW, because the wave driven component of alongshore transport dominates in these scenarios. For low wave scenarios, southward transport was found for the transects north of the inlet for waves from WNW, WSW, and SSW. The WNW scenario can be intuitively explained as north of the inlet, the tidal currents are obstructed by the ETD and thus have a smaller influence on the alongshore transport while waves from WNW are not obstructed north of the inlet. This results in an average transport in southward direction for the WNW scenario. The southward transport in the scenarios with waves from WSW and SSW is only found for bed load transport and is therefore relatively small. It is however, counterintuitive to find southward transport in these scenarios as the wave driven and tide driven alongshore transport are both northward along most of the coast. This behavior could be a result of an eddy current that forms as the tidal current flows along the ETD and flow separation occurs. This has been found at protruding coastal features such as headlands but also occurs at protruding beach nourishments (Radermacher et al., 2017). The eddy current, together with reduced wave driven alongshore current north of the inlet, as waves are obstructed by the shoals of the ETD, could be an explanation for the southward transport present for waves from SW directions.

The presence of both lower and higher waves in the wave climate was found to help keep the inlet open. When a single wave reaches a threshold where tidal currents are relatively too weak to keep the inlet open, the inlet closes off completely. This happened in our scenarios for waves of ± 4m and when tides were turned off. In a wave climate, the presence of high waves for a short amount of time can make large morphological change to the ETD and inlet, while the lower waves that dominate the system

timewise keep the inlet open and stabilize the influence the large waves have (Bruneau et al., 2011; Ridderinkhof et al., 2016).

The cyclic behavior as observed in the results from the wave climate (Boechat Albernaz et al., 2023), in the form of ebb delta breaching (Fitzgerald et al., 2000), where the ebb channel on the ETD switches between single and double channel configurations by breaching a subtidal shoal. Was not found in any of the single wave scenarios. The other form of cyclic behavior described in our results consisted of shoals periodically forming very near to the inlet, which then moved along the downdrift margin of the channel out to the ETD. This mode of cyclic behavior was present in both the wave climate and single low waves at an angle of around 25 degrees to shore normal. This behavior was very cyclical but seems to correspond to periodical buildup of sediment that becomes available as the downdrift barrier erodes.

The erosional origin of this shoal formation shows that these cycles have a different origin than the sediment bypassing processes normally associated with tidal inlet systems (Fitzgerald et al., 2000; Lenstra et al., 2019b). When the shoal arrives at the ETD, the behavior of shoal migration does however behave in a very similar manner as described in(Ridderinkhof et al., 2016). We do not yet have an explanation as to how this mechanism where shoals form through sediment availability from erosional processes comes to be in the model and the stability of the inlet location should be improved upon.

The wave climate includes all the other wave scenarios that were run, and intuitively the sediment transport balance in a system with a wave climate should be in the middle of the single wave scenarios. The ETD growth and basin infilling are not very quick compared to high waves, and the ETD growth and basin infilling are larger than for low waves. The wave climate scenario showed to be the most in balance with the initial setup, the inlet channel confined a little bit but remained constant and active throughout the run. Higher waves closed the inlet off, and lower waves surprisingly made the inlet wider and shallower. Within the basin, for higher waves the width of the inlet constricts inflow reducing tidal prism which in turn reduces the rate of morphological development while in the low wave scenarios the tidal prism increased as the supratidal areas in the basin eroded away.

Wave direction mostly affects the alongshore transport rate, which is here found to influence the inlet stability. The inlet moved more quickly downdrift for waves from WNW and WSW and slower for very oblique waves from both the north and south. This is consistent with the maximum alongshore transport for waves with between 30 and 45 degrees angle of incidence (Bird, 2000). Another effect of wave direction on the tidal inlet system originates from the interaction of waves from the same direction or opposite to the tide propagation. In this study, due to phase differences in cross-shore and alongshore tidal currents, the ebb currents leave the inlet in the opposite direction as the tidal propagation resulting in the ebb channel and ETD to bend to the southwest. This means that waves from the south push against the front of the ETD and the channel to the north, rotating the channel. This mechanism also favors the formation of the seaward channel margin bar and terminal lobe of the ETD. Waves from the north push both the ETD and the channel more towards the shore, this effect is clearest for waves from NNW as this shortens the seaward reach of the channel and thereby the ETD volume is much smaller in this case. Sufficient wave energy that push against the ETD and its channel orientation can push them downdrift (Sha, 1990). This resulted in a downdrift oriented channel for the wave of ± 4m from WSW and for waves of ±2.4 m from WSW it was found that the shape of the ETD resembled sediment bypassing processes associated with wave dominated inlets (Fitzgerald et al., 2000).

The modelling limits we encountered during this study were related to the steepening and stability of the coast. Steepening of the coast causes unrealistic wave breaking properties and therefore unrealistic sediment transport. This was the case for higher waves, where the high wave energy results in transport rates that were not numerically possible. This was also encountered by (Lenstra K. J. H., 2020), who suggested the improved parameterization of the wave related bed transport (Albernaz et al., 2019) could improve these results. Another measure to improve model stability would be the usage of flexible mesh techniques (Symonds et al., n.d.), this reduces cell sizes in places where more precise calculations are necessary, such as right at the coast.

The only measure that was taken to improve model stability for the higher wave scenarios was decreasing the morfac (morphological acceleration factor), but this increased the modelling time by so much that a lowest morfac of 25 was chosen for 4m high waves. These model runs also showed that the inlet closed off quickly in the model as the wave driven alongshore transport outweighed the capacity of the tides to keep the inlet open. However, it would have been useful to have more stable results of the ± 2.4m wave runs with a lower morfac, the morfac of 50 produced a stable model only for one of the wave directions at this height and here the coast steepened as well. The morfac values of 25 and 50 for the higher waves are still very high as in literature the morfac is often as low as time allows, with a morfac of 20 being most frequent in relevant studies (Lenstra K. J. H., 2020; Ridderinkhof et al., 2016).

The long modelling times are in part due to the fact that each model run was started with an undisturbed morphology with a basin that was relatively deep and imported a lot of sediment. The importing of sediment limited how much sediment there was available for the ETD, and thereby the dynamic behavior of the ETD was also limited for all the runs. This spin up time can be limited by using a bathymetry of a run that has already imported a lot of sediment to the basin. The model without waves resulted in a bathymetry with a very developed basin and almost no morphology at the seaward side of the inlet, this could serve as a great starting point when researching the dynamics of the ETD.

4.3 Recommendations

The before mentioned shortcomings of this study have led to insights on how to improve future modelling studies. The deep basin that limited the sediment available for the ETD in these model runs could be improved upon by using a disturbed run where the basin infilling and channel formation have stabilized (Figure 15 B). The bathymetry of our model run without waves could be used for such a disturbed morphology model (Figure 21). At 50 years, this scenario has a developed basin morphology, and the basin infilling reached a value where most scenarios stabilized. If this bathymetry is used as a starting point the basin will not import as much sediment. This means the spin up time of the development of the ETD and tidal inlet can be shorter because less of the sediment availability is directed into the basin. This method can improve both modelling duration as our understanding of how a certain wave or set of waves act directly on a tidal inlet and what mode of sediment bypassing relates to certain waves.

This study used a selection of waves selected from the wave climate by (Boechat Albernaz et al., 2023). The waves from this wave climate proved to be too far apart in terms of wave height to see certain trends of when behavior of the system changes. For instance, the inlet with a wave of 2.4m WNW showed to be close to filling in, but the step to a wave of 4m from the same direction was far past the filling in threshold. The waves that are picked for future studies into the physical mechanisms of tidal inlet systems should be more evenly spread and could be based on inlet stability (Bruun & Gerritsen, 1960). Another interesting approach would be to model different wave climate conditions, as well as combining a parallel wave climate with storm events that run high waves for a short period of time in series (Ridderinkhof, de Swart, et al., 2016).

This research improved our understanding of how the tidal inlet systems behave in modelled settings, and how different wave conditions react to the same boundary conditions. We found some unknowns in our model such as the washing out phase in the low wave runs, and very unstable inlets for waves from 25 degrees to shore normal. Another focus in future modelling studies could be larger basins which have a larger tidal prism, and this makes the range within which the system is dynamic larger (Lenstra K. J. H., 2020). These types of models are being used to predict real tidal inlet systems in nature and future research should focus on both technical advancements in parameterization and how to better relate these models to these real tidal inlet systems.

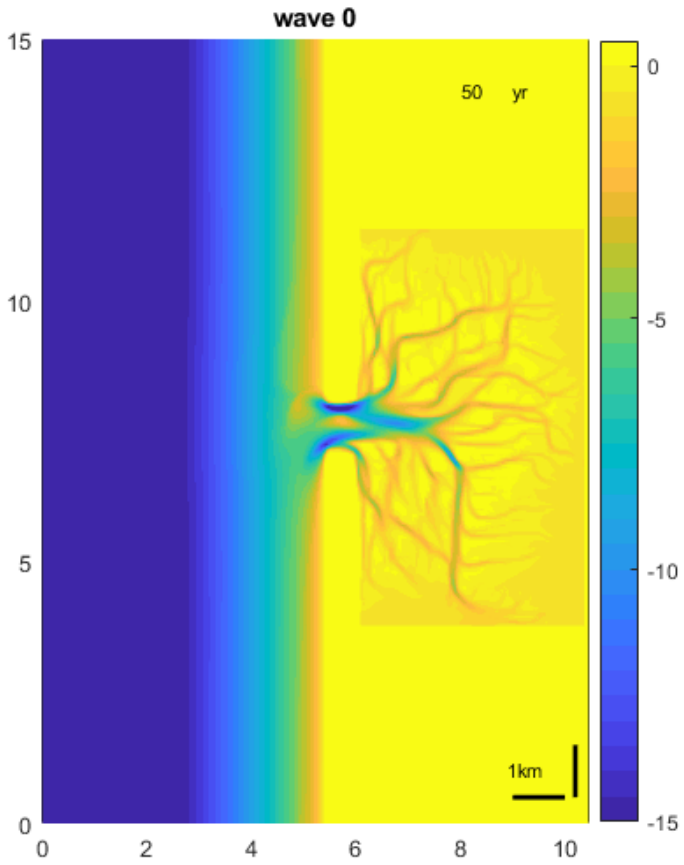

Figure 21, bathymetry of the control run without waves after 50 years. Example of a disturbed initial bathymetry.

5 Conclusion

Morphodynamic model runs provided insight into the dynamics of tidal inlet morphology and an the role of different single wave conditions versus a wave climate. In this specific case, only the wave climate produced cyclic behavior associated to sediment bypassing processes in the form of ebb tidal delta breaching. The single waves did not show cyclic behavior because the necessary balance between wave energy and strength of tidal currents was not reached. A form of cyclic behavior related to erosional processes occurred for both the wave climate and waves from both directions at ± 25 degrees from shore normal. It was found that with low waves the tidal inlet widens through time as the downdrift barrier erodes and tidal currents export sediment from the inlet. This left the basin prone to wave erosion which reduced supratidal area. At higher waves the inlet confined (2.4m) and closed (4m), this reduced the tidal prism and the potential basin infilling rate.

Waves with a direction opposed to the ebb flow out of the inlet (SW) showed different behavior than waves from NW, as waves from SW push on the direction the main ebb channel develops on the ETD and waves from NW push on the ETD laterally. This caused the ETD for waves from NW to be pushed towards the coast and for waves from SW the ETD rotated from an SW to a NW direction depending on wave height. For high waves (4m) opposite to the tidal outflow, the channel moves completely downdrift, for low waves (1 m) the waves push on the mouth of the channel and the terminal lobe of the ETD is more pronounced and for medium waves (2.4m) the channel moves slowly in downdrift direction but the channel breaches in updrift direction. The sediment bypassing processes for medium waves was found to be a mix of a wave dominated inlet and ebb tidal delta breaching.

6 References

Albernaz, M. B., Ruessink, G., Jagers, H. R. A., & Kleinhans, M. G. (2019). Effects of wave orbital velocity parameterization on nearshore sediment transport and decadal morphodynamics. *Journal of Marine Science and Engineering*, *7*(6). https://doi.org/10.3390/jmse7060188

Bird, E. (2000). *Coastal Geomorphology: an introduction.* Wiley.

Boechat Albernaz, M., Brückner, M. Z. M., van Maanen, B., van der Spek, A. J. F., & Kleinhans, M. G. (2023). Vegetation Reconfigures Barrier Coasts and Affects Tidal Basin Infilling Under Sea Level Rise. *Journal of Geophysical Research: Earth Surface*, *128*(4). https://doi.org/10.1029/2022JF006703

Booij, N., Ris, R. C., & Holthuijsen, L. H. (1999). A third-generation wave model for coastal regions: 1. Model description and validation. *Journal of Geophysical Research: Oceans*, *104*(C4), 7649–7666. https://doi.org/10.1029/98JC02622

Bruun, P., & Gerritsen, F. (1960). STABILITY OF COASTAL INLETS. *Coastal Engineering Proceedings*, *1*(7), 23. https://doi.org/10.9753/icce.v7.23

Cayocca, F. (2001). Long-term morphological modeling of a tidal inlet: the Arcachon Basin, France. In *Coastal Engineering* (Vol. 42). www.elsevier.comrlocatercoastaleng

Dastgheib, A., Roelvink, J. A., & Wang, Z. B. (2008). Long-term process-based morphological modeling of the Marsdiep Tidal Basin. *Marine Geology*, *256*(1–4), 90–100. https://doi.org/10.1016/j.margeo.2008.10.003

Davis, R. A., & Hayes, M. O. (1984). What is a wave-dominated coast? *Marine Geology*, *60*(1–4), 313–329. https://doi.org/10.1016/0025-3227(84)90155-5

Davis R, & Dalrymple R. (2012). *Principles of Tidal Sedimentology*.

De Swart, H. E., & Zimmerman, J. T. F. (2009). Morphodynamics of tidal inlet systems. In *Annual Review of Fluid Mechanics* (Vol. 41, pp. 203–229). https://doi.org/10.1146/annurev.fluid.010908.165159

Elias, E. P. L., Van Der Spek, A. J. F., Wang, Z. B., & De Ronde, J. (2012). Morphodynamic development and sediment budget of the Dutch Wadden Sea over the last century. *Geologie En Mijnbouw/Netherlands Journal of Geosciences*, *91*(3), 293–310. https://doi.org/10.1017/S0016774600000457

FitzGerald, D. M. (1988). *Shoreline erosional-depositional processes associated with tidal inlets* (pp. 186–225). https://doi.org/10.1029/LN029p0186

Fitzgerald, D. M., Kraus, N. C., & Hands, E. B. (2000). *Natural Mechanisms of Sediment Bypassing at Tidal Inlets*.

Hayes, M. O. (1979). Barrier island morphology as a function of tidal and wave regime. *Jm Leatherman, SP, Ed., Barrier Islands.*, 1–28.

Isobe, M., & Horikawa, K. (1982). Study on Water Particle Velocities of Shoaling and Breaking Waves. *Coastal Engineering in Japan*, *25*(1), 109–123. https://doi.org/10.1080/05785634.1982.11924340

Lenstra K. J. H. (2020). *Cyclic channel-shoal dynamics of ebb-tidal deltas*.

Lenstra, K. J. H., Ridderinkhof, W., & van der Vegt, M. (2019a). Unraveling the Mechanisms That Cause Cyclic Channel-Shoal Dynamics of Ebb-Tidal Deltas: A Numerical Modeling Study. *Journal of Geophysical Research: Earth Surface*, *124*(12), 2778–2797. https://doi.org/10.1029/2019JF005090

Lenstra, K. J. H., Ridderinkhof, W., & van der Vegt, M. (2019b). Unraveling the Mechanisms That Cause Cyclic Channel-Shoal Dynamics of Ebb-Tidal Deltas: A Numerical Modeling Study. *Journal of Geophysical Research: Earth Surface*, *124*(12), 2778–2797. https://doi.org/10.1029/2019JF005090

Lenstra, K. J. H., & van der Vegt, M. (2021). The impact of sea-level rise and basin area reduction on the cyclic behavior of tidal inlet systems. *Continental Shelf Research*, *214*. https://doi.org/10.1016/j.csr.2020.104323

Lesser, G. R., Roelvink, J. A., van Kester, J. A. T. M., & Stelling, G. S. (2004). Development and validation of a three-dimensional morphological model. *Coastal Engineering*, *51*(8–9), 883–915. https://doi.org/10.1016/j.coastaleng.2004.07.014

Leuven, J. R. F. W., de Haas, T., Braat, L., & Kleinhans, M. G. (2018). Topographic forcing of tidal sandbar patterns for irregular estuary planforms. *Earth Surface Processes and Landforms*, *43*(1), 172–186. https://doi.org/10.1002/esp.4166

Nahon, A., Bertin, X., Fortunato, A. B., & Oliveira, A. (2012). Process-based 2DH morphodynamic modeling of tidal inlets: A comparison with empirical classifications and theories. *Marine Geology*, *291–294*, 1–11. https://doi.org/10.1016/j.margeo.2011.10.001

Nicolas Bruneau, André B. Fortunato, Guillaume Dodet, Paula Freire, Anabela Oliveira, & Xavier Bertin. (2011). Future evolution of a tidal inlet due to changes in wave climate, Sea level and lagoon morphology (Ó bidos lagoon, Portugal). *Continental Shelf Research*, *31*, 1915–1930.

O'Brien, M. P. (1969). *Equilibrium Flow Areas of Tidal Inlets on Sandy Coasts*. 676–686. https://doi.org/10.1061/9780872620087.039

Radermacher, M., de Schipper, M. A., Swinkels, C., MacMahan, J. H., & Reniers, A. J. H. M. (2017). Tidal flow separation at protruding beach nourishments. *Journal of Geophysical Research: Oceans*, *122*(1), 63–79. https://doi.org/10.1002/2016JC011942

Ranasinghe, R., Swinkels, C., Luijendijk, A., Roelvink, D., Bosboom, J., Stive, M., & Walstra, D. J. (2011). Morphodynamic upscaling with the MORFAC approach: Dependencies and sensitivities. *Coastal Engineering*, *58*(8), 806–811. https://doi.org/10.1016/j.coastaleng.2011.03.010

Ridderinkhof, W., de Swart, H. E., van der Vegt, M., & Hoekstra, P. (2016). Modeling the growth and migration of sandy shoals on ebb-tidal deltas. *Journal of Geophysical Research: Earth Surface*, *121*(7), 1351–1372. https://doi.org/10.1002/2016JF003823

Ridderinkhof, W., Hoekstra, P., van der Vegt, M., & de Swart, H. E. (2016). Cyclic behavior of sandy shoals on the ebb-tidal deltas of the Wadden Sea. *Continental Shelf Research*, *115*, 14–26. https://doi.org/10.1016/j.csr.2015.12.014

Rijkswaterstaat. (2017). *The yearly coastal measurements (in Dutch: De jaarlijkse kustmetingen or jarkus) [Dataset]*. Https://Opendap.Deltares.Nl/Thredds/Catalog/Opendap/Rijkswaterstaat/Jarkus/Caralog.Html.

Roelvink, J. A. (2006). Coastal morphodynamic evolution techniques. *Coastal Engineering*, *53*(2–3), 277–287. https://doi.org/10.1016/j.coastaleng.2005.10.015

Ruessink, B. G., Ramaekers, G., & van Rijn, L. C. (2012). On the parameterization of the free-stream non-linear wave orbital motion in nearshore morphodynamic models. *Coastal Engineering*, *65*, 56–63. https://doi.org/10.1016/j.coastaleng.2012.03.006

Sha, L. P. (1990). Surface sediments and sequence models in the ebb-tidal delta of Texel Inlet, Wadden Sea, The Netherlands. *Sedimentary Geology*, *68*(1–2), 125–141. https://doi.org/10.1016/0037-0738(90)90123-B

Symonds, A. M., Vijverberg, T., Post, S., Van Der Spek, B.-J., Henrotte, J., & Sokolewicz, M. (n.d.). *COMPARISON BETWEEN MIKE 21 FM, DELFT3D AND DELFT3D FM FLOW MODELS OF WESTERN PORT BAY, AUSTRALIA*.

Tambroni, N., & Seminara, G. (2006). Are inlets responsible for the morphological degradation of Venice Lagoon? *Journal of Geophysical Research: Earth Surface*, *111*(F3), n/a-n/a. https://doi.org/10.1029/2005JF000334

van der Vegt, M., Schuttelaars, H. M., & de Swart, H. E. (2009). The influence of tidal currents on the asymmetry of tide-dominated ebb-tidal deltas. *Continental Shelf Research*, *29*(1), 159–174. https://doi.org/10.1016/j.csr.2008.01.018

Van Rijn, L. C., Walstra, D. J. R., & van Ormondt, M. (2004). *Description of TRANSPOR2004 and Implementation in Delft3D-ONLINE*. http://resolver.tudelft.nl/uuid:ea12eb20-aee3-4f58-99fb-ebc216e98879

Walton, T. L., & Adams, W. D. (1976). *Capacity of inlet outer bars to store sand*.

Wang, Z. B., Elias, E. P. L., Van Der Spek, A. J. F., & Lodder, Q. J. (2018). Sediment budget and morphological development of the Dutch Wadden Sea: Impact of accelerated sea-level rise and subsidence until 2100. *Geologie En Mijnbouw/Netherlands Journal of Geosciences*, *97*(3), 183–214. https://doi.org/10.1017/njg.2018.8

Wang, Z. B., Hoekstra, P., Burchard, H., Ridderinkhof, H., De Swart, H. E., & Stive, M. J. F. (2012). Morphodynamics of the Wadden Sea and its barrier island system. *Ocean and Coastal Management*, *68*, 39–57. https://doi.org/10.1016/j.ocecoaman.2011.12.022

Appendix

A. Time series of full runs

Overview of wave conditions

Wave	Wave height	Wave period	Wave direction
#	(Hs) m	(Tp) sec	deg
1	1.20	4.1	201
4	1.08	4.2	248
5	2.53	5.5	247
6	3.96	6.5	250
7	0.80	3.5	270
8	1.02	4.7	297
9	2.33	5.7	296
10	4.02	6.9	296
11	0.81	4.2	333

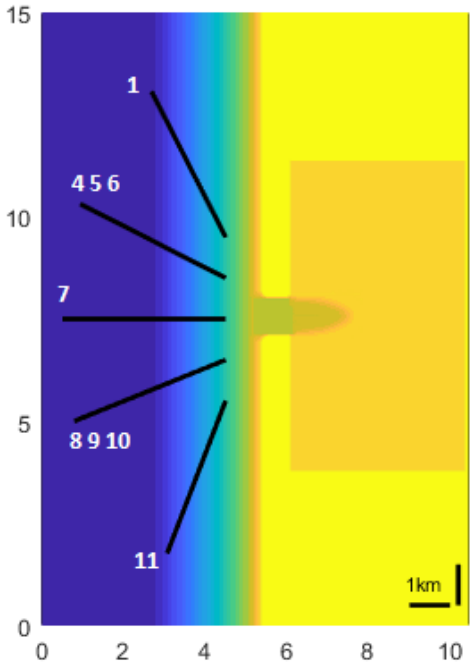

I. Low waves 100 years every 10 years

Wave 1

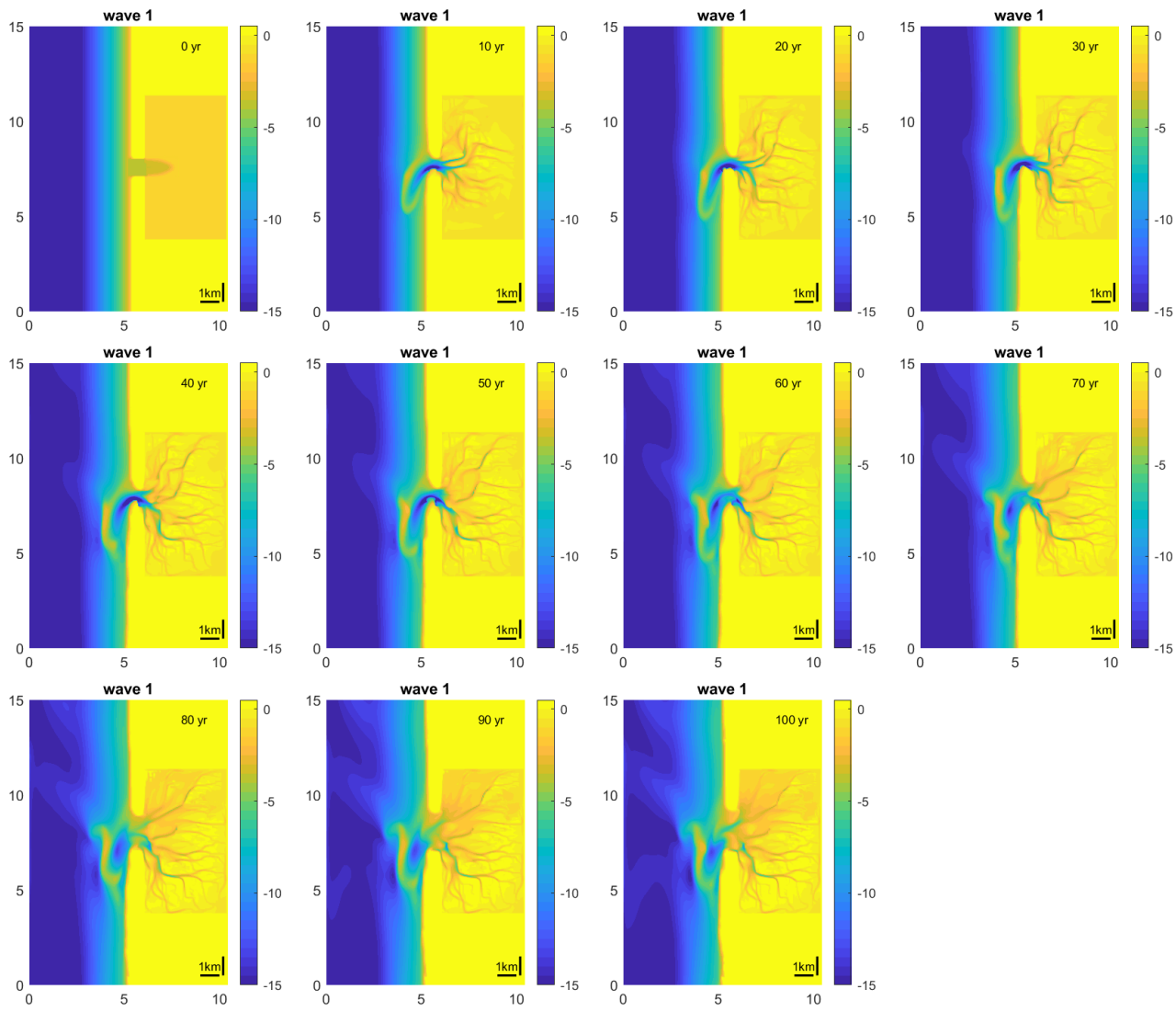

Wave 4

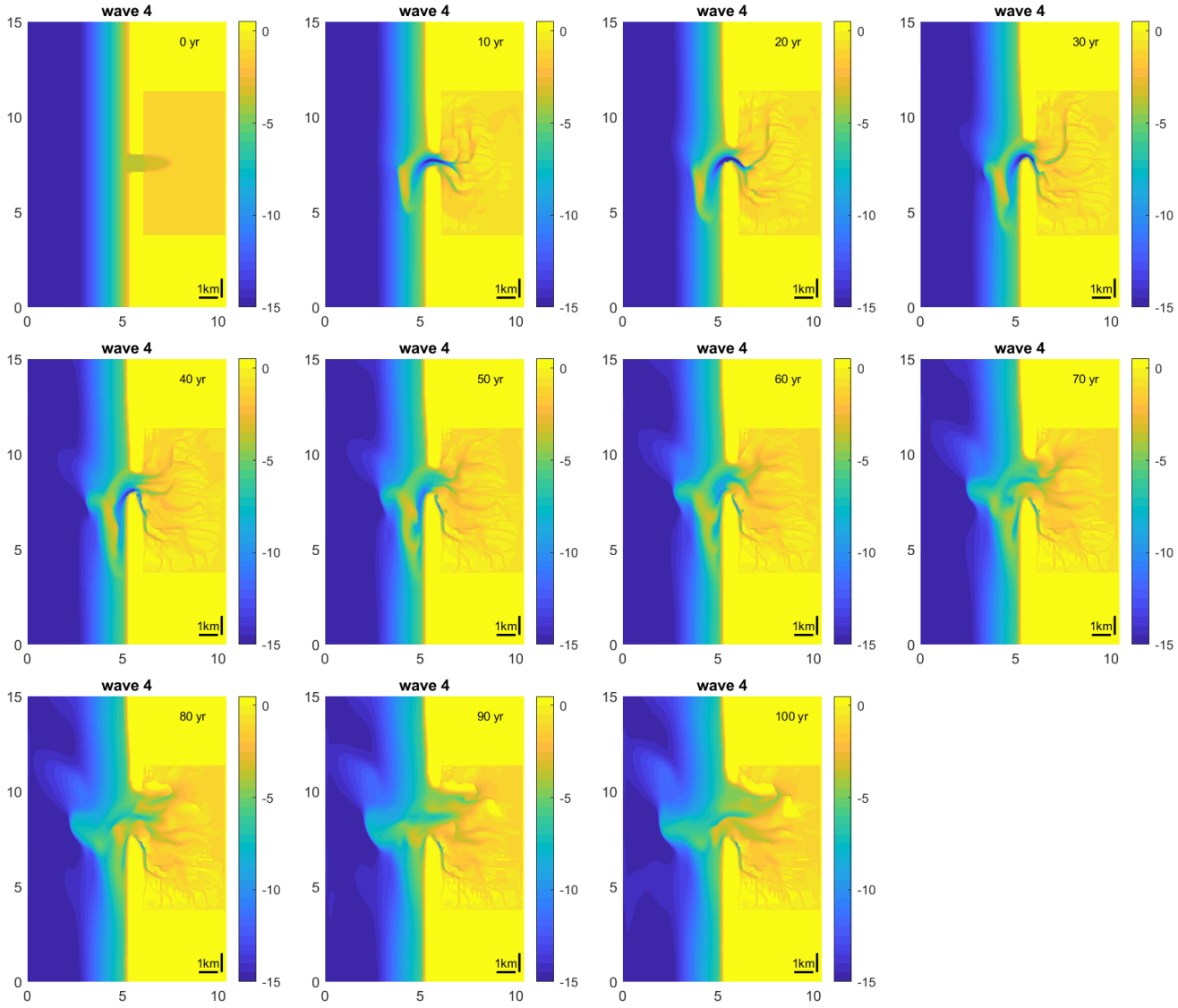
wave 4
0 yr
10 yr
20 yr
30 yr
40 yr
50 yr
60 yr
70 yr
80 yr
90 yr
100 yr
1km
0
5
10
15
-5
-10
-15

Wave 7

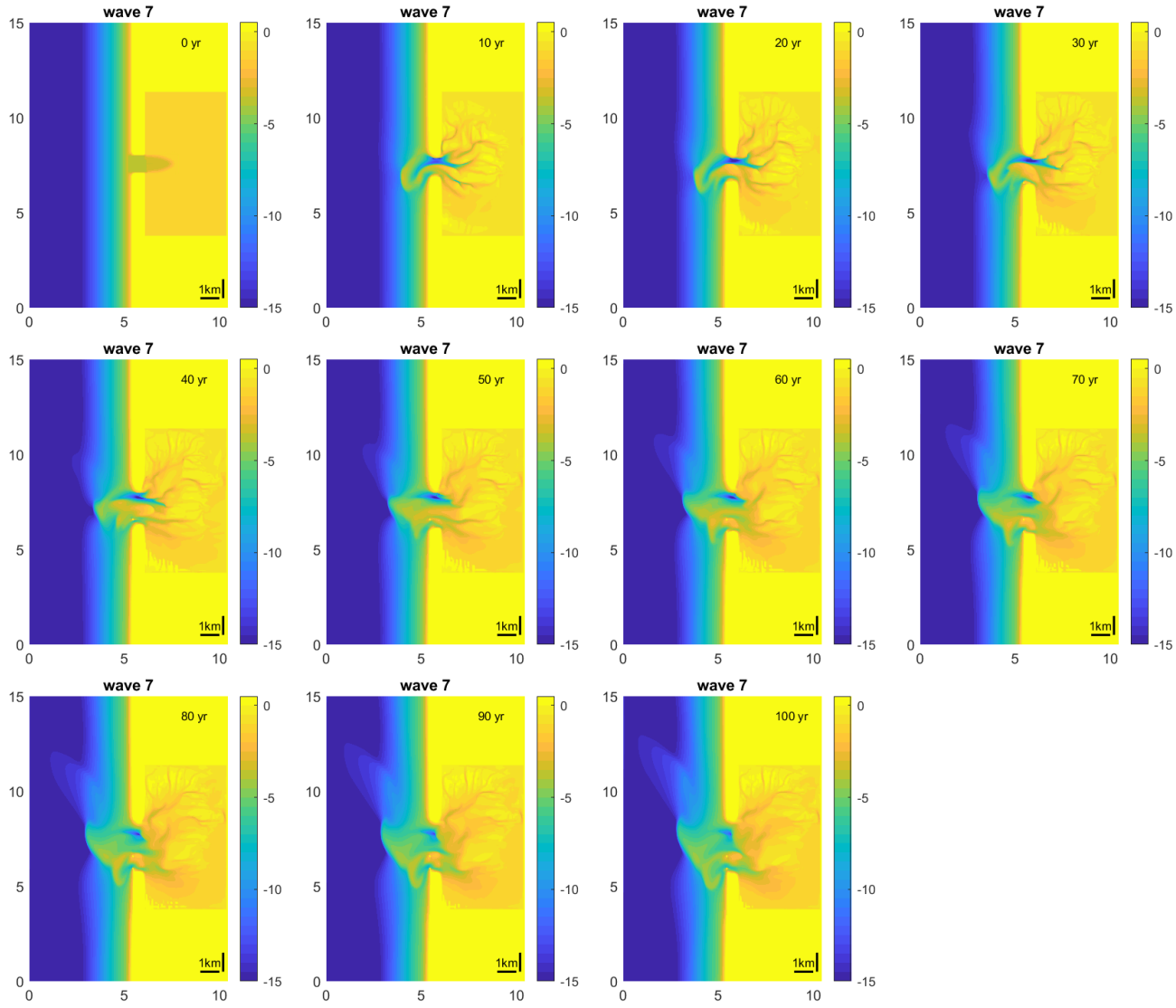
wave 7
0 yr
10 yr
20 yr
30 yr
40 yr
50 yr
60 yr
70 yr
80 yr
90 yr
100 yr
1km

Wave 8

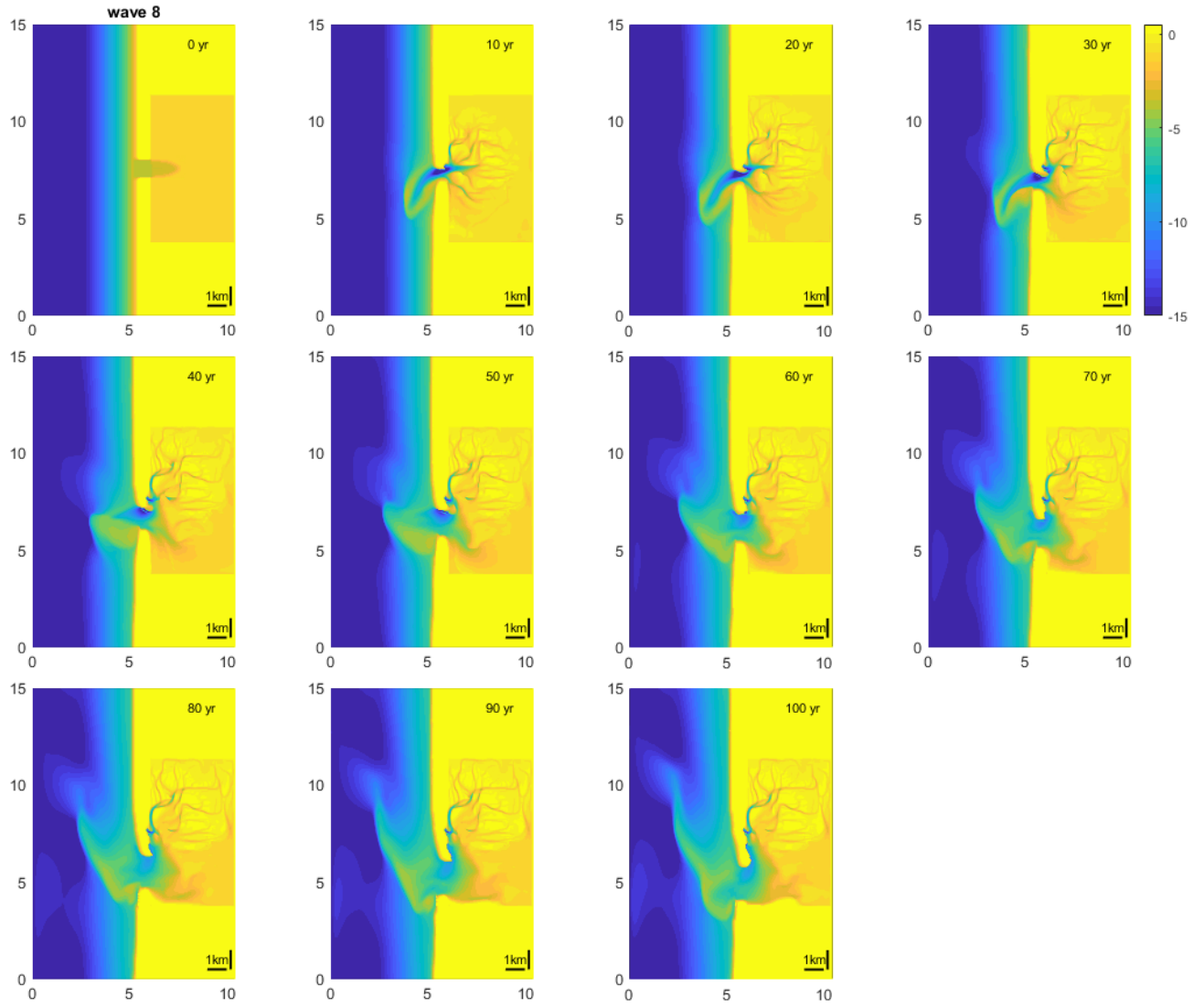
wave 8
0 yr
10 yr
20 yr
30 yr
40 yr
50 yr
60 yr
70 yr
80 yr
90 yr
100 yr
1km
0
-5
-10
-15

Wave 11

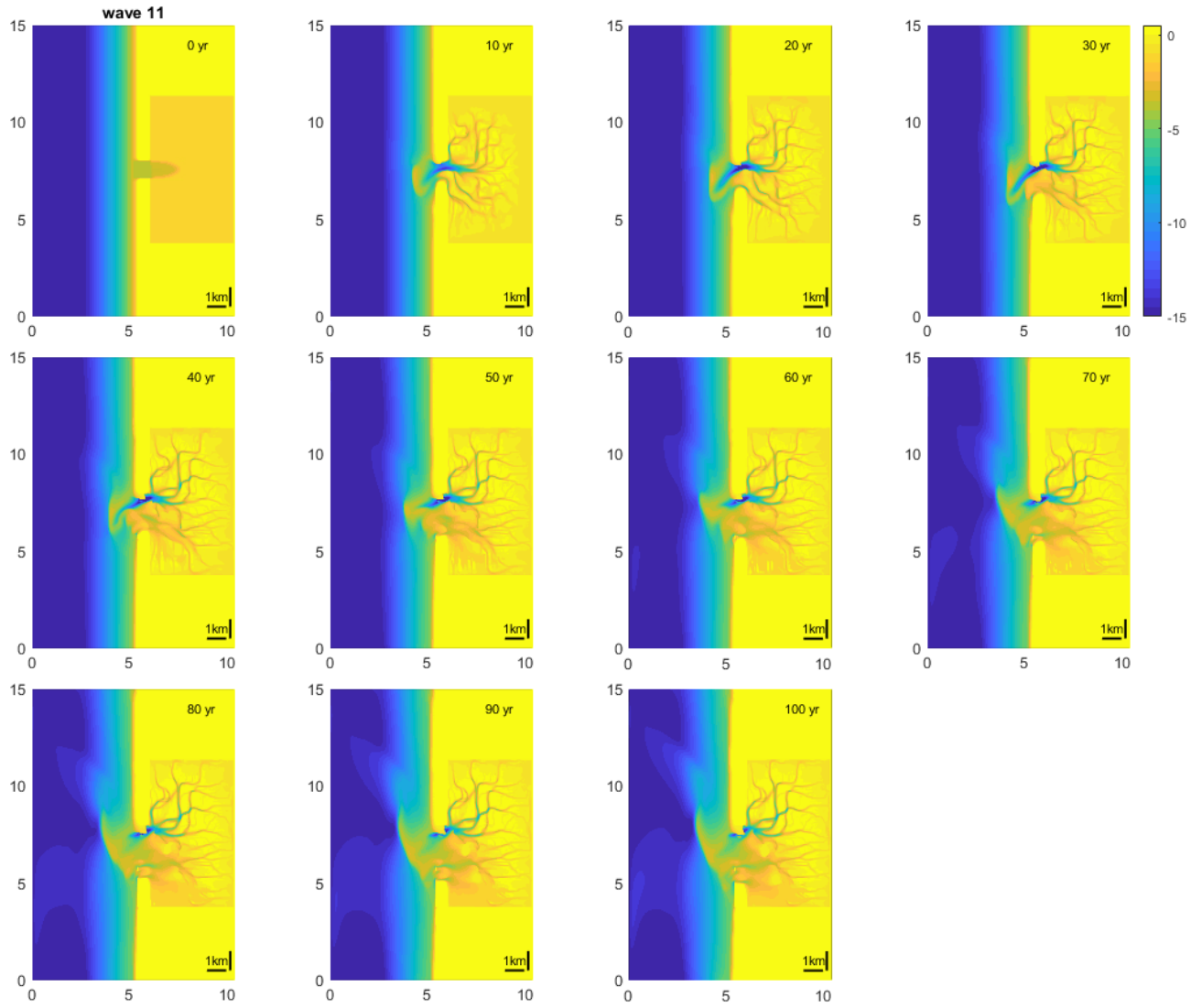
wave 11
0 yr
10 yr
20 yr
30 yr
40 yr
50 yr
60 yr
70 yr
80 yr
90 yr
100 yr
1km
0
-5
-10
-15

II. Low wave WSW 160 years every 20 years

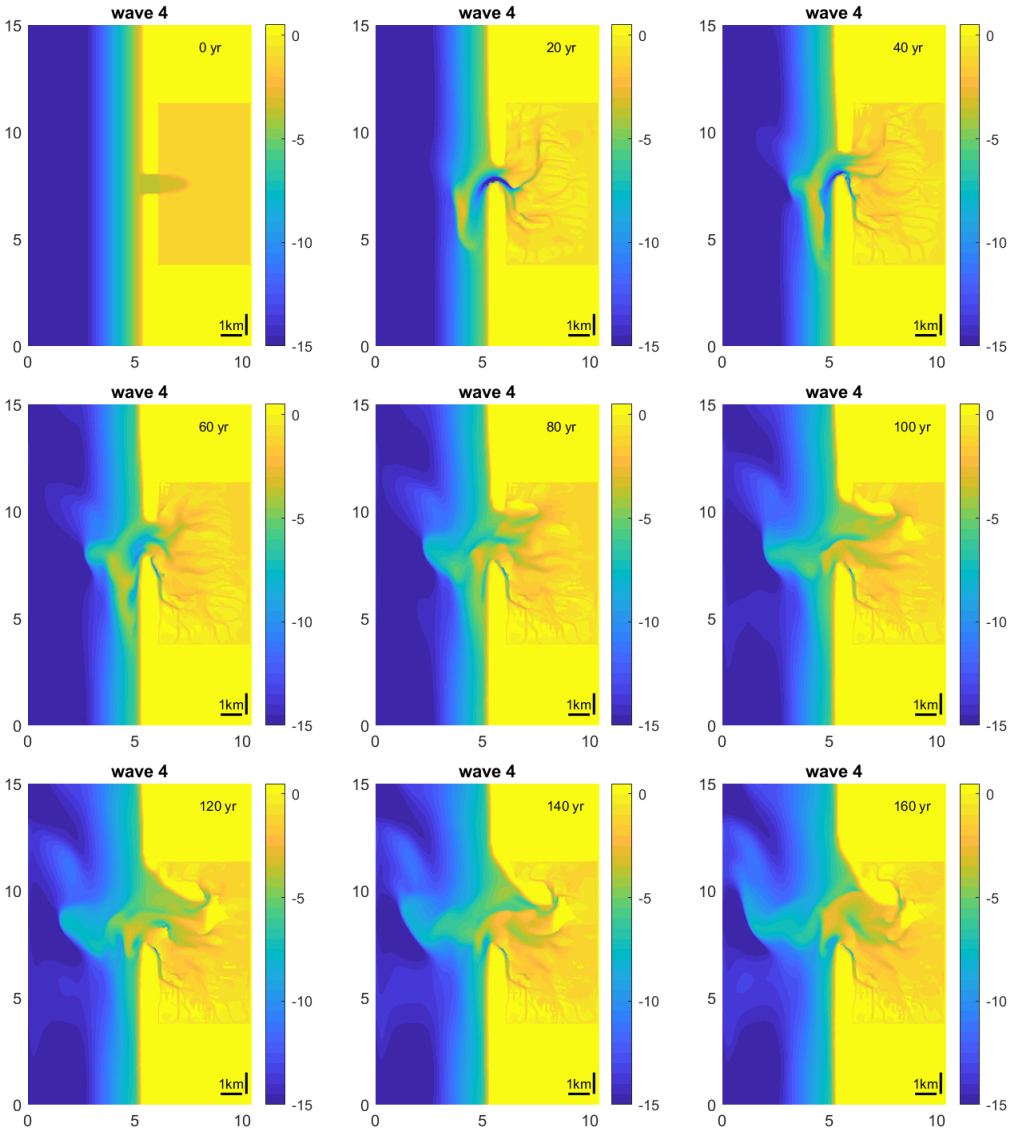

III. Wave climate 100 years every 10 years

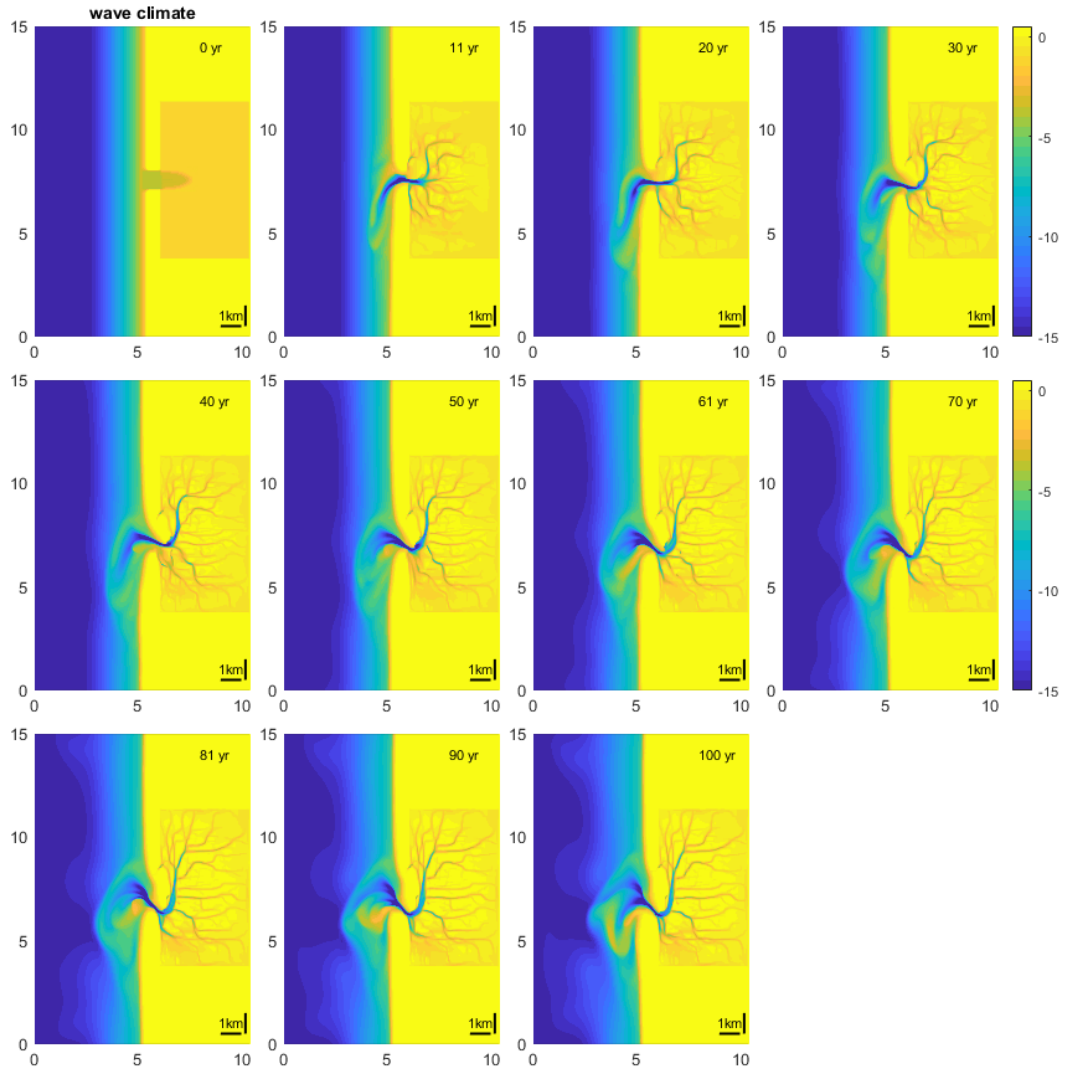

IV. Medium wave 40 years every 5 years

Wave 9

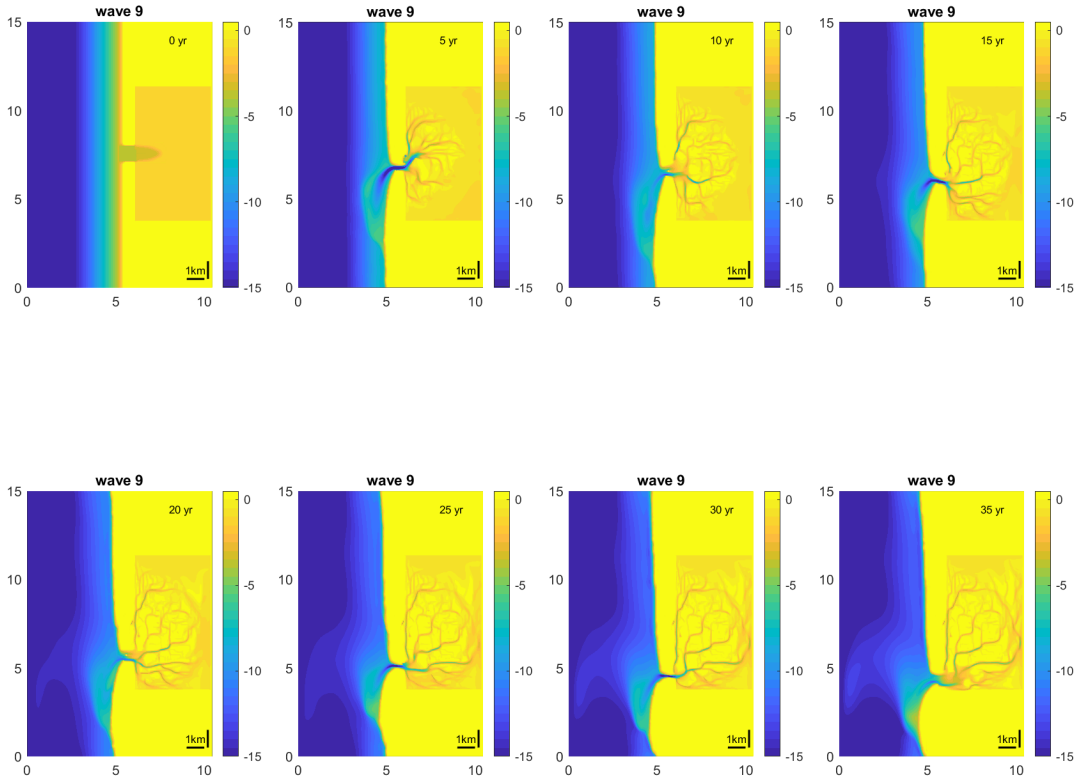

B. Transport plots

Overview of measuring transects where transport was measured

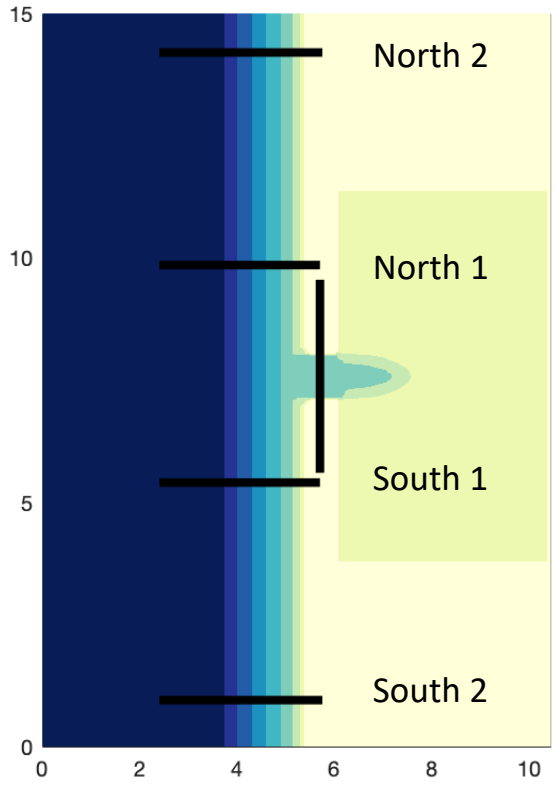

I. Transport for each individual measuring transect

North

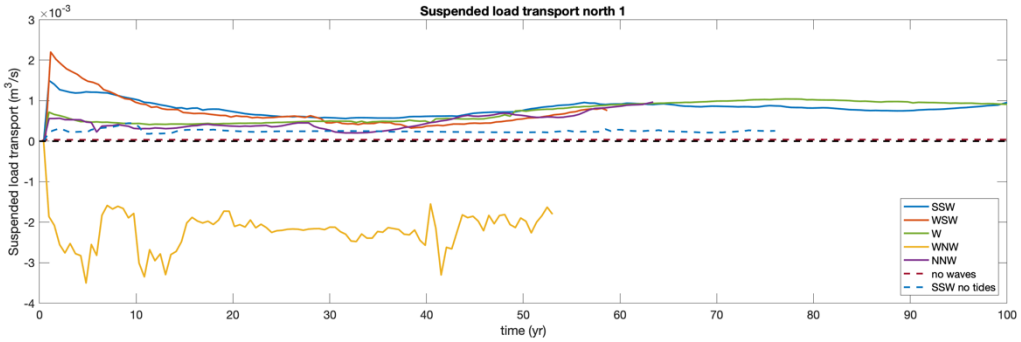

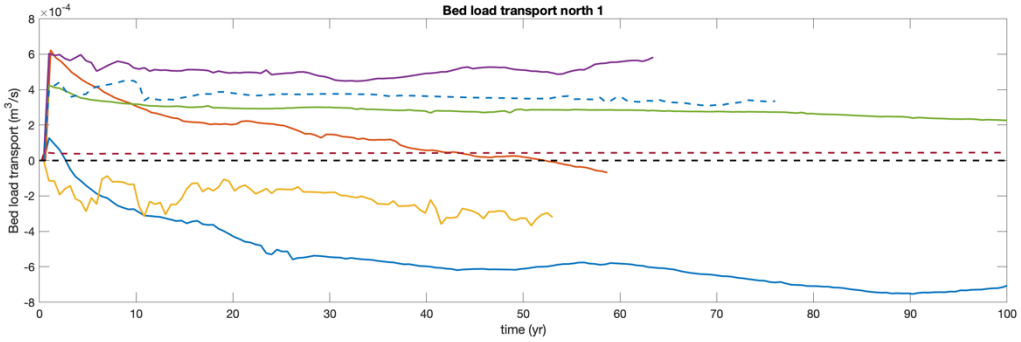

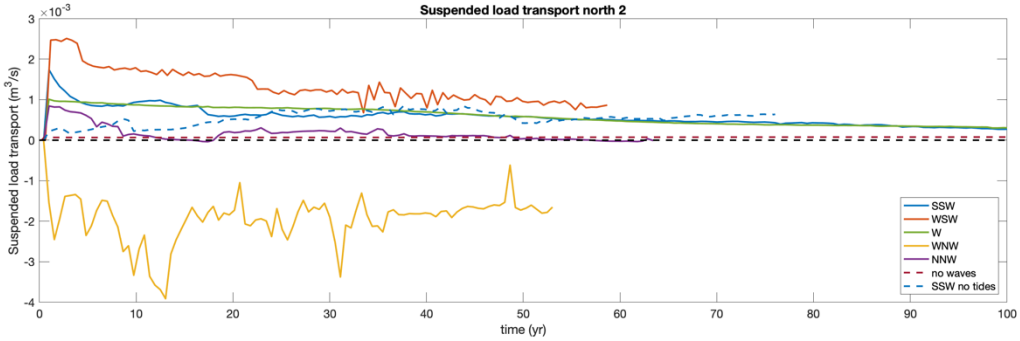

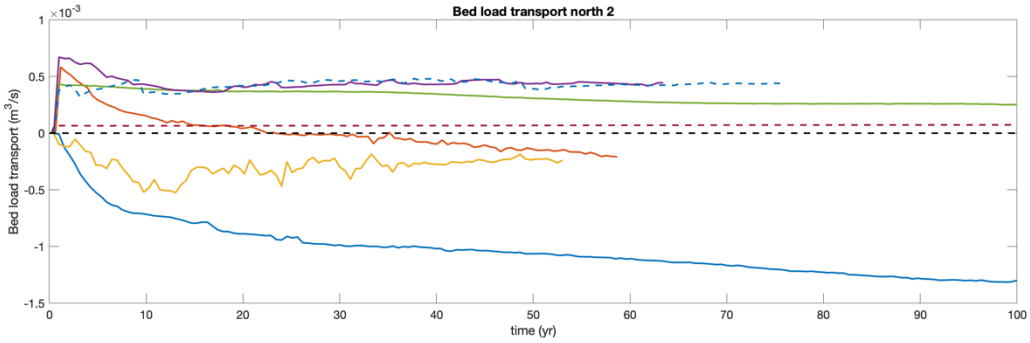

South

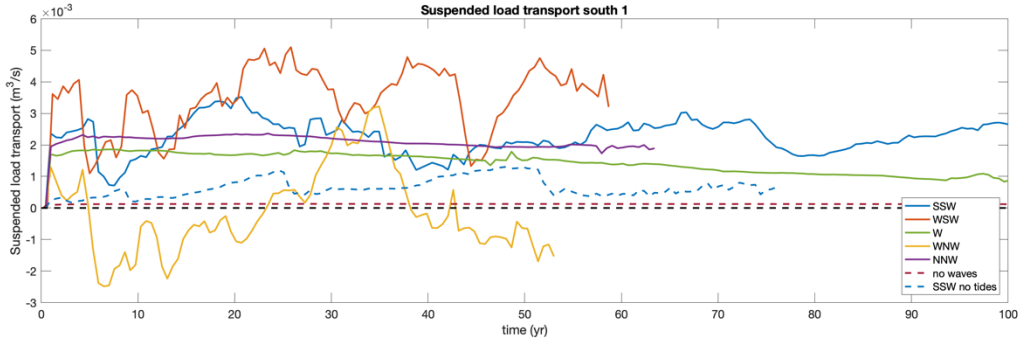
Suspended load transport south 1
×10^-3
Suspended load transport (m^3/s)
time (yr)
SSW
WSW
W
WNW
NNW
no waves
SSW no tides

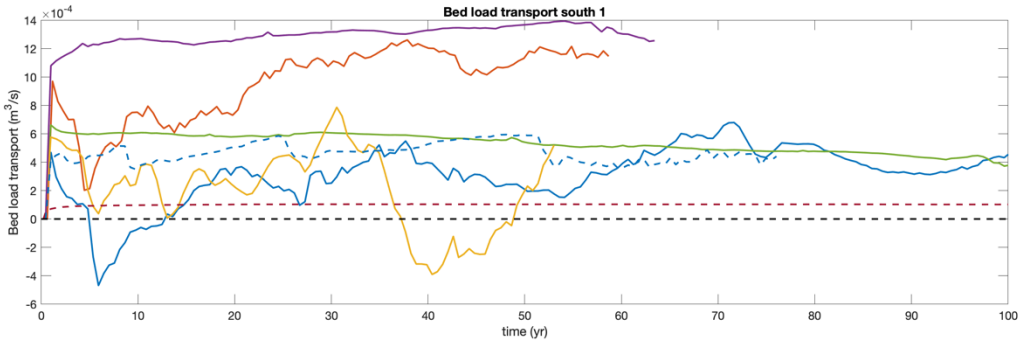
Bed load transport south 1
×10^-4
Bed load transport (m^3/s)
time (yr)

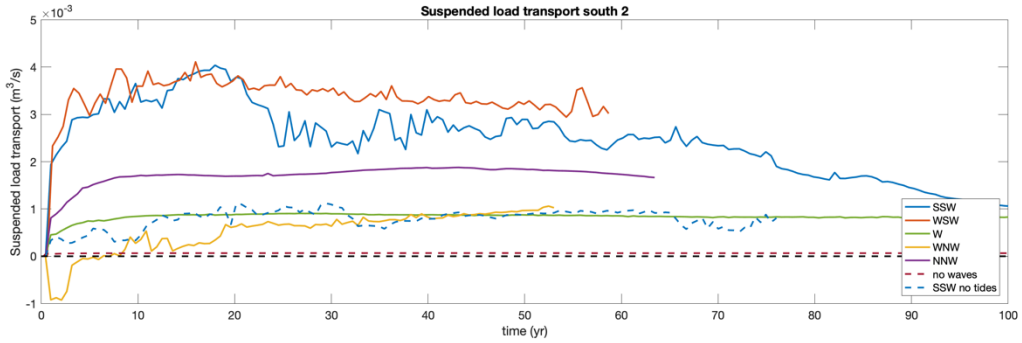
Suspended load transport south 2
×10^-3
Suspended load transport (m^3/s)
time (yr)
SSW
WSW
W
WNW
NNW
no waves
SSW no tides

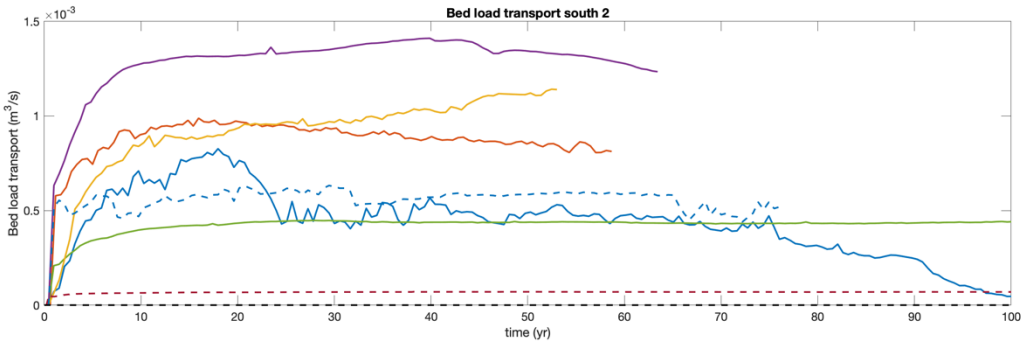
Bed load transport south 2
×10^-3
Bed load transport (m^3/s)
time (yr)

II. Mean transport for measuring transects

North (north 1 and north 2)

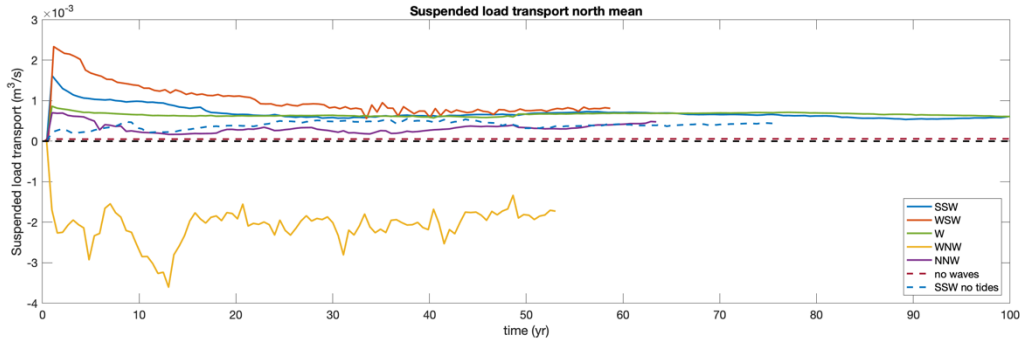

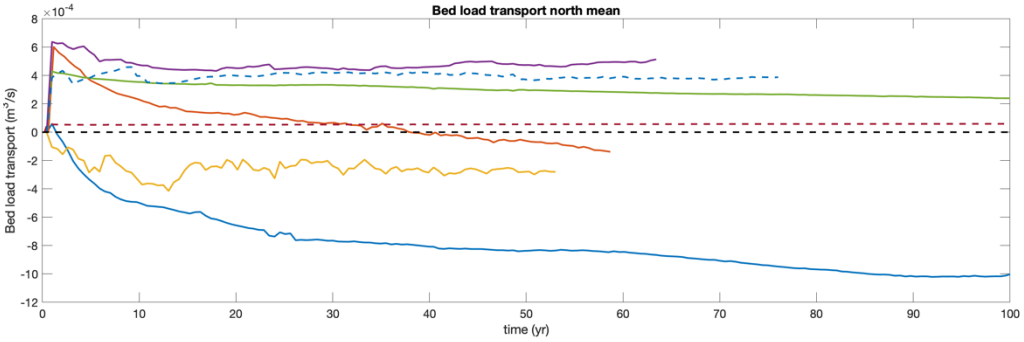

South (south 1 and south 2)

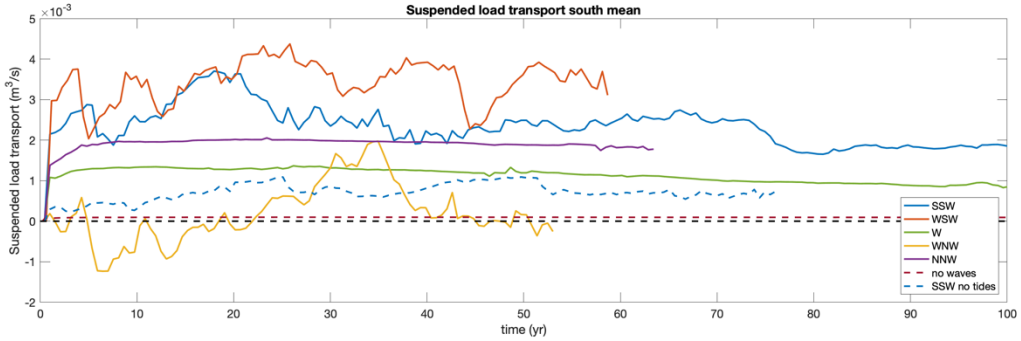

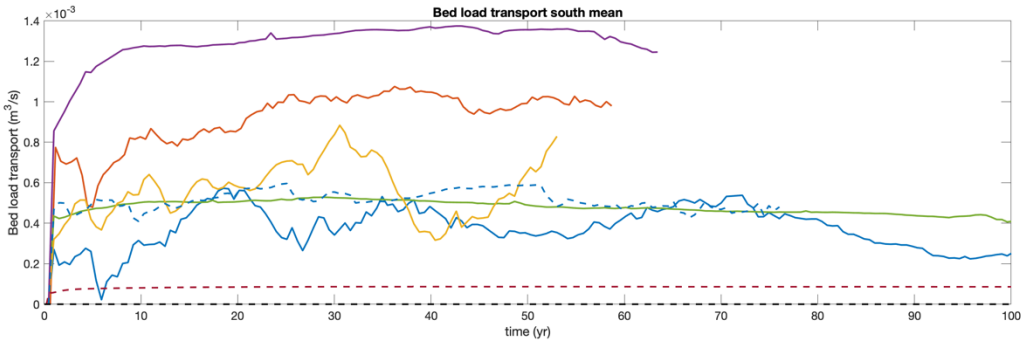

Close to inlet (north 1 and south 1)

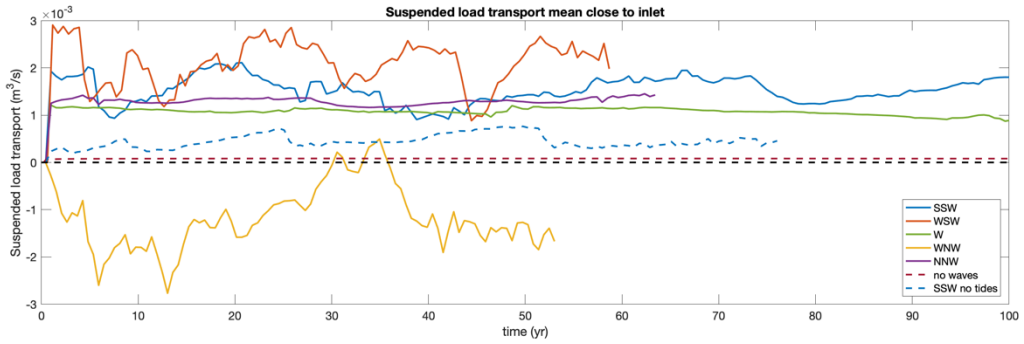

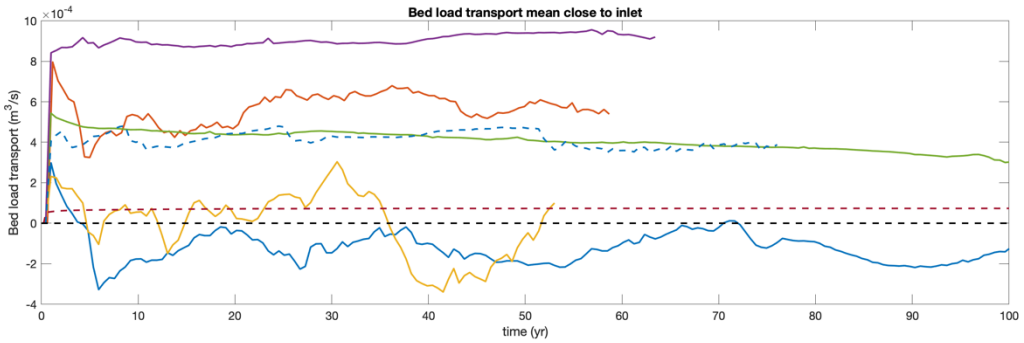

Far from inlet (north 2 and south 2)

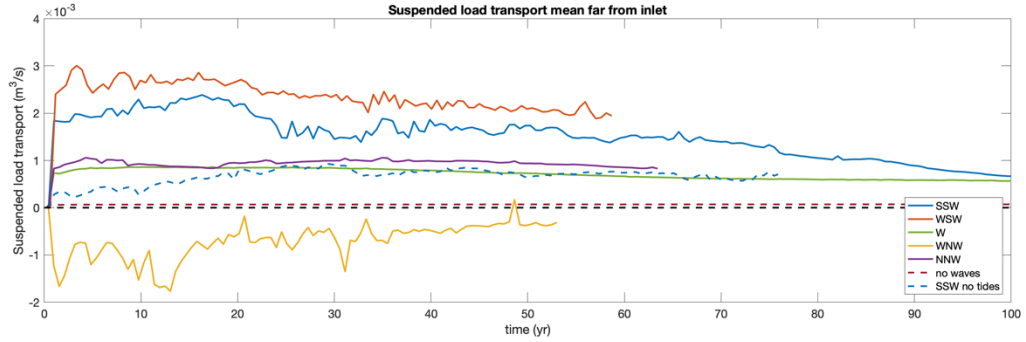

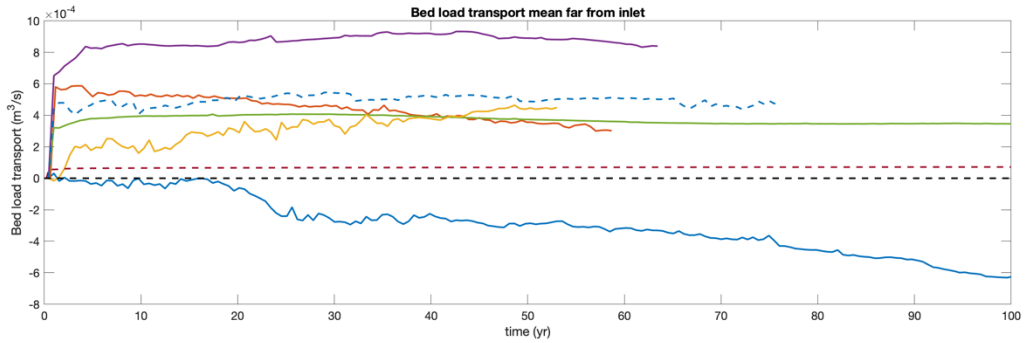

C. Timestacks

I. Timestacks for low waves

Wave 1

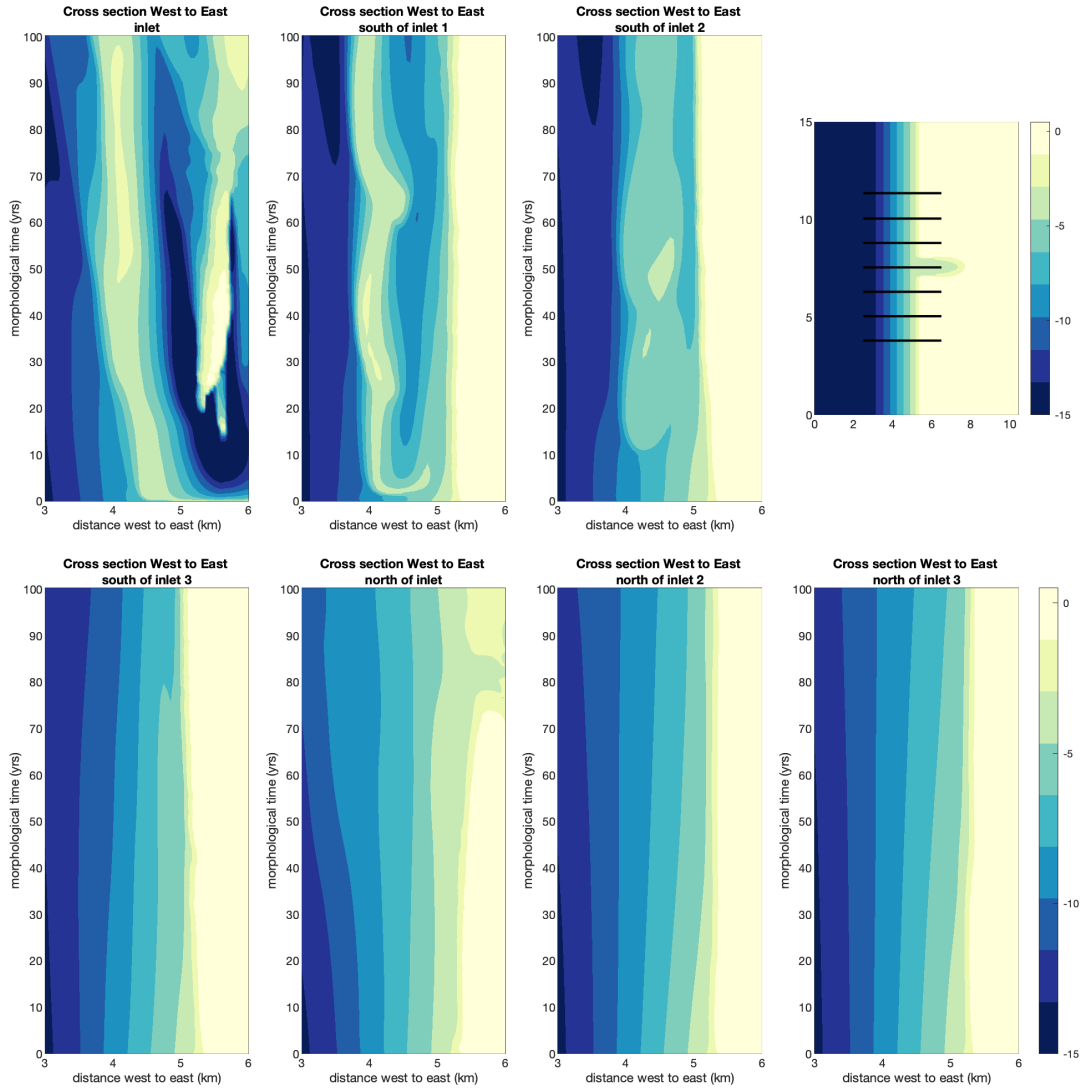

Wave 4

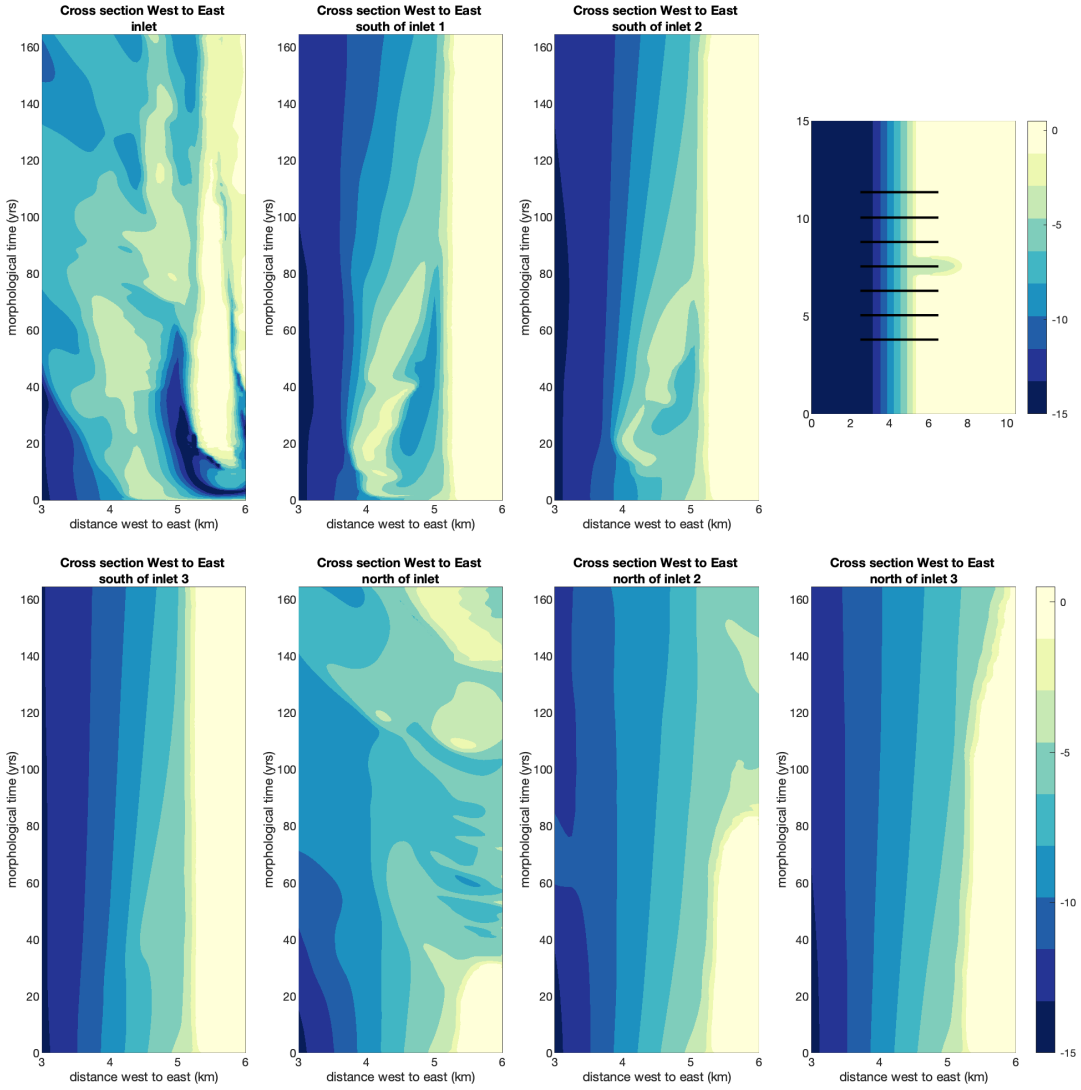
Cross section West to East inlet
Cross section West to East south of inlet 1
Cross section West to East south of inlet 2
Cross section West to East south of inlet 3
Cross section West to East north of inlet
Cross section West to East north of inlet 2
Cross section West to East north of inlet 3
morphological time (yrs)
distance west to east (km)

Wave 7

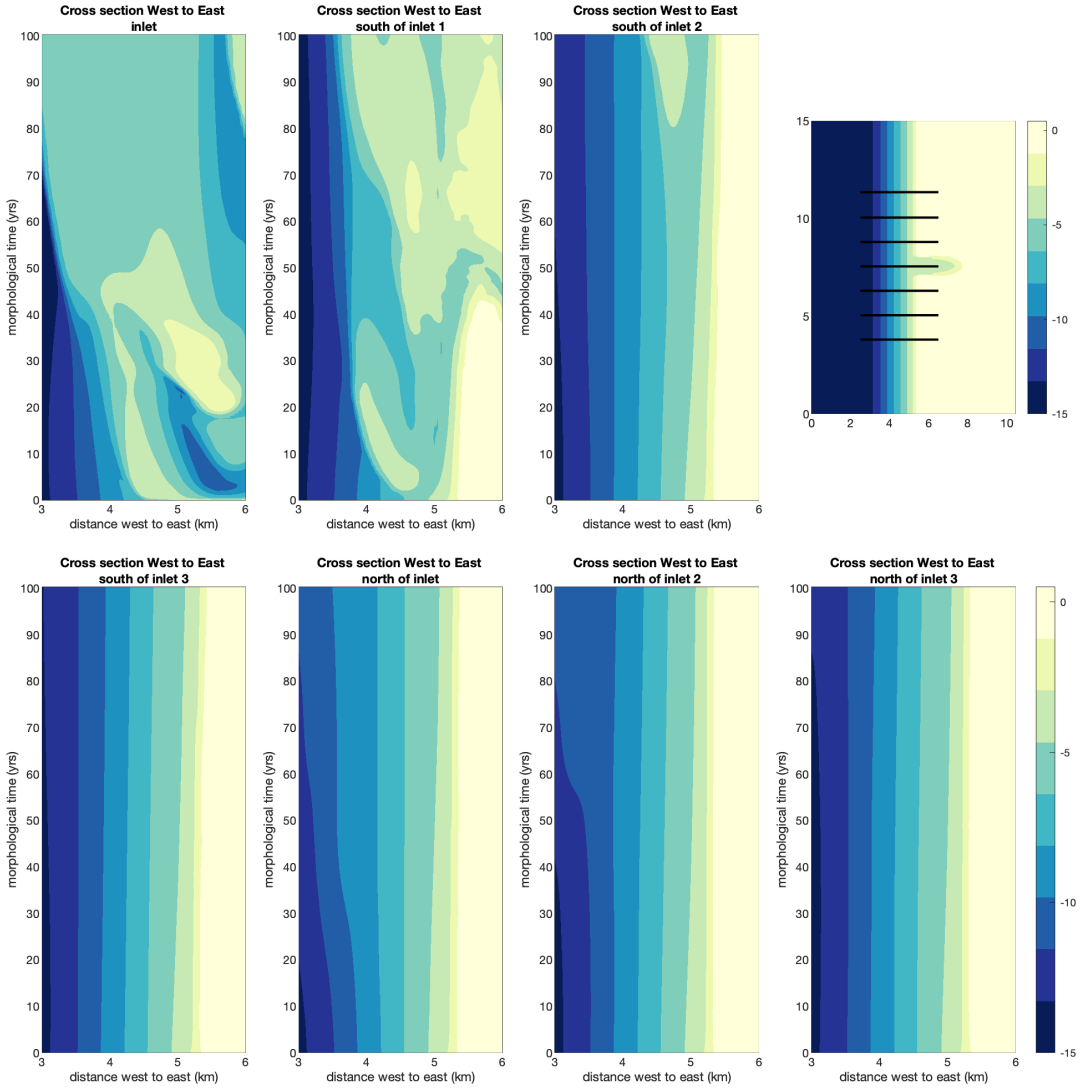
Cross section West to East inlet
Cross section West to East south of inlet 1
Cross section West to East south of inlet 2
Cross section West to East south of inlet 3
Cross section West to East north of inlet
Cross section West to East north of inlet 2
Cross section West to East north of inlet 3
morphological time (yrs)
distance west to east (km)

Wave 8

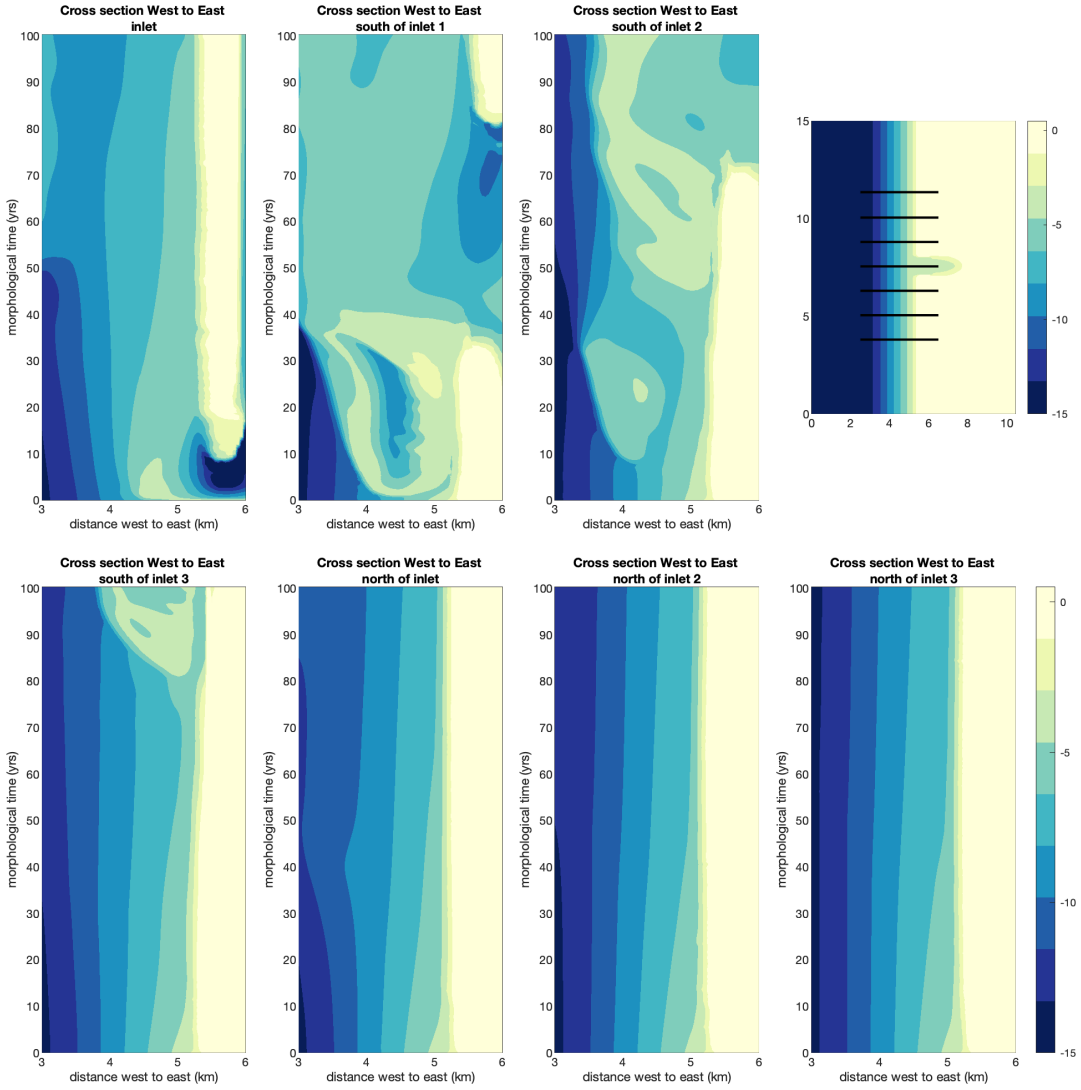
Cross section West to East inlet
Cross section West to East south of inlet 1
Cross section West to East south of inlet 2
Cross section West to East south of inlet 3
Cross section West to East north of inlet
Cross section West to East north of inlet 2
Cross section West to East north of inlet 3
morphological time (yrs)
distance west to east (km)

Wave 11

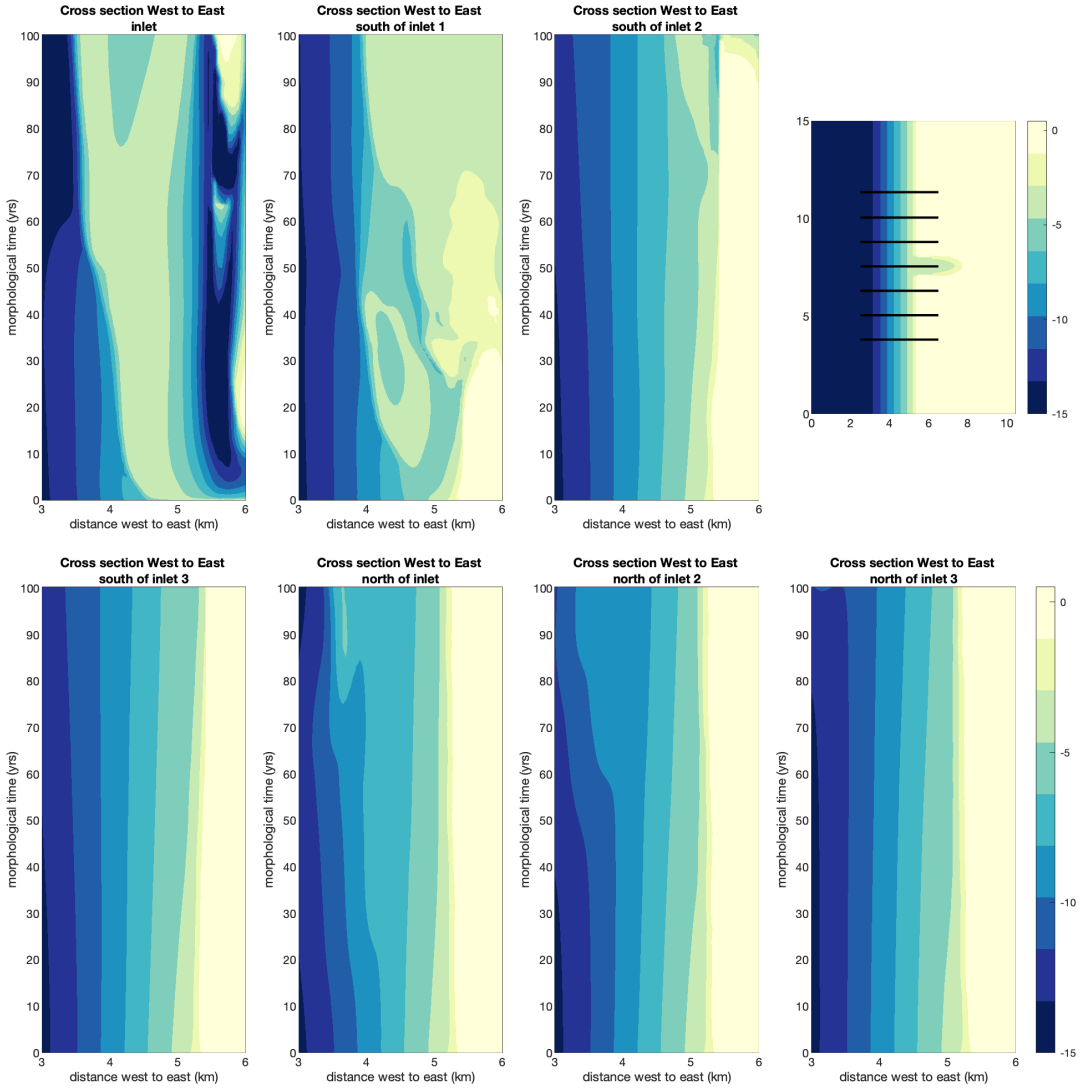
Cross section West to East inlet
Cross section West to East south of inlet 1
Cross section West to East south of inlet 2
Cross section West to East south of inlet 3
Cross section West to East north of inlet
Cross section West to East north of inlet 2
Cross section West to East north of inlet 3
morphological time (yrs)
distance west to east (km)

II. Timestacks for medium and high waves

Wave 5

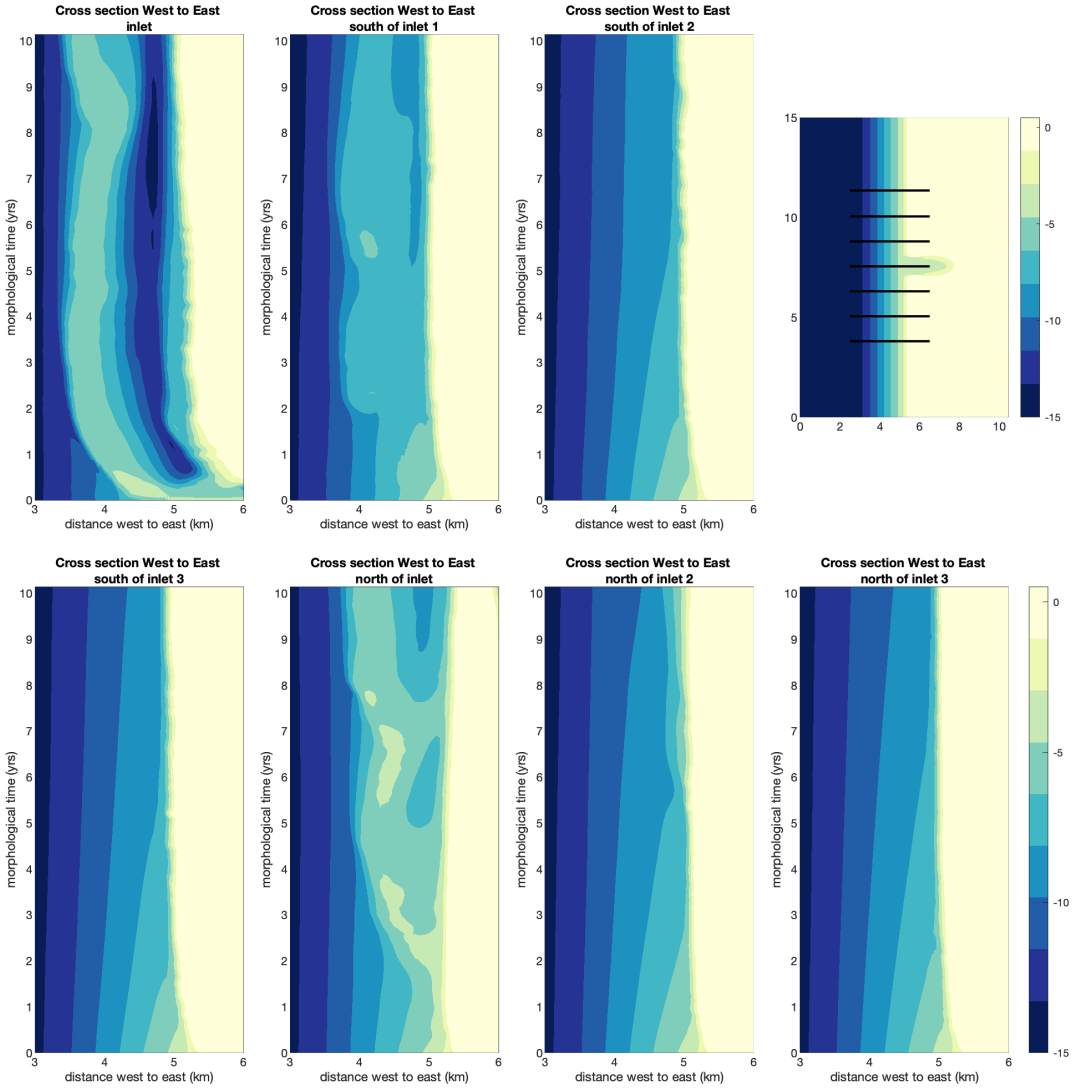

Wave 6

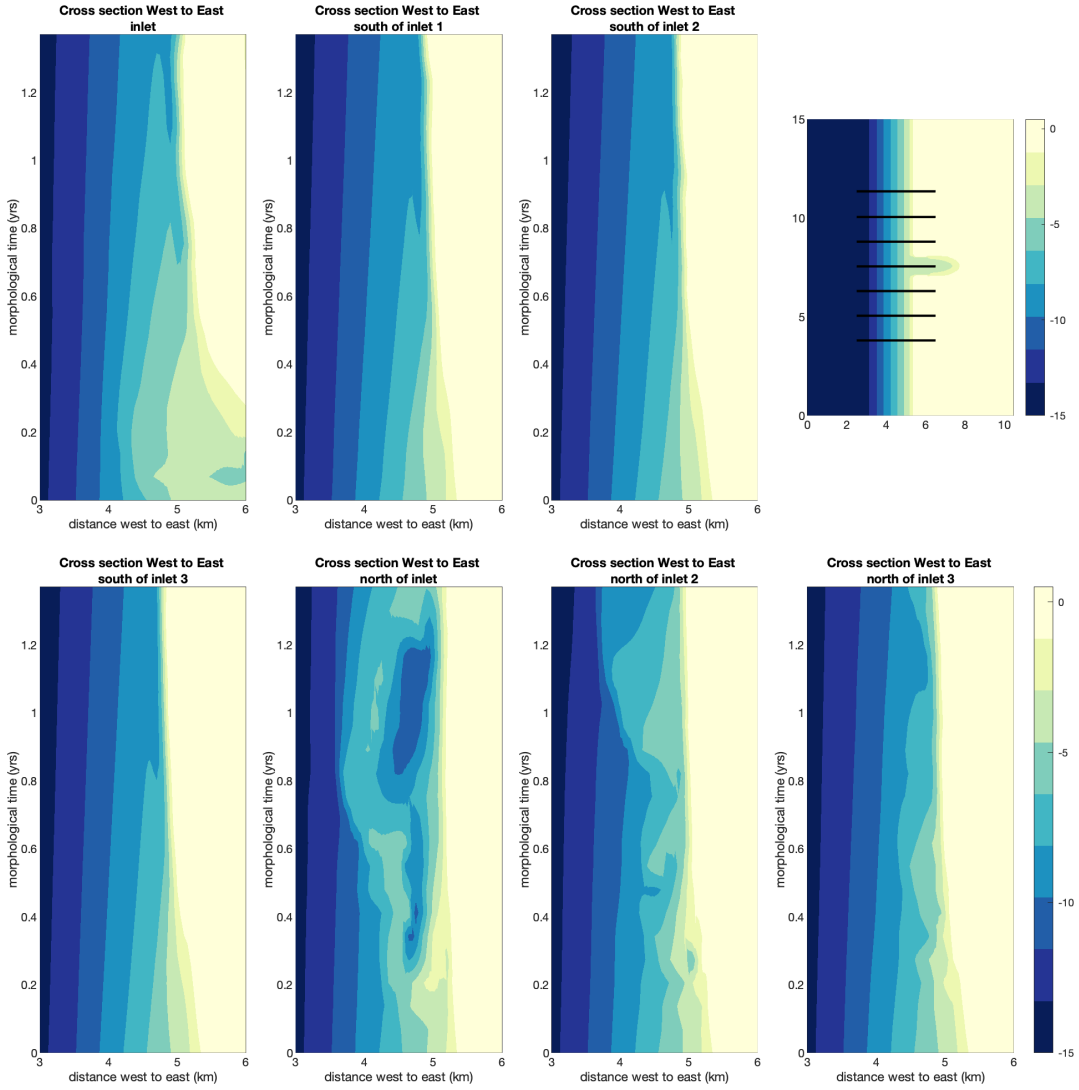
Cross section West to East inlet
Cross section West to East south of inlet 1
Cross section West to East south of inlet 2
Cross section West to East south of inlet 3
Cross section West to East north of inlet
Cross section West to East north of inlet 2
Cross section West to East north of inlet 3
morphological time (yrs)
distance west to east (km)

Wave 9

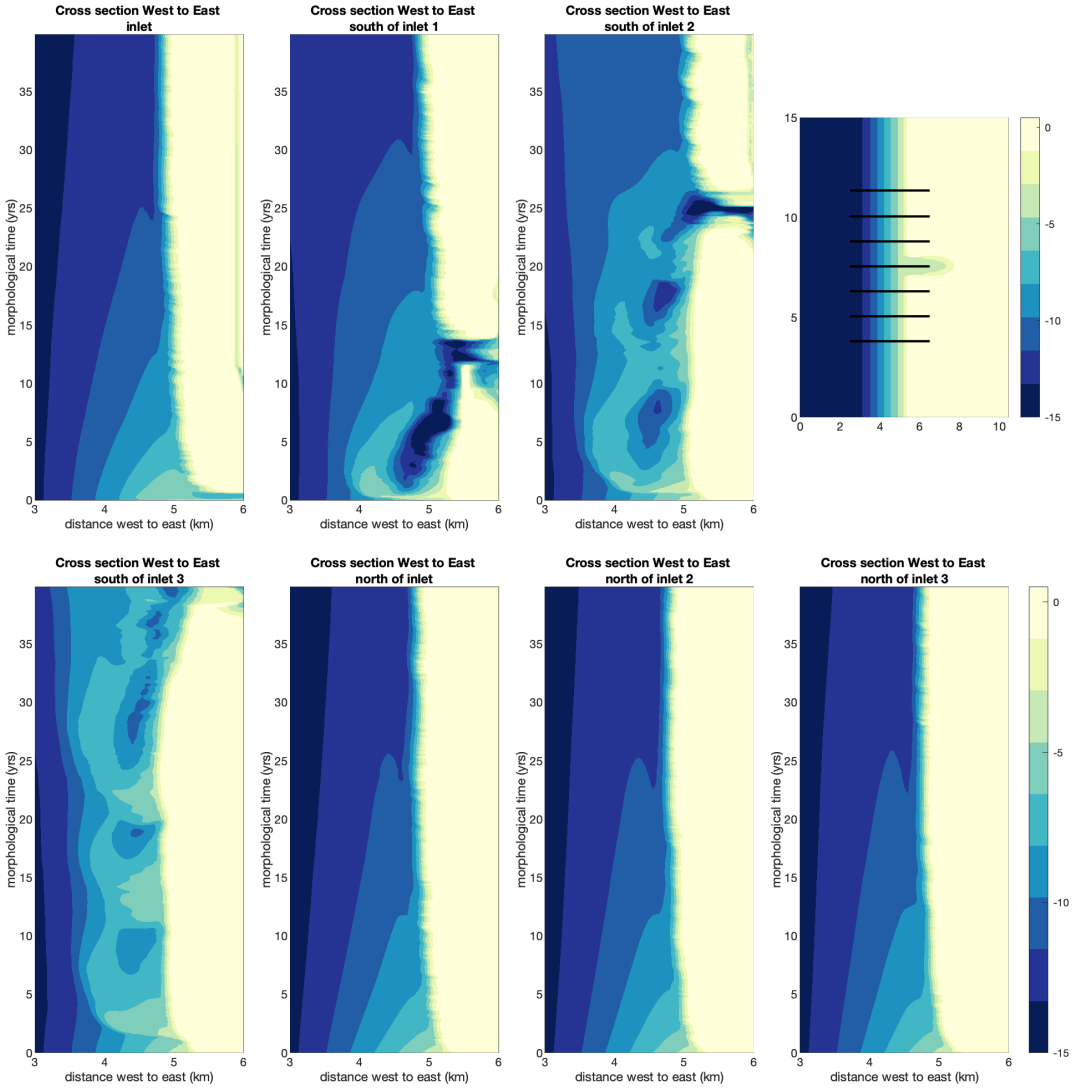
Cross section West to East inlet
Cross section West to East south of inlet 1
Cross section West to East south of inlet 2
Cross section West to East south of inlet 3
Cross section West to East north of inlet
Cross section West to East north of inlet 2
Cross section West to East north of inlet 3
morphological time (yrs)
distance west to east (km)

Wave 10

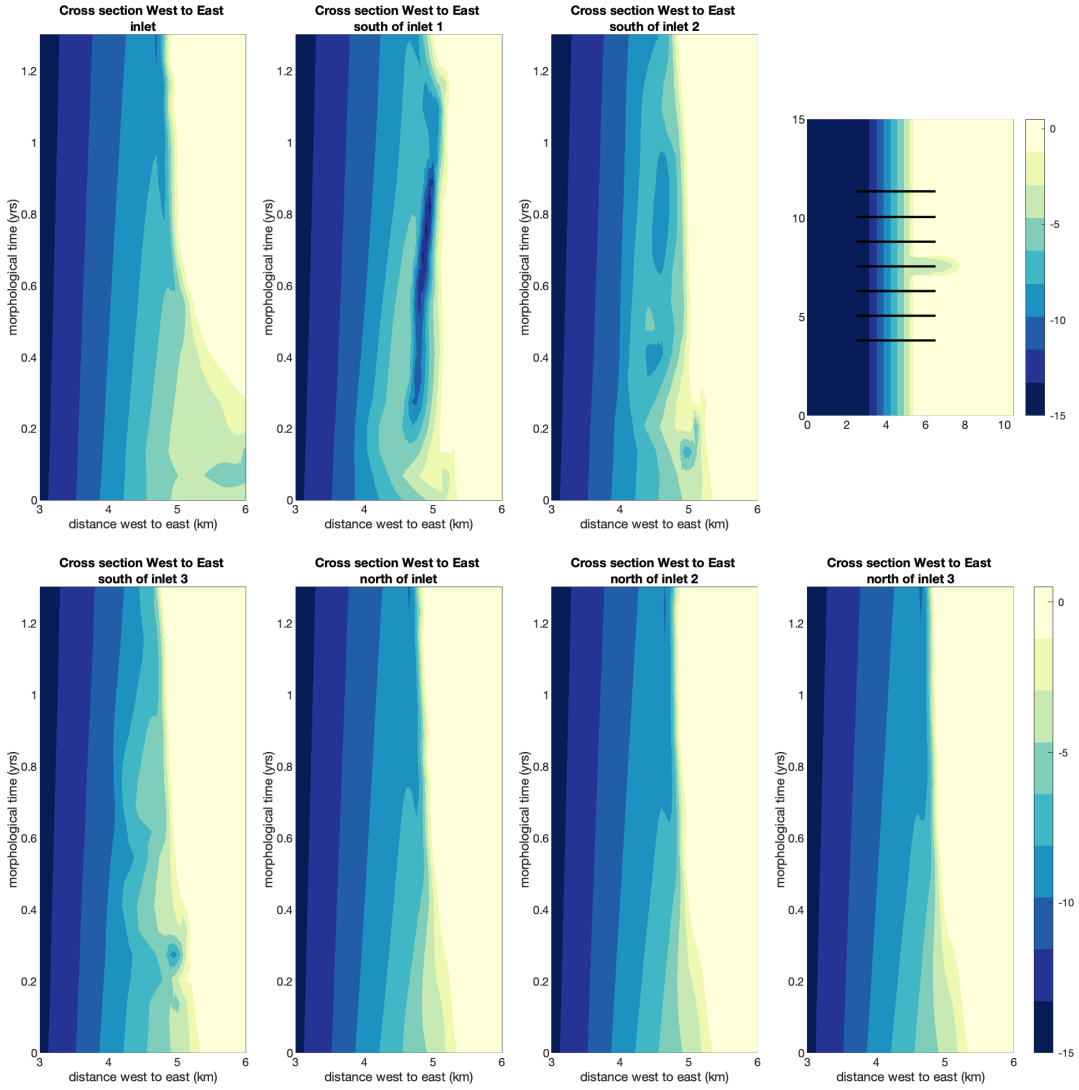
Cross section West to East inlet
Cross section West to East south of inlet 1
Cross section West to East south of inlet 2
Cross section West to East south of inlet 3
Cross section West to East north of inlet
Cross section West to East north of inlet 2
Cross section West to East north of inlet 3
morphological time (yrs)
distance west to east (km)

III. Timestacks for control waves and wave climate

No waves

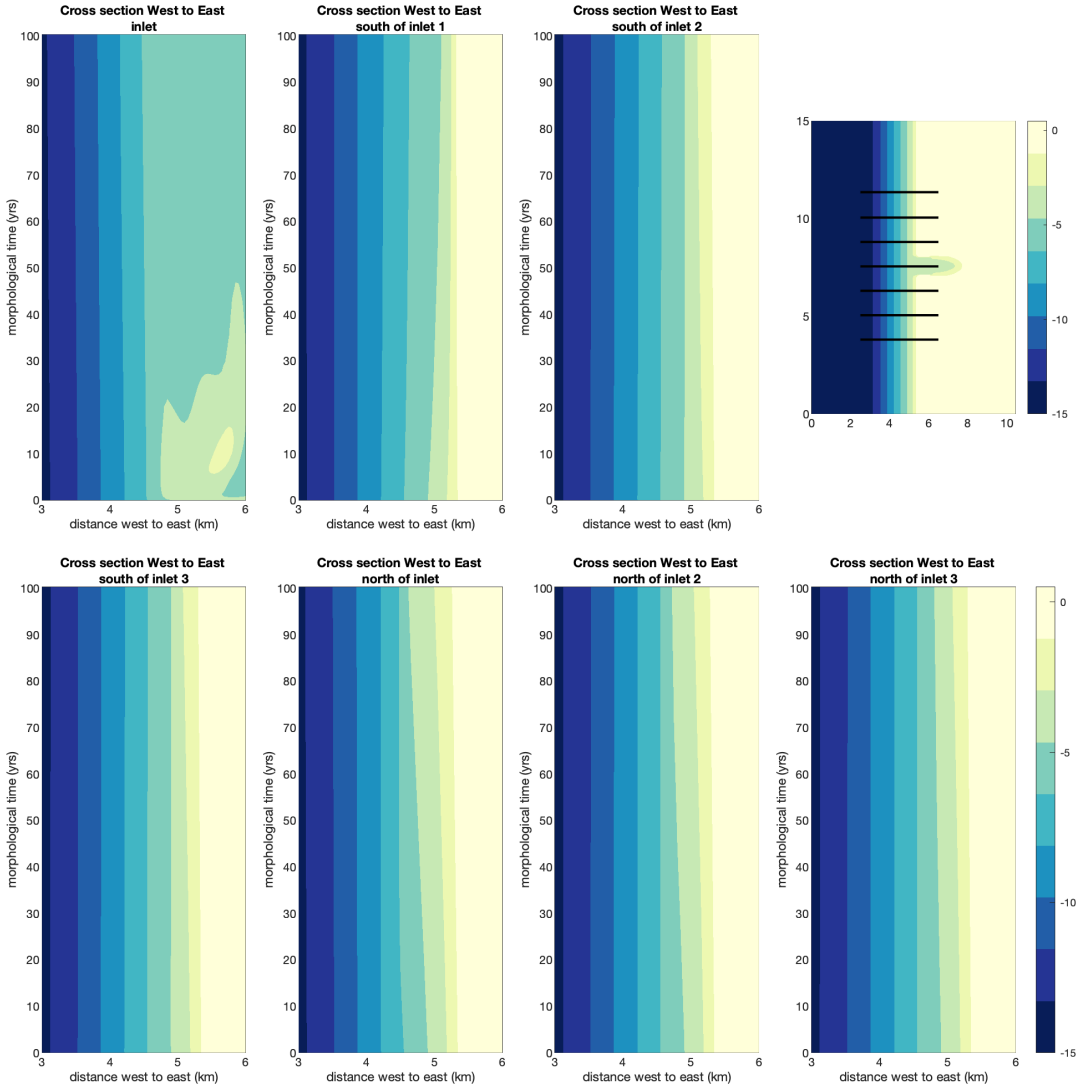

No tides, Wave 1.2m SSW

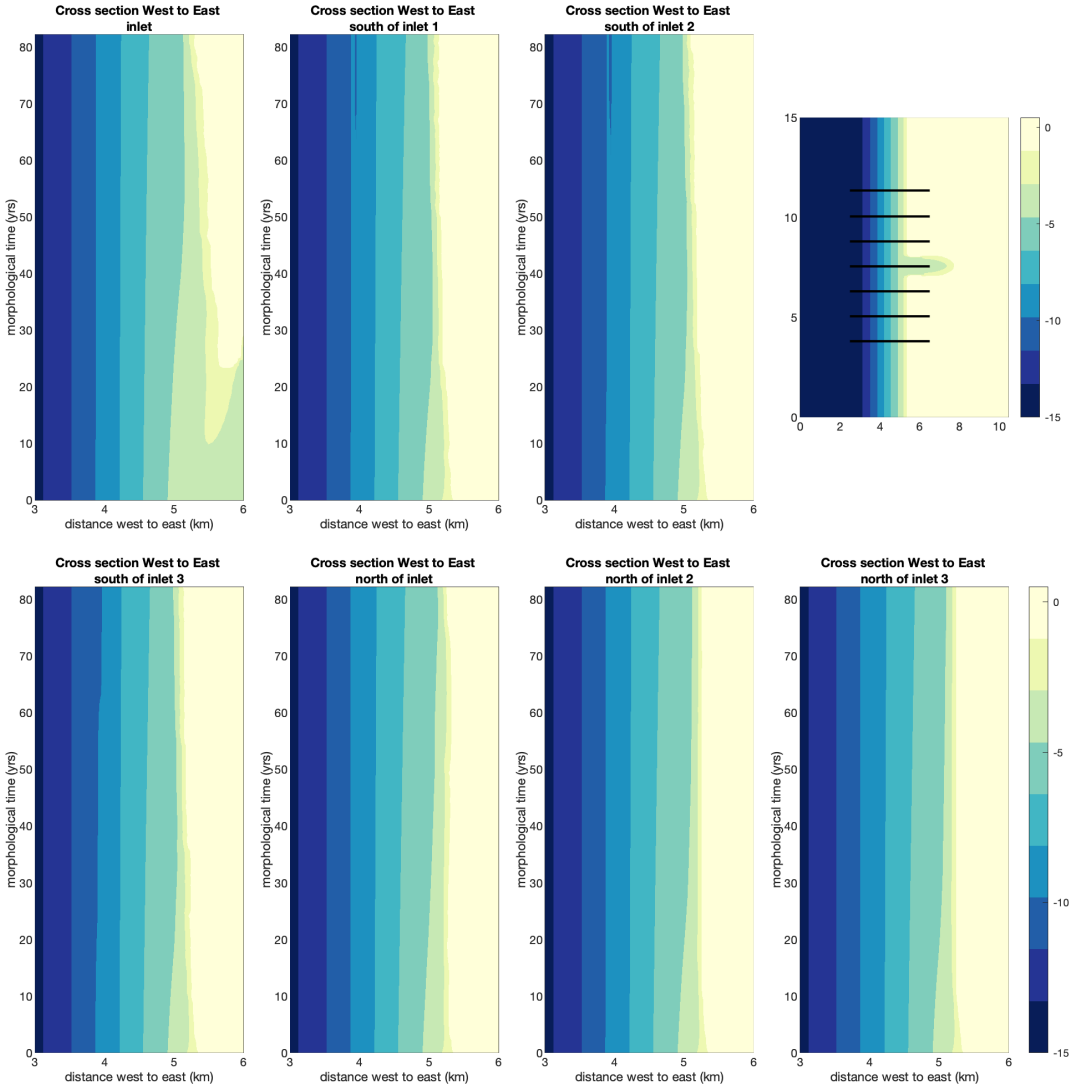

Wave climate